

Experimental Investigation of Pressure Drop and Flow Regimes of Newtonian and Non-Newtonian Two-Phase Flow

Master's Thesis

In Mechanical Engineering

Prepared by:

Serag Alfarek

#201497443

Supervisor: **Dr. Aziz Rahman**

May 2018

Faculty of Engineering and Applied Science

Memorial University

Abstract

Numerous commercial applications in the nuclear, oil and gas, and chemical industries use two-phase flows. When using flows, it is critical to follow the procedures to ensure that the equipment is safe and that the process is efficient. Experimental researchers of two-phase flows focus on developing the fundamental knowledge about it and on enhancing credible experimental databases. It is crucial for validating predictions of computer simulations (i.e. Computational Fluid Dynamics (CFD) software) and the development of theoretical models. Hence, the purpose of this thesis is to assess the pressure drop for Newtonian liquid/gas and non-Newtonian liquid/gas multiphase flows with various operations and to observe the accuracy of the existing empirical models. Partially, the study also aims at predicting the flow patterns of Newtonian and the non-Newtonian flow. However, the estimation of adding a solid particle to the flow loop was not carried out due to the time limitation and commercial constraints. A Manometer and a differential pressure (dP) cell sensor were used to conduct the experimental measurements of pressure drop. In addition, the flow regimes through a horizontal 72.6-mm-ID pipe was observed by a high-speed camera. For the Newtonian model, water and air were instilled. For the non-Newtonian model, xanthan gum solution made out of xanthan gum and water, and air was injected. The experimental results were in line with the empirical models. The experiment results showed that there is a correlation with an increase of the pressure drop and the increase in the gas flow rate. Moreover, the pressure drop increases when the concentration of Xanthan gum solution increases.

Acknowledgments

I would never have been able to finish my dissertation without the guidance of my supervisor, help from friends, and support from my family and wife.

I would like to express my deepest gratitude to my supervisor, Dr. Mohamed Aziz Rahman for his excellent guidance, caring, patience, and providing me with an excellent atmosphere for doing research and letting me experience the concept of multiphase flow in the field and practical issues beyond the textbooks, patiently corrected my writing and financially supported my thesis.

I would also like to thank all the people that helped me to update the multiphase flow experimental set-up. Particularly, I want to thank Mr. Craig Mitchell and Mr. Matt Curtis for their encouragement. Special Thanks goes out to my friend Mr. Abdelsalam Ihmoudah who was always willing to help and give his best suggestions. It would have been a lonely lab without him.

Finally, I would like to thank my wife and my son. They have always been there cheering me up and stood by me through the good times and bad.

Contents

Abstract	iii
Acknowledgments	iii
List of Tables	vii
List of Figures	x
1 Introduction	1
1.1 Purpose	1
1.2 Applications	1
2 Background	2
2.1 Flow Through Pipes	2
2.1.1 Resistance to Flow in a Pipe	2
2.1.2 Frictional Head Loss and Frictional Pressure Drop	6
2.2 Multi-Phase Flow	9
2.2.1 Multi-Phase Flow Models	11
2.3 Flow Regime	13
2.3.1 Flow Regimes Classification	13
2.3.2 Visualization of Flow Regimes	13
2.3.3 Flow Regimes Maps	17
2.4 Fluids Characterization	19
2.4.1 Newtonian Fluids	19
2.4.2 Non-Newtonian Fluids	20
2.5 Two-Phase Flow Basic Definitions and Terminology	27
2.6 Newtonian Pressure Drop Calculations	37
2.6.1 Pressure Drop in a Single-Phase Flow	37
2.6.2 Pressure Drop in a Multiphase Flow	38
2.7 Non-Newtonian Pressure Drop Calculations	42
2.7.1 Pressure Drop in a Single-Phase Flow	42

2.7.2	Pressure Drop in a Multiphase Flow	45
3	Experimental Apparatus	47
3.1	Process Flow Loop	47
3.2	Flow Loop Equipment	49
3.2.1	Storage Tank.....	49
3.2.2	Pump	49
3.2.3	Liquid Flow Meter	50
3.2.4	Gas Flow Meter.....	51
3.2.5	Pressure Sensor.....	53
3.2.6	Differential Pressure (dP Cell) Sensor	53
3.2.7	Manometer.....	55
3.2.8	Thermocouples	56
3.3	Flow Loop Valves.....	57
3.3.1	Pneumatic Ball Valves.....	57
3.3.2	Pressure Relief Valve.....	57
3.3.3	Pressure Regulator	58
3.3.4	Air Filter	59
3.3.5	Check Valves	60
3.4	Data Acquisition System – NI cDAQ-9178	61
3.5	Mega Speed MS55K - High Speed Camera	64
3.6	Rheology Measurement Equipment	67
4	Experimental Procedure	70
4.1	Rheology Determination of Non-Newtonian Test Fluid.....	70
4.2	Flow Test Experimental Procedure	73
4.2.1	Newtonian Procedure	73
4.2.2	Non-Newtonian Procedure	74
5	Flow Test Results and Analysis	77
5.1	Lab Test Fluid Rheology	77

5.2	Pressure Drop Measurements	79
5.2.1	Single-Phase Flow	79
5.2.2	Single-Phase Pressure Drop vs Reynolds Number	82
5.2.3	Two-Phase Flow.....	83
5.2.4	Two-Phase Pressure Drop vs Reynolds Number	89
5.2.5	Phase Pressure Drop Comparisons.....	90
5.3	Flow Regime Visualizations.....	93
5.3.1	Newtonian Flow Regimes.....	93
5.3.2	Non-Newtonian Flow Regimes.....	94
5.3.3	Flow Regime Maps.....	95
6	Discussion	99
7	Conclusion	101
	References	103
	Appendix A: Pressure Drop Correlations	103
	Appendix B: Solid/Liquid/Gas Multiphase Flow	103

Nomenclature

Abbreviation	Description	Unit
D	inside diameter of pipe	m
A	cross-sectional area	m^2
L	actual length of pipe	m
L_e	equivalent length due to pipe fittings	m
L_T	total length of pipe	m
v_{sl}	superficial liquid velocity	m/s
v_{sg}	superficial gas velocity	m/s
v_m	mixture velocity	m/s
Q_l	liquid flow rate	L/min
Q_g	gas flow rate	L/min
\dot{m}_l	liquid mass flow rate	Kg/s
\dot{m}_g	gas mass flow rate	Kg/s
\dot{m}	total mass flow rate	Kg/s
G	total mass flow flux	$Kg/m^2.s$
μ_l	liquid viscosity	cP
μ_g	gas viscosity	cP
μ_m	mixture viscosity	cP
μ_p	plastic viscosity	cP
μ_{NS}	no-slip viscosity	cP
η	kinematic viscosity	cP
ρ_l	liquid density	Kg/m^3
ρ_g	gas density	Kg/m^3
ρ_m	mixture density	Kg/m^3
ρ_{NS}	no-slip density	Kg/m^3
g	gravitational constant	$Kg.m/s^2$
C_l	liquid volume fraction	<i>dimensionless</i>
C_g	gas volume fraction	<i>dimensionless</i>
$E_L(0)$	in-situ liquid holdup	<i>dimensionless</i>
$E_L(\theta)$	actual in-situ liquid holdup	<i>dimensionless</i>
Re	Reynold's Number	<i>dimensionless</i>
Re_{NS}	no-slip Reynold's Number	<i>dimensionless</i>
Re_{tp}	two-phase Reynold's number	<i>dimensionless</i>

f	friction factor	<i>dimensionless</i>
f_F	Fanning friction factor	<i>dimensionless</i>
f_{NS}	no-slip friction factor	<i>dimensionless</i>
f_{tp}	two-phase friction factor	<i>dimensionless</i>
h_f	head loss	m
ΔP	pressure drop	Pa
ΔP_{tp}	two-phase pressure drop	Pa
$(-\Delta P)_f$	frictional pressure loss	Pa
$(-\Delta P)_g$	gravity pressure loss	Pa
$(-\Delta P)_a$	acceleration pressure loss	Pa
τ	shear stress	Pa
τ_w	wall shear stress	Pa
τ_0	yield stress	Pa
γ	shear rate	sec^{-1}
K	flow consistency	$\text{Pa}\cdot\text{s}^n$
n	flow behavior index	<i>dimensionless</i>
Fr_m	Froude mixture number	<i>dimensionless</i>
C	Lockhart-Martinelli constant	<i>dimensionless</i>
X	Lockhart-Martinelli parameter	<i>dimensionless</i>
ϕ_l	liquid multiplier	<i>dimensionless</i>
ϕ_g	gas multiplier	<i>dimensionless</i>
J	Farooqi and Richardson correction factor	<i>dimensionless</i>
N_{vl}	liquid velocity number	<i>dimensionless</i>
α	void fraction	<i>dimensionless</i>
x	wetness fraction	<i>dimensionless</i>
S	slip ratio	<i>dimensionless</i>
k/D	relative pipe roughness	<i>dimensionless</i>
β	volumetric quality	<i>dimensionless</i>

List of Tables

Table 1 - P&ID Legend	48
Table 2 - Specifications of Omega PX409 Sensor [36]	54
Table 3 - Specifications of Comark C9555 Manometer [38].....	55
Table 4 - NI cDAQ-9178 Specifications [41].....	62
Table 5 - Mega Speed MS55K Specifications [42].....	65
Table 6 - Experiment Sample Concentration = 1 g/L	77
Table 7 - Experiment Sample Concentration = 2 g/L	77
Table 8 - Comparison Flow Regime Area Limits of The Experimental Results with Literature review	97

List of Figures

Figure 1 - Elements of Fluid Flow in Pipes	3
Figure 2 - Velocity Profile of General Flow Types [4].....	4
Figure 3 - General Types of Fluid Flow in Pipes based on Reynold's Number	5
Figure 4 - Moody's Diagram [5].....	8
Figure 5 - Different Fields of Multiphase Flow [8]	10
Figure 6 - Visualization System [13].....	14
Figure 7 - Gas-Liquid Flow Patterns in Horizontal Pipelines (Adapted from Hubbard, 1966 [16])	15
Figure 8 - Flow Regimes Map for Gas-Liquid Flow in Horizontal Pipes (Adapted from Mandhane et al., 1974 [18])	18
Figure 9 - Flow Regimes Map for Gas-Liquid Flow in Horizontal Pipes (Adapted from Taitel and Dukler, 1976 [19]).....	18
Figure 10 - Shear Stress as a Function of Shear Rate for Several Kind of Fluids [20].....	20
Figure 11 - Viscosity of Newtonian, Shear Thinning and Shear Thickening Fluids as a Function of Shear Rate [20]	20
Figure 12 - Shear Thinning Flow.....	21
Figure 13 - Bingham Body Flow.....	21
Figure 14 - Shear Thickening Flow	22
Figure 15 - Thixotropic Flow	22
Figure 16 - Velocity Profile for Different Fluids [20].....	23
Figure 17 - Fluid Classification based on Time Dependency	23
Figure 18 - The Conformation Change in Xanthan Gum Solutions when Shear is Applied and Removed	25
Figure 19 - Xanthan Gum Viscosity vs Concentration in Standardized Tap Water [24].....	26

Figure 20 - The Conformation Change in Xanthan Gum Solutions with Heating and Cooling.....	26
Figure 21 - Correlations for void fraction and frictional pressure drop (Adapted from Lockhart and Martinelli, 1949 [26]).....	41
Figure 22 - Simplified Diagram of Process Flow Loop	47
Figure 23 - Schematic of The Flow Loop.....	48
Figure 24 - Storage Tank of The Flow Loop	49
Figure 25 - Goulds Pump and TB Wood Inverter.....	50
Figure 26 - Omega FTB-730 Turbine Flow Meter	51
Figure 27 - Branched Air Pipeline and Gas Flow Meters	52
Figure 28 - Omega FLR6750D Gas Flow Meter [33]	52
Figure 29 - Omega Pressure Sensor PX603 [34]	53
Figure 30 - Omega PX409 Sensor [35]	54
Figure 31 - Omega PX409 Sensor Setup.....	54
Figure 32 - Comark C9555 Manometer.....	55
Figure 33 - Omega TC-(*)-NPT Sensor [39].....	56
Figure 34 - Installed Control Valves for The Liquid Flow (on The Left) and The Air Flow (on The Right) .	57
Figure 35 - Jaybell Pressure Relief Valve	58
Figure 36 - TORPING Air Filter 52.160 and TOPRING Pressure Regulator 52.360	59
Figure 37 - Liquid Ball Check Valve (on The Left) and Air Check Valve.....	60
Figure 38 - NI cDAQ-9178 Chassis [41].....	61
Figure 39 - NI cDAQ-9178 Setup.....	63
Figure 40 - SignalExpress Interface Signals Monitoring	63
Figure 41 - SignalExpress Signal outputs Interface	64

Figure 42 - Mega Speed MS55K - High Speed Camera	65
Figure 43 - Mega Speed MS55K Visualization	66
Figure 44 - Mega Speed MS55K High-Speed Imaging Software	66
Figure 45 - Acculab Vicon Scale	67
Figure 46 - Graduated Beaker	67
Figure 47 - Marsh Funnel Viscometer	68
Figure 48 - Density Mud Balance	68
Figure 49 - High-Speed Multi Mixer.....	69
Figure 50 - Rotational Viscometer.....	69
Figure 51 - OFITE 8-Speed Model 800 Viscometer [43].....	71
Figure 52 - Rheogram for Experiment Sample Concentrations.....	78
Figure 53 - Effect of Shear Rate on Viscosity of Xanthan Gum Concentrations	78
Figure 54 - Single-Phase Water Flow - Experimental and Correlations Pressure Drop Results.....	79
Figure 55 - Single-Phase Air Flow - Experimental and Correlations Pressure Drop Results.....	80
Figure 56 - 1g/L Xanthan Gum Solution - Experimental and Correlations Pressure Drop Results	81
Figure 57 - 2g/L Xanthan Gum Solution - Experimental and Correlations Pressure Drop Results	81
Figure 58 - Single-Phase Pressure Drop vs Reynolds Number	82
Figure 59 - 2-P Water and Air Flow - Experimental and Correlations Pressure Drop Results	83
Figure 60 - 2-P Air and Water Flow - Experimental and Correlations Pressure Drop Results	84
Figure 61 - Two-Phase 1g/L Xanthan Gum Solution and Air Flow - Experimental and Correlations Pressure Drop Results	85
Figure 62 - Two-Phase Air Flow and 1g/L Xanthan Gum Solution - Experimental and Correlations Pressure Drop Results	86

Figure 63 - Two-Phase 2g/L Xanthan Gum Solution and Air Flow - Experimental and Correlations Pressure Drop Results	87
Figure 64 - Two-Phase Air Flow and 2g/L Xanthan Gum Solution - Experimental and Correlations Pressure Drop Results	88
Figure 65 - Two-Phase Pressure Drop vs Reynolds Number.....	89
Figure 66 - Newtonian Experimental Pressure Drop Comparison - Single Phase vs Two Phase.....	90
Figure 67 - Non-Newtonian Experimental Pressure Drop Comparison - Single Phase vs Two Phase	91
Figure 68 - Newtonian and Non-Newtonian Experimental Pressure Drop Comparison - Single Phase vs Two Phase	92
Figure 69 - Newtonian Flow Regimes Visualized by High-Speed Camera Mega Speed MS55K	93
Figure 70 - Non-Newtonian Flow Regimes Visualized by High-Speed Camera Mega Speed MS55K.....	94
Figure 71 - Comparison Taitel and Duckler (1976) and Mandhane (1974) Flow Regime Maps with Flow Regimes Visualizations Through a 3 in (76.2 mm)-ID Horizontal Pipe.	95
Figure 72 – Typical Velocity and Shear Stress Distributions Near a Wall in Turbulent Flow (Adapted from Kay and Nedderman, 1985 [52]).....	125
Figure 73 - Forces Acting a Spherical Particle Within a Flow (Adapted from Green and Perry, 2007 [53])	125
Figure 74 - Solid-Liquid flow regimes in horizontal pipelines (Adapted from Multiphase Design Handbook, 2005 [54]).....	126
Figure 75 - Solid-Gas-Liquid flow regimes in horizontal pipelines (Adapted from Multiphase Design Handbook, 2005 [54])	128
Figure 76 - Flow Loop Schematic of Design 1	129
Figure 77 - Flow Loop Schematic of Design 2.....	131
Figure 78 - Flow Loop Schematic of Design 3.....	132

1 Introduction

1.1 Purpose

It is critical to comprehend the impact of the frictional elements in pressure loss to improve the accuracy of the process system design [1]. There is a wide use of two-phase flow in the process and related industries as it includes various flow regimes, such as annular, slug, stratified, and bubble. There are great pressure fluctuations in the slug and stratified regimes which can impair the equipment, as they impact mass and transfer phenomena of the equipment [2]. This study aims at accurately evaluating the pressure drop for Newtonian and non-Newtonian two-phase flow. Moreover, its aim is to predict the flow patterns to create a flow regime map. Finally, it will analyze the effects of the changes in non-Newtonian fluid concentrations and the flow rates on the pressure drop.

1.2 Applications

Multiphase units are used in a wide range of commercial industries, such as gas and oil, refining, and mining in regard to some broad fields of matter. Some important applications are sizing of process equipment, liquid management, and well drilling operations. Accordingly, it is highly challenging, yet critical, for engineers to select the right multiphase pressure drop in liquid accumulation and pigging [3]. To prevent problems such as large liquid surges, flow instabilities, and high liquid hold up, pipe diameter and pump design selection needs precise pressure drop measurements. The attention should be paid to the following issues:

1. Pressure drop in flow-lines
2. Liquid management
 - 2.1. Liquid inventory control operation
 - Rate changes, shut-down and restart
 - Water accumulation
 - Pigging
 - 2.2. Pipeline diameter selection

3. Prediction and control of slugging
4. Sizing of process equipment, e.g. separators/slug catchers
5. Drag reduction
6. Remote multiphase boosting
7. Oil, grease, slurries transport in pipeline
8. Separator pressure set-point

2 Background

2.1 Flow Through Pipes

There are numerous purposes of pipe flow under pressure. In all industries which use chemical and mechanical engineering, the understanding of fluid flow is critical. Both manufacturing and chemical industries rely on large flow networks to ensure smooth transport of raw materials and products from various processing units. Accordingly, it is crucial to have a comprehensive knowledge about fluid flow in pipes. The flow requires energy input of liquid or gas to flow through the pipe. It is necessary due to frictional energy loss, also known as frictional pressure drop and frictional head loss. It occurs as a result of the internal friction within the fluid and the friction between the fluid and the pipe wall. A significant amount of energy in pipe flow is lost because of frictional resistances. Pipe losses in a piping system depend on several system features, including the shape of flow path, sudden or gradual changes in the cross-section, obstructions in the flow path, changes in direction of flow, and pipe friction.

2.1.1 Resistance to Flow in a Pipe

During a fluid flows throughout a pipe, local eddy currents within the fluid are generated because of the internal roughness of the pipe. As a result, a resistance is added to the flow of the fluid. Because of the velocity profile in a pipe the fluid elements located in the middle of the pipe flow faster than elements located near to the wall. Accordingly, friction will take part between layers within the fluid. The move of fluid elements in the mutual relation is related to the pressure drop known as well as frictional losses. In a case of

pipes with smooth walls such as polyethylene, brass, copper, and glass, the impact on the frictional resistance is small. However, the impact on the frictional resistance is large when the pipes have less smooth walls, including steel, cast iron, and concrete, as these materials create big eddy currents. The rougher is the inner wall, the higher is the pressure loss as a result of friction. Also, there is a correlation between the rise in the average velocity and the pressure losses. As the velocity is in the direct relationship to the flow rate, then: $\text{Velocity} = \text{Volumetric flow rate} / \text{Cross sectional area of the pipe}$.

A drop or rise in a flow rate results in respective decrease or increase in velocity. Hence, the smaller pipe is, the larger amount of the liquid touches the pipe, which generates friction. There is also the impact of the pipe size on velocity. When a flow rate is constant, the decrease in the pipe size results in an increase of velocity, which in turn, leads to a rise in friction. Considering that the fluid moves throughout the entire pipe, the friction losses are cumulative. The friction losses, hence, increase with the distance travelled. However, high viscosity fluids are slower and overall without eddy currents. Hence, the inner roughness of the pipe does not impact the frictional resistance.

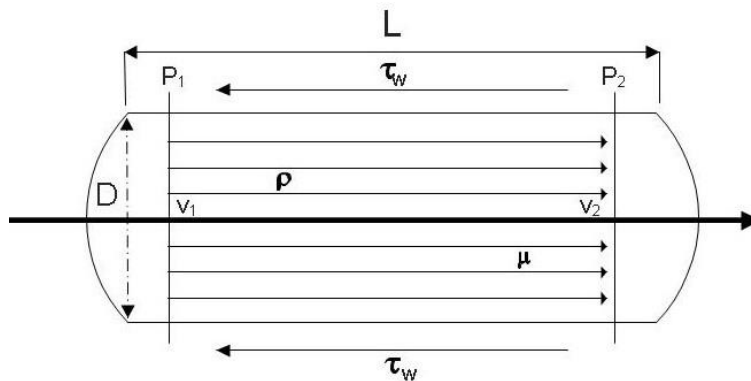


Figure 1 - Elements of Fluid Flow in Pipes

Overall, three types of fluid flow in pipes exist:

Turbulent Flow

In this case, the fluid moves erratically and takes the form of eddies and cross currents. Overall, it occurs in larger pipes and with high flow rates.

Laminar Flow

Overall, it occurs in small pipes, with highly viscous fluid, and with low flow velocities. When the velocity is low, fluids have a tendency to flow without lateral mixing. In this case, adjacent layers slide next to each other like cards. There are no eddies and cross currents. In fact, it can be described as a series of liquid cylinders in the pipe, where the cylinder that touches the pipe does not move, whereas the fastest parts are inner ones.

Transitional Flow

Transitional flow is a combination of turbulent and laminar flow. The laminar flow takes part close to the edges, whereas the turbulence occurs in the middle of the pipe.

All flows behave differently in regard to frictional energy loss during to flow and there are different equations predicting this behavior. Reynolds examined the conditions for the transformation of one flow into another. He discovered that there is a critical velocity at which the laminar flow becomes the turbulent one, and that it is based on four quantities: average velocity of the liquid, density, viscosity, and the diameter of the tube. It is possible to combine those four factors into one group. Hence, the transformation of the flow takes part at a definite value of the group. The name of the grouping of the variables is Reynolds Number (Re). Laminar or turbulent flow is determined by Reynolds Number.

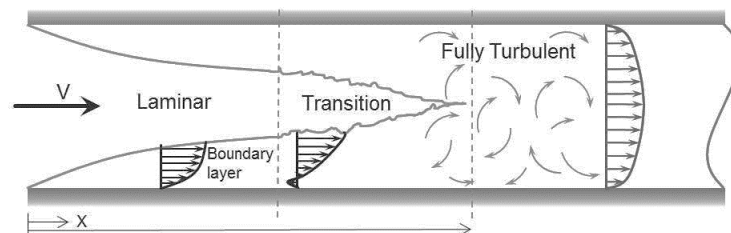


Figure 2 - Velocity Profile of General Flow Types [4]

The Reynolds number shows the ratio of inertial (resistant to change or motion) forces to viscous forces.

$$Re = \frac{D \rho v}{\mu} = \frac{\text{inertia force}}{\text{viscous force}} \quad (1)$$

Where:

D = Diameter of the pipe (m),

ρ = Density of fluid (kg/m^3),

v = Average velocity of the fluid (m/s),

μ = Viscosity of fluid (cP).

It is possible to write the Reynolds number in terms of kinematic viscosity (η)

$$\eta = \frac{\mu}{\rho} \quad (2)$$

The Reynolds number is critical for the analysis of all kinds of flow with a significant velocity gradient (i.e. shear). It shows what is the relative importance of the viscous effect in comparison to the inertia effect.

The flow is

- Transient when $2100 < Re < 4000$
- Laminar when $Re < 2100$
- Turbulent when $Re > 4000$

In comparison to inertial forces, viscous forces dominate in laminar regions. Under conditions of laminar flow, there is a proportional relationship between the velocity and the pressure drop per unit length. However, it is not possible to reproduce experimental results in transition regions. Lastly, inertial forces dominate in turbulent regions. Regarding turbulent flow, the pressure drop is proportional to the velocity when it is increased to a power of 2.

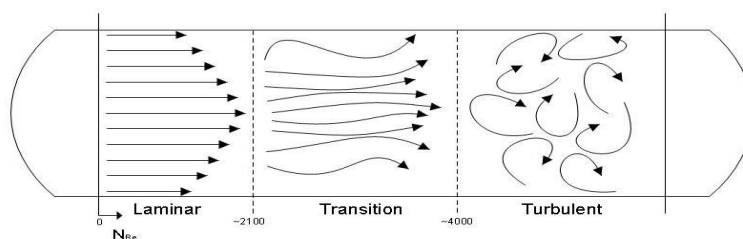


Figure 3 - General Types of Fluid Flow in Pipes based on Reynold's Number

2.1.2 Frictional Head Loss and Frictional Pressure Drop

It is possible to express the energy loss in pipe flow because of friction as a pressure drop and not as a head loss. Commonly, mechanical and chemical engineers use pressure drop, whereas civil engineers head loss. The following shows the relationship between frictional pressure drop and frictional head loss [5]:

$$(-\Delta P)_f = \rho g h_{fs} \quad (3)$$

Where:

$(-\Delta P)_f$ = Frictional pressure drop (Pa),

h_{fs} = Frictional head loss due to skin friction (Pa),

ρ = Density of fluid (kg/m³),

g = acceleration due to gravity (m/s²).

Head Loss as a result of skin friction (h_{fs}) can be related to wall shear.

$$h_{fs} = \frac{(-\Delta P)_f}{\rho g} = \frac{4\tau_w L}{\rho g D} \quad (4)$$

Where L is the length of the pipe, τ_w the shear stress at the wall of the pipe, and ΔP_f is pressure drop as a result of friction losses.

$$f = \frac{\tau_w}{\rho v^2 / 2} \quad (5)$$

$$h_{fs} = \frac{(-\Delta P)_f}{\rho g} = 4f \left(\frac{L}{D} \right) \left(\frac{v^2}{2g} \right) \quad (6)$$

Where, f is the Fanning friction factor

- Only requires L, D, v and f to obtain friction loss
- Valid for turbulent and laminar flow
- Valid for both Newtonian and Non-Newtonian fluids

There are correlations between the Reynolds number and the fanning friction factor for turbulent and laminar flow in a broad range of pipes. In a case laminar flow, first principles serve to develop a relation between the friction factor and the Reynolds number. The

Hagen-Poiseuille equation relates the frictional pressure drop to pipe dimension, viscosity, and fluid velocity:

$$(-\Delta P)_f = \frac{32\mu Lv}{D^2} \quad (7)$$

Equation (7) (the Hagen-Poiseuille equation) shows equating the pressure drop as a result of friction with the overall pressure drop throughout the pipe. When it is combined with the Fanning equation provided by Equation (6), the results in relation for laminar flow are the following:

$$f = \frac{16}{Re} \quad (8)$$

It is not possible to apply the first principle analysis to develop a relation between Reynolds number and friction factor in a case of turbulent flow. There are various empirical correlations for turbulent flow in smooth pipes, such as Blasius equations:

$$f_{Blasius} = \frac{0.079}{Re^{0.25}} \quad (9)$$

This correlation is valid for $4000 < Re < 10^5$

There is no theoretical basis of the Blasius equation. Hence, it is only an empirical equation. However, it is highly convenient to apply. The Kármán-Nikuradse equation well represents the whole turbulent region:

$$\frac{1}{\sqrt{f}} = 4.0 \log Re\sqrt{f} - 0.4 \quad (10)$$

For $Re > 4000$, turbulent

The research has confirmed that a rough pipe in turbulent flow will have a higher friction factor in relation to a given Reynolds number than the smooth one. The friction factor is reduced when the pipe is made smoother. If it happens that smoothing does not result in the reduction of friction factor for a given Reynolds number, the tube is regarded as hydraulically smooth.

**The equations 1 to 10 were obtained from [5].*

Regarding turbulent flow, f the friction factor, depends on the relative roughness of the pipe, k/D (k - average roughness height of the pipe; D - the inner diameter of the pipe) and the Reynolds number. The overall behavior of turbulent pipe flow when there is surface roughness is established. In a case k is small in comparison to the pipe diameter D (i.e. $k/D \rightarrow 0$), f depends solely on Re . In a case k/D has a significant value and Re is low, then the flow is regarded to be in a smooth regime in which roughness have no impact. With the rise in Re , the flow is transformed into transitionally rough. This phase is a transition regime as the friction factor becomes higher than the smooth value. At this point, it is a function of both Re and k . If the Re continues to rise, the flow will reach a fully rough regime. In this regime, f is completely independent of Re . In a case of smooth pipe flow, the effect of k on the flow is entirely submerged by the viscous sub layer. Accordingly, the friction factor f is independent of the effect of k on the flow, but it is a function of Re . When the pipe flow is rough, then the viscous sub layer thickness is small in comparison to roughness height. Accordingly, f is independent of Re , and it is the function of k/D , as the roughness of the pipe dominates the flow. The friction factor chart summarizes the frictional characteristics of both rough and smooth round pipes. It is a log-log plot of Fanning friction factor (f) vs Re on the basis of the Moody's chart (Figure 4).

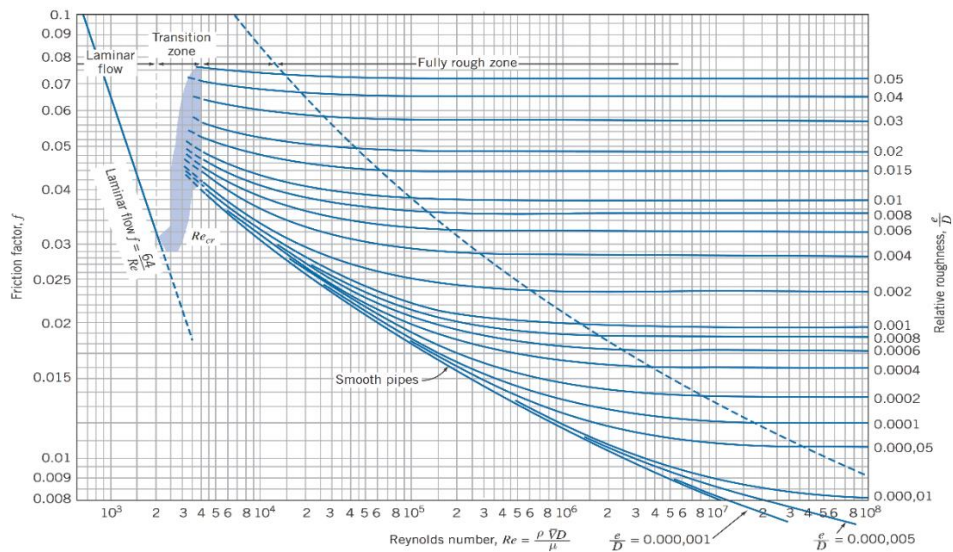


Figure 4 - Moody's Diagram [5]

2.2 Multiphase Flow

A phase refers to one state of the subject. It can be gas, liquid, and solid [6]. The term multiphase flow refers to fluid flow that encompasses more than one component or a phase or component flowing throughout a pipeline [7]. There is a greater variety of applications of multiphase flow than single phase flow because of differences in density. Hence, because of different viscosities and densities, the viscous impediment at the pipe wall differs among phases. Besides, typically different phases do not flow at same velocities. The variations in the internal average velocities between phases results lead to slip (Sidsel et al., 2005). The definition of phase holdup is that it is the fraction of pipe volume occupied by a certain phase. To illustrate, void fraction refers to the in-situ gas volume fraction, whereas liquid holdup is the in-situ liquid volume fraction, which is expressed as:

$$H_L = 1 - H_G \quad (11)$$

The variance in the physical distribution of the phases in the pipe flow is the differentiating aspect of multiphase flow. It is also known as flow regime and flow pattern. The flow regime is dependent on the relative magnitudes of the forces impacting the fluids, such as surface tension forces, inertia, turbulence, and buoyancy. These forces importantly vary by fluid properties, pipe inclination, pipe diameter, and flow rates.

Multiphase flow is a type of flow with a variety of application in many petroleum and chemical industries. It is possible to observe various forms of a flow pattern, known as a Multiphase flow pattern, when two or more phases flow at the same time as shown in Figure 5. It is a critical phenomenon for gas and oil industries, as they rely on Boiling Water Reactors, steam generators, steam flow in water type boiler tubes, and pipeline transportation of oil and gas mixtures.

The aim of this study is to shed light on the development in the technological and research aspects. Depending on the users' needs, flows combining various flow parameters are either preferred or to be avoided. The multiphase flow depends on parameters such as the momentum difference between vapor and liquid, interfacial area per unit volume,

momentum, and mass exchange rate. Most commonly, the multiphase flow is used in the petroleum industries. In this case, the preference is for having a minimum pressure loss during the transportation of liquid or gas petroleum compounds through a pipeline. An adequate estimation of the flow regime that corresponds to flow parameters allows industries to work within its preferred operational limits. Overall, petroleum industries aspire to transport liquid petroleum products by using gas or air as a driving force. Such flow is able to transport liquid petroleum in a vertical section, which leads to a slug or bubbly flow. However, if designed improperly, the outcome can be an annular flow with a small amount of liquid petroleum products and great amount of air.

The first research on multiphase flow was conducted by Lockhart- Martinelli in 1949. His method had been standard in that period and achieved satisfactory results regarding two-phase flow in a horizontal pipe. Nevertheless, there are inconsistencies when applying his method to flows with three and more phases. Hence, in 1954, Baker carried out experiments which resulted in important changes in the equations of Lockhart- Martinelli regarding flow patterns in horizontal pipelines. More precisely, Baker (1954) proposed new correlations for all flow regimes for two-phase flow. Nonetheless, Dukler et al. (1964) did an experiment with Lockhart-Martinelli's and Baker's pressure drop correlations applied to a large number of data points. Their experiment revealed that correlations of Lockhart-Martinelli are superior in approximating flow regimes, apart from the case of wavy flow. So far, only several studies have focused the pressure drop features related to flow pattern. New knowledge about multiphase flow regime development will significantly contribute to financial savings in the industrial sector.

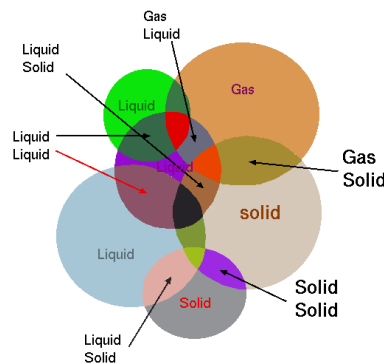


Figure 5 - Different Fields of Multiphase Flow [8]

2.2.1 Multiphase Flow Models

Dispersed Phase and Separated Flows

The term dispersed phase flows refer to flows which have one phase consisting of discrete elements, or more precisely not connected, such as bubbles in a liquid and droplets in a gas. When the flow is separated, there is a line separating two phases. An overcontact annular flow has a gaseous core and a liquid layer on the pipe wall. Put differently, it is possible to stay in the same medium while passing from one point to another within the same phase in a separated flow.

Gas - Liquid Flows

Many applications have gas–liquid flows. Good examples are droplets in the conveying gas stream and the motions of bubbles. Bubble columns have their application in the process industries. In power generation systems, atomization has a crucial role in generating small droplets for combustion. Moreover, in materials processing, droplet formation and impaction are critical for spray forming. Power systems, such as nuclear reactors and fossil fuel plants, commonly use heat exchangers and steam-water flows in pipes. Gas–liquid flows in pipes are able to take configurations, including annular flow, with a droplet-laden gaseous core flow and a liquid layer on the wall, and bubbly flow.

Gas - Solid Flows

In general, gas–solid flows are regarded as a gas with suspended solid particles. This category of flow involves fluidized beds and pneumatic transport. This flow is the basis of pollution control devices such as electrostatic precipitators and cyclone separators. In fossil–fuel power systems, the combustion of coal depends on the burning and dispersion of coal particles. For instance, the performance of the rocket is affected by the micron-size particles found in exhausts of solid-propellant rocket. Furthermore, the motion of particles down an inclined plane or chute is also a gas–solid flow. In these, so-called granular flows, there is a greater significance of particle-wall and particle-particle interactions than of the forces because of the interstitial gas. When the particles stop moving, the problem is reduced to flow by a porous medium having the viscous force on

the particle surfaces as the primary mechanism impacting the gas flow (i.e. A pebble-bed heat exchanger). Although there is no exact 'flowing' in this phase, it is still considered as a kind of multiphase flow.

Liquid - Solid Flows

Liquid–solid flows refer to flows characterized by the liquid carrying solid particles, known as slurry flows. They have a broad range of application in flow of mud and the transport of ores and coals. Such flows that attract significant attention of engineering researchers can be regarded as phase flows. Another instance of porous media flow is the flow of liquid through a solid.

Three-Phase Flows

There are common engineering problems in regard to three-phase flows. To illustrate, bubbles in a slurry flow are an example of three phases in a joint flow. However, there is a gap in the literature on three-phase flows. For a long time, the design of multiphase systems has relied on empiricism. Nevertheless, the qualification of fundamental parameters and process control have been improved due to the development of measurement techniques. The progress in computational capacity has led to the innovations in numerical models, which complement the engineering system design. The technological field of numerical models is quickly progressing, and it has significant implications for improving the efficacy of processes and operations and enables the development of new technologies [9].

2.3 Flow Regime

The flow of gas-liquid mixtures in pipes and similar parts of process equipment is widely used and highly significant. However, depending on the distance, the quality taken as the mass fraction of gas in the two-phase flow is variable. It is illustrated by the flow in numerous gas-oil pipelines. Besides, the quality can change as a result of condensation or boiling, even when the total mass flow rate does not change. It should be underlined that various flow regimes take part at different liquid and gas flow rates and that different materials are used. Hence, to precisely calculate pressure losses in two-phase flow, it is first required to predict the flow regime. Afterwards, an adequate pressure drop calculation procedure is used [10].

2.3.1 Flow Regimes Classification

The flow regimes are categorized into three primary classes:

Regimes for horizontal flow in pipes - the heavier phase (water) is closer to the bottom, due to the gravity. Commonly, the liquid phase is pushed by the gas phase toward the flow direction.

Regimes for vertical flow in pipes - The liquid phase is concentrated on the pipe walls. It forms either an unstable or stable film. There are different formations of flow regimes and flow velocity, depending if it is a downward or upward flow.

Regimes for sloped pipes - They are not widely used. The most important factors are the slope angle and the direction of the flow (downwards or upwards) [11].

2.3.2 Visualization of Flow Regimes

The most challenging feature of managing two-phase flows in pipelines is their tendency to develop various flow patterns. In a gas liquid flow through the horizontal pipe, the gas can appear in a form of small bubbles in the liquid. This type of flow is formed when the amount of liquid in the pipe is much bigger than the amount of gas. Besides, when the liquid flow is sufficiently fast to generate a turbulent flow, then the gas is mixed rapidly with the liquid, and it can go to the top of the pipeline. On the contrary, if there is a small

flow rate of liquid carried by the enormous gas flow rate, the water will take a form of a small film on the pipe wall [12]. Reflector light and a high-speed camera were used for recording to ensure quality visualization as represented in Figure 6.

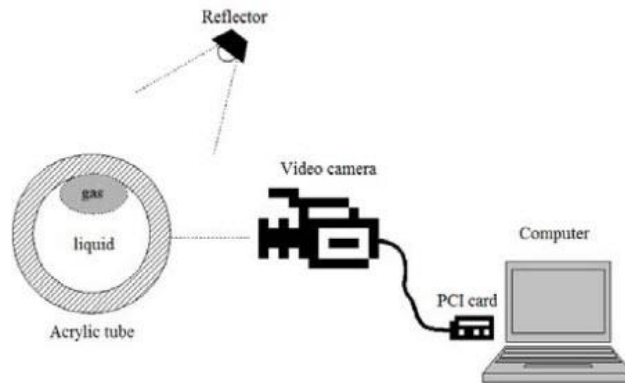


Figure 6 - Visualization System [13]

2.3.2.1 Gas - Liquid Flow Regimes – Horizontal

This section introduces the fundamental theory of two-phase and related flow regime. Typically, the term two phase flow indicates the simultaneous flow of liquid and gas through a pipeline system. Furthermore, as the interface of liquid and gas is deformable. Accordingly, it is challenging to predict which regions are occupied by liquid and by gas phase. During the flow of two phases throughout a pipeline, various types of interface distribution can be formed. Typical distributions are:

- *Annular flow* - the liquid flow takes a form on a film and it is located on the wall of the pipe.
- *Stratified flow* - the gas is lighter than liquid and it flows on the top; two phases are separated.
- *Slug flow* - gas bubbles take a form of a large slug, commonly in a shape of a bullet.
- *Bubbly flow* - small sized bubbles are dispersed with liquid.

Typically, the multiphase flow rate is characterized by its superficial flow velocity and liquid superficial velocity. The superficial velocity is the term used to describe gas-liquid

multiphase flow. It is also used in the flow regime maps. Under the condition of the superficial velocity, the fluid flows without the other fluid being present. Hence, there is no slip between the phases to consider [14]. Put differently, following Crowe [9], superficial velocity (v_{sg} , v_{sl}) refers to the total amount of fluid (Q_{gas} , Q_{liquid}) throughput divided by the cross-section area (A) of the pipe ($v_{sg} = Q_{gas}/A$, $v_{sl} = Q_{liquid}/A$). The volume fraction is the ratio of the gas or liquid flow rate and the total fluid flow rate. The input volume fraction of individual phases can be different than in-situ volume fraction. Also, the buoyancy force and gravity significantly impact heat transfer in the pipeline system, volume fraction, pressure drop, and the flow regime [15]. The flow regimes for horizontal pipe are illustrated in Figure 7.

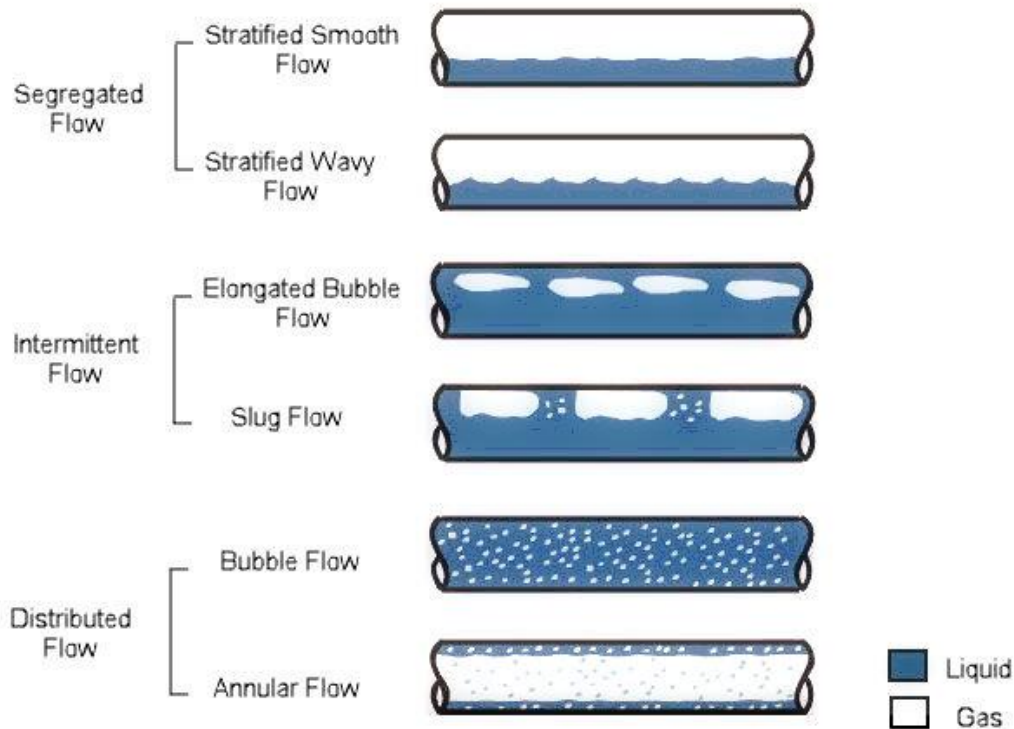


Figure 7 - Gas-Liquid Flow Patterns in Horizontal Pipelines (Adapted from Hubbard, 1966 [16])

There is a consensus about certain descriptions for gas-liquid flow regimes. Focusing on horizontal and near horizontal pipes, Hubbard (1966) proposed three main categories of flow regimes: distributed, intermittent, and segregated flow as illustrated in Figure 7.

Distributed Flow

- i. Bubble Flow:*** here are small gas bubbles flowing on the top of the pipe.
- ii. Annular Flow:*** the gas flow rate should be high enough to allow the formation of the liquid film surrounding the pipe walls. Also, the liquid can take part of droplets distributed through the continuous gas stream, which flows in the center of the pipe. As a result of gravity, the liquid interface is thicker on the bottom of the pipe.

Intermittent Flow

- i. Slug Flow:*** when the amplitude of the waves flowing on the liquid surface is large enough and accordingly bridges the top of the pipe, then the flow is transformed into the slug flow regime. In this regime, the flow of gas takes a form of intermittent slugs, and smaller bubbles are noticed in the liquid.
- ii. Elongated Bubble (Plug) Flow:*** the rising rate of gas flow creates more frequent collision between the bubbles, and eventually they merge into an elongated bubble (plugs).

Segregated Flow

- i. Wavy Flow:*** the boundary between liquid and gas is usually not smooth, as there are ripples on the surface of the liquid. Hence, wavy flow takes the form of ripples as a result of the flowing of the gas at the top of the pipe. The gas flow rate increases simultaneously with a rise in amplitude.
- ii. Stratified Flow:*** a continual gas flow is generated by the merging of the lumps on the top of the pipe. Typically, the gas-liquid boundary typical of stratified flow is smooth.

2.3.3 Flow Regimes Maps

To predict flow patterns, numerous types of flow regimes maps were proposed in the literature. Baker (1954), Beggs and Brill (1973), Mandhane et al. (1974) (Figure 8) developed different empirical maps on the basis of the experimental data. Furthermore, Taitel and Dukler (1976) (Figure 9) are known for a mechanistic approach. Commonly, the classification of regimes in multiphase flow is based on the distribution of the interfaces, the disposition of the phases within the tube, and their shape [15]. The purpose of flow regime maps is to predict flow regime on the bases of some parameters and to provide information about liquid hold-up, pressure, gradient, etc. Transition lines illustrates various flow patterns shown as regions. Lines show that the flow regime changes into another because of the change in a given flow parameter.

Empirical maps are based on the experimental data, which has the coordinate axis consisting of momentum flux, mass, phases superficial velocities, and dimensionless groups. The flow patterns found in the literature usually focus on air and water. It is crucial to provide generalizations according to the available data to include different parameters such as operational conditions, pipe dimensions, and fluid properties.

To precisely determine the transition lines, the number of studies experiments should be considered as well as the parameters on the map coordinate axis knowing that two-phase flow has transient interfaces. However, the analysis and comparison of the transition lines are challenging as different authors use different terms and classify flow patterns differently. The theoretical maps are based on models which include mathematical expressions of the mechanisms of pattern transition. They are developed on the basis of physical concepts and not on the flow regime data. Accordingly, they are fully predictive.

This study has chosen the empirical map of Mandhane et al. (1974) and the theoretical map of Taitel and Dukler (1976) as they are widely accepted [17].

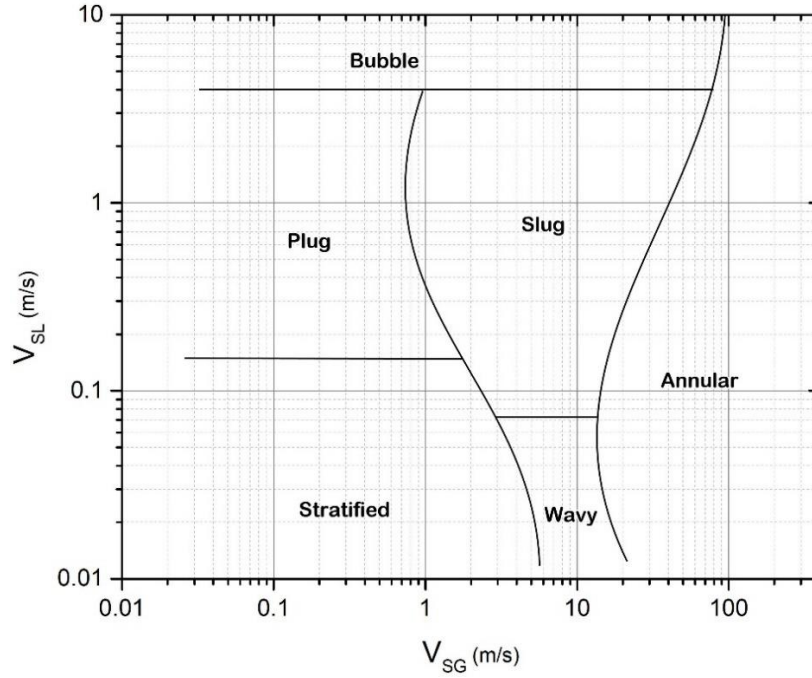


Figure 8 - Flow Regimes Map for Gas-Liquid Flow in Horizontal Pipes (Adapted from Mandhane et al., 1974 [18])

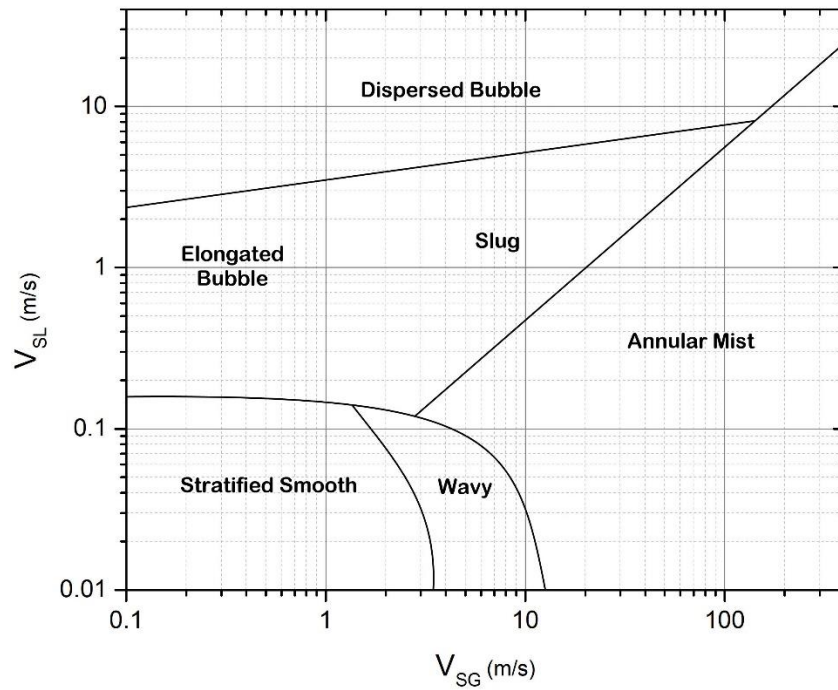


Figure 9 - Flow Regimes Map for Gas-Liquid Flow in Horizontal Pipes (Adapted from Taitel and Dukler, 1976 [19])

2.4 Fluids Characterization

On the basis of the viscosity behavior which is a function of deformation history, shear stress, and shear rate, the fluids are divided into Newtonian or non-Newtonian [20].

2.4.1 Newtonian Fluids

Sir Issac Newton (1642 - 1726) described the flow behavior of fluids with a linear relation between shear stress (τ) and shear rate ($\dot{\gamma}$), named the Newton's Law of Viscosity. In this equation, the proportionality constant (μ) denotes the viscosity of the fluid:

$$\tau = \mu \times \dot{\gamma} \quad (12)$$

Newtonian fluids are honey, organic solvents, and water. Their viscosity depends on temperature. Accordingly, as it can be observed from Figure 10, a plot of shear stress versus shear rate shows a linear rise in stress with a rise in shear rates. The viscosity of the fluid is illustrated by the slope. In conclusion, as seen in Figure 11, the viscosity of Newtonian fluids is constant regardless of the speed of their flow through a channel or pipe. Accordingly, viscosity is independent of the shear rate.

Bingham plastics are an exception to this rule, as these fluids need some minimum stress before initiating the flow, which is a non-Newtonian feature. However, when the flow starts, they keep exhibiting behavior typical of Newtonian fluids, such as the linear relationship between the shear stress and shear rate. Remarkably, mayonnaise behaves in this way.

Typically, Newtonian fluids consist of small isotropic (whose properties and shape are symmetric) molecules. They are not oriented by flow. Nevertheless, there are also fluids consisting of large anisotropic molecules that exhibit Newtonian behavior. To illustrate, polymer or low concentration protein solutions can have a constant viscosity, no matter what the shear rate is. Also, some samples exhibit Newtonian behavior at low shear rates in plateaus termed the zero-shear viscosity region.

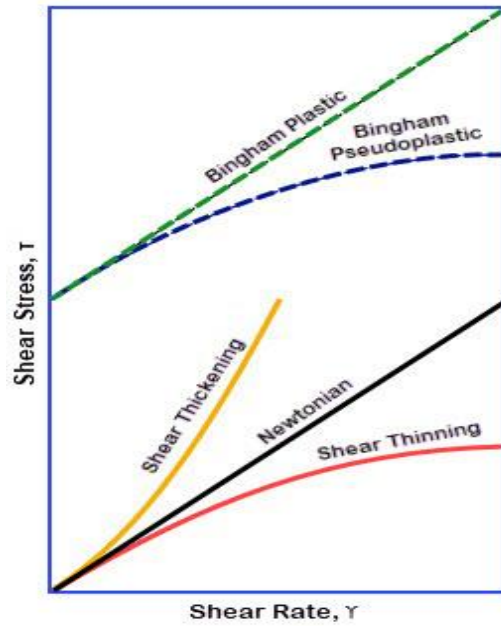


Figure 10 - Shear Stress as a Function of Shear Rate for Several Kind of Fluids [20]

2.4.2 Non-Newtonian Fluids

The majority of fluids in reality is non-Newtonian. Accordingly, their viscosity depends on the deformation history (Thixotropic fluids) or the shear rate - shear thickening or thinning. Unlike Newtonian fluids, as shown in Figure 11, a non-linear relation between shear stress and shear rate is typical for non-Newtonian fluids. In addition, their viscosity is time-dependent, and they have a yield stress.

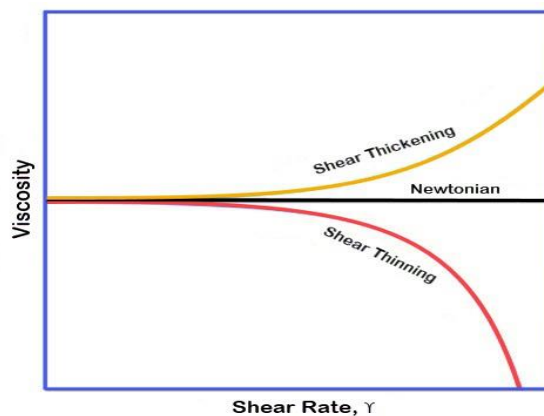


Figure 11 - Viscosity of Newtonian, Shear Thinning and Shear Thickening Fluids as a Function of Shear Rate [20]

2.4.2.1 Types of Non-Newtonian Behavior

Shear Thinning (Pseudo-plastic) Flow

Pseudo-plasticity or Shear Thinning behavior refers to the reduction of apparent viscosity with shear rate. It is a typical behavior of dispersed systems (i.e. Emulsions, inks, and latex), paints, and concentrated polymer solutions. To exhibit this behavior, the system must have a structure able to be reversibly broken down when the stress is first applied and subsequently removed. Figure 12 illustrates common rheograms:

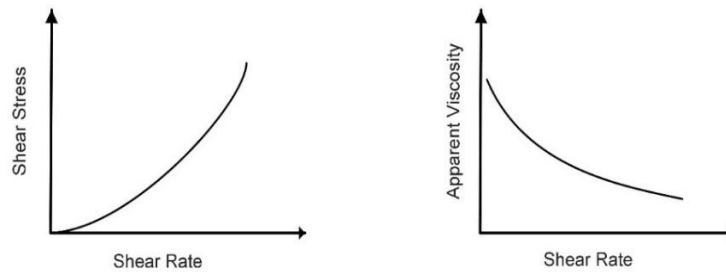


Figure 12 - Shear Thinning Flow

As can be observed from Figure 12, the apparent viscosity or the slope of the shear stress-shear rate curve quickly arises when the shear rate gets closer to zero. Commonly, when the curve is extrapolated to zero, consequently the shear rates intersects positively on the shear stress axis. The term yield stress refers to this intercept. A fluid with a positive intercept and a linear shear stress - shear rate function demonstrates ideal plastic flow. It is labeled as the Bingham body. Figure 13 presents the rheogram for this kind of flow. The apparent viscosity gets close infinity (i.e., a solid) while the shear rate gets close to zero. If the applied shear stress is under the critical yield stress or shear stress, the fluid will behave like an elastic solid.

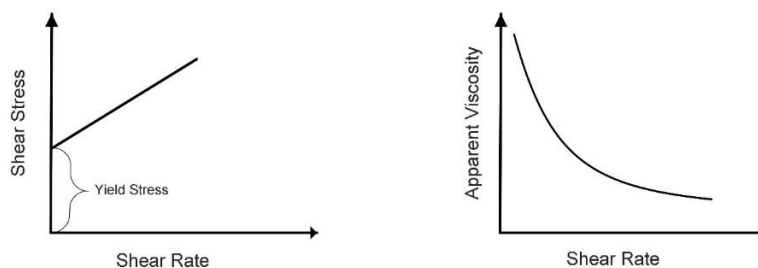


Figure 13 - Bingham Body Flow

Shear Thickening (Dilatant) Flow

With the rise in the shear rate, the apparent viscosity rises reversibly as seen in Figure 14. This kind of behavior is not as frequent as Shear Thinning. Some wrongly argue that the fluid is required to dilate (Dilatant) when flowing [21]. Dilatant fluids are suspensions of glass rods and concentrated clay suspensions. The Dilatancy mechanism is based on four factors which enhance interaction of particles, namely density, size, anisotropy of shape, and concentration [22]. In this way, the effective concentration and the occupied volume are efficiently increased. There is a greater inertia in denser and larger particles. Hence, when the shear is applied to them, they first retard and subsequently accelerate. Because energy is needed to achieve this, a higher apparent viscosity or an additional resistance to flow emerge.

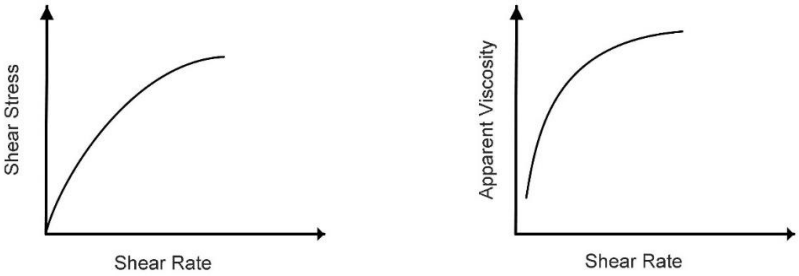


Figure 14 - Shear Thickening Flow

Thixotropic Flow

While the apparent viscosity of shear thickening (Dilatant), shear thinning (Pseudo-plastic) and Newtonian fluids is time-independent other fluids exhibit with same properties are time-dependent. Rheopexy is a behavior when time-independent fluids show increasing in viscosity as they are undergoing shear stress which is evident in Figure 15.

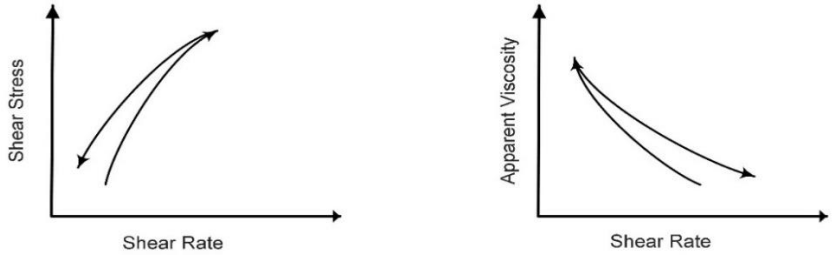


Figure 15 - Thixotropic Flow

Fluid flow depends very much on the viscosity of fluids, which is determined by the characteristics of the flow. Figure 16 shows three velocity profiles on the basis of the fluid behavior. In all cases, viscosity is determined by the shear rate at the walls, namely the slope of the velocity profile close to the wall. To precisely determine if the fluid is non-Newtonian or Newtonian, it is crucial to characterize viscosity and to consider a range of shear rates for the application. Frequently, viscometers available on the market are able to measure index viscosity. However, they do not adequately characterize true and absolute viscosity and shear rate. For the developing and modeling applications with the fluid flow, it is essential to consider the absolute viscosity, as one of the most significant parameters. Hence, the characterization of viscosity should be conducted at a shear rate relevant to the particular process. Figure 17 shows the fluid category depending on time reliance.

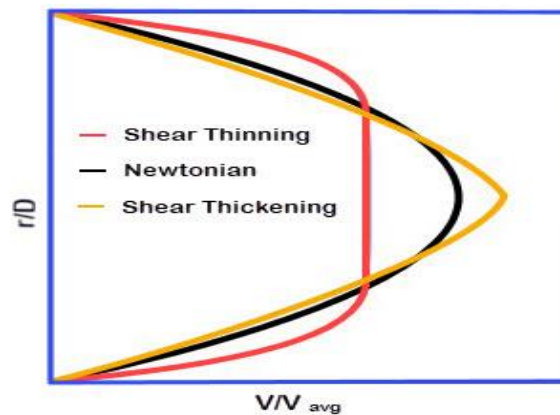


Figure 16 - Velocity Profile for Different Fluids [20]

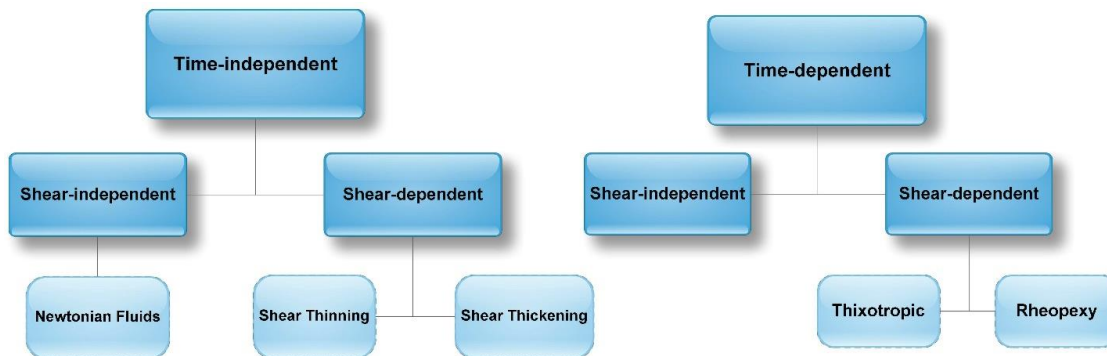


Figure 17 - Fluid Classification based on Time Dependency

2.4.2.2 Rheological Mathematical Models

Herschel-Bulkley Model

The Herschel-Bulkley model is applicable to fluids with yield stress and a non-linear behavior. The model is precise as its equation includes three parameters, that are based on data, adjustable (Pevere & Guibaud, 2006). The Herschel-Bulkley model is expressed in Equation (13), where τ_0 represents the yield stress [23].

$$\tau = \tau_0 + K\gamma^n \quad (13)$$

The consistency index parameter (K) provides information the viscosity of the fluid. Nevertheless, fluids need to have a comparable flow behavior index (n), so that their K -values are compared. If the flow behavior index is near 1, the fluid passes into a shear thickening fluid from a shear thinning. The fluid behaves as a shear thickening fluid if n is above 1: Following Seyssiecq and Ferasse (2003), Equation 13 provides information about fluid behavior:

$\tau_0 = 0$ & $n = 1 \rightarrow$ *Newtonian Behavior*

$\tau_0 > 0$ & $n = 1 \rightarrow$ *Bingham Behavior*

$\tau_0 = 0$ & $n < 1 \rightarrow$ *Shear Thinning (Pseudoplastic) Behavior*

$\tau_0 = 0$ & $n > 1 \rightarrow$ *Shear Thickening (Dilatant) Behavior*

Power-Law Model

The model is applicable to shear thinning fluids without exhibiting a yield stress (Pevere et al., 2006). Equation 14 included n -value which provides information about fluid behavior:

$$\tau = K\gamma^{n-1} \quad (14)$$

$n = 1 \rightarrow$ *Newtonian Behavior*

$n < 1 \rightarrow$ *Shear Thinning (Pseudoplastic) Behavior*

$n > 1 \rightarrow$ *Shear Thickening (Dilatant) Behavior*

Bingham Model

The Bingham model (Equation 15) encompasses the flow curve of a material when there is a yield stress and viscosity is constant at stresses higher than the yield stress. According to Seyssiecq and Ferasse (2003), this is a pseudo-Newtonian fluid behavior. The yield stress (τ_0) is the shear stress (τ) at a shear rate (γ) zero and the viscosity (μ) is the slope of the curve at stresses above the yield stress.

$$\tau = \tau_0 + \mu\gamma \quad (15)$$

$\tau_0 = 0 \rightarrow$ *Newtonian Behavior*

$\tau_0 > 0 \rightarrow$ *Bingham Behavior*

2.4.2.3 Xanthan Gum Solution

Xanthan gum solutions are a kind of highly pseudoplastic shear thinning fluids. It enhances the distribution of remedial amendments when deliver into low permeability zones of subsurface heterogeneous formations [24]. Viscosity decreases with the rise in the shear stress rate, but it promptly recovers when shear rate is reduced. Xanthan solutions are not significantly thixotropic. The high-molecular weight molecule causes pseudoplasticity, as it uses polymer entanglement and hydrogen bonds to form complex molecular aggregates. This network of entangled, stiff molecules is highly ordered. The gum's suspending properties are outstanding because of high viscosity at low shear rates. Disaggregation of the network and subsequent alignment of individual polymer molecules toward shear force causes shear thinning pseudoplasticity. Nevertheless, aggregates are quickly rearranged when the shearing stops, as shown in Figure 18.

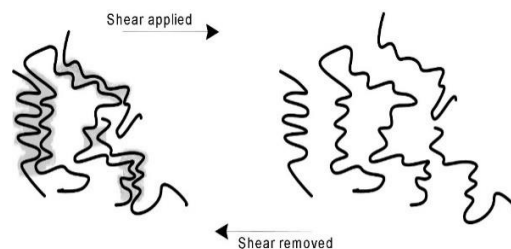


Figure 18 - The Conformation Change in Xanthan Gum Solutions when Shear is Applied and Removed

Figure 19 illustrates the relationship between concentration and viscosity in xanthan gum, which is crucial for its suspension-stabilizing properties.

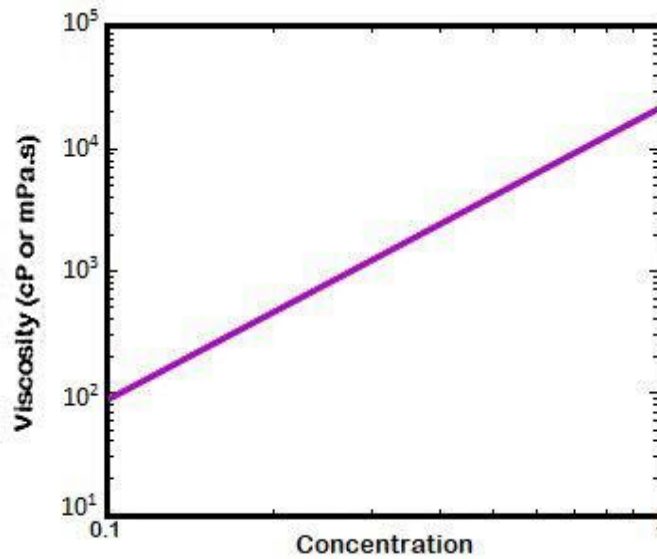


Figure 19 - Xanthan Gum Viscosity vs Concentration in Standardized Tap Water [24]

Xanthan gum solutions have the unique ability to keep viscosity (γ) until they reach a definite "melting temperature" (T_m) at which the viscosity decreases significantly a reversible molecular conformation change, as shown in Figure 20.

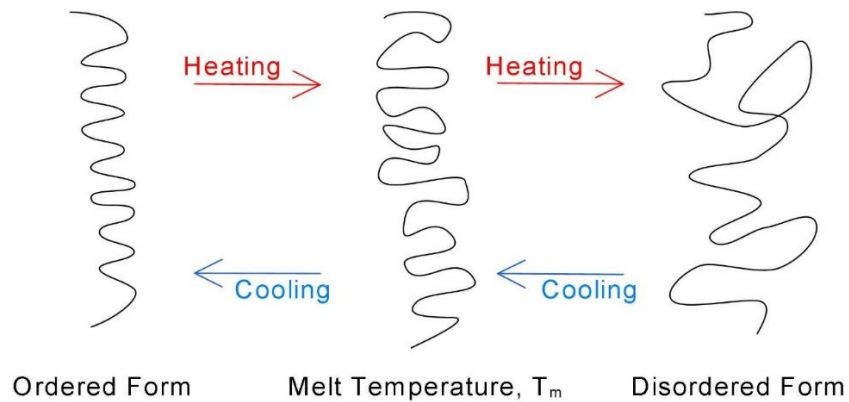


Figure 20 - The Conformation Change in Xanthan Gum Solutions with Heating and Cooling

To achieve optimal results, it is necessary to hydrate xanthan gum before using it. Hydration depends on the following factors:

- Desired concentration
- Size of the particles
- Temperature
- Composition of the hydration medium
- Agitation rate of the hydration medium
- Dispersion of the particles

The gum particles need be well dispersed to hydrate properly. If not, they have a tendency to stick together during the mixing process. As a result, they form swollen lumps, also known as "fisheyes" [25].

2.5 Two-Phase Flow Basic Definitions and Terminology

The total mass flow rate (\dot{m}) (In kg per second) is the sum of the mass flow rate of liquid phase (\dot{m}_l) and the mass flow rate of gas phase (\dot{m}_g) [5].

$$\dot{m} = \dot{m}_l + \dot{m}_g \quad (16)$$

The total volumetric flow rate (Q) (in cubic meter per second) is the sum of the volumetric flow rate of liquid phase (Q_l) and the volumetric flow rate of gas phase (Q_g).

$$Q = Q_l + Q_g \quad (17)$$

The volumetric flow rate of liquid phase (Q_l) relates to the mass flow rate of liquid phase (\dot{m}_l) as the following:

$$Q_l = \frac{\dot{m}_l}{\rho_l} \quad (18)$$

The volumetric flow rate of gas phase (Q_g) relates to the mass flow rate of gas phase (\dot{m}_g) as the following:

$$Q_g = \frac{\dot{m}_g}{\rho_g} \quad (19)$$

The total mass flux of the flow (G) is the total mass flow rate (\dot{m}) divided by the pipe cross-sectional area (A).

$$G = \frac{\dot{m}}{A} \quad (20)$$

It should be underlined that this mass velocity is the actual velocity. The volumetric flow rate is not constant (as the density is not constant) along the flow rate. The definition is the following:

$$Q_l = \frac{G_l}{\rho_l} = v_{sl} \quad (21)$$

In a case of gas:

$$Q_g = \frac{G_g}{\rho_g} = v_{sg} \quad (22)$$

The quality (dryness fraction) (x) is the ratio of the mass flow rate of gas phase (\dot{m}_g) to the total mass flow rate (\dot{m}).

$$x = \frac{\dot{m}_g}{\dot{m}} = \frac{\dot{m}_g}{\dot{m}_l + \dot{m}_g} \quad (23)$$

Comparably, the value of $(1 - x)$ is known as the “wetness fraction.” The final two fractions are constant along the tube length if the liquid and gas masses are constant.

The volumetric quality (β) is the ratio of the volumetric flow rate of the gas phase (Q_g) to the total volumetric flow rate (Q).

$$\beta = \frac{Q_g}{Q} = \frac{Q_g}{Q_l + Q_g} \quad (24)$$

The volumetric quality (β) relates to the mass quality (x) as the following:

$$\beta = \frac{xv_g}{xv_g + (1-x)v_l} = \frac{1}{1 + \left(\frac{1-x}{x}\right) \left(\frac{\rho_g}{\rho_l}\right)} \quad (25)$$

The void fraction (α) is the ratio of the pipe cross-sectional area (or volume) taken by the gas phase to the pipe cross-sectional area (or volume).

$$\alpha = \frac{A_g}{A} = \frac{A_g}{A_l + A_g} \quad (26)$$

This fraction varies along the tube length because the gas density is not constant along the tube length. The liquid fraction or liquid holdup is

$$L_H = 1 - \alpha = \frac{A_l}{A} \quad (27)$$

The superficial velocity of liquid phase flow (v_{sl}) is the velocity when the liquid flows alone in the pipe. Its definition is the volumetric flow rate of liquid phase (Q_l) divided by the pipe cross-sectional area (A).

$$v_{sl} = \frac{Q_l}{A} \quad (28)$$

The superficial velocity of gas phase flow (v_{sg}) is the velocity when the gas flows alone in the pipe. Its definition is the volumetric flow rate of gas phase (Q_g) divided by the pipe cross-sectional area (A).

$$v_{sg} = \frac{Q_g}{A} \quad (29)$$

The definition of the mixture velocity of flow (v_m) is the total volumetric flow rate (Q) divided by the pipe cross-sectional area (A).

$$v_m = \frac{Q}{A} \quad (30)$$

The mixture velocity of flow (v_m) (In meter per second) is expressed as superficial velocity of liquid phase flow (v_{sl}) and the superficial velocity of gas phase flow (v_{sg}) in the following:

$$v_m = v_{sl} + v_{sg} \quad (31)$$

The definition of the average velocity of liquid phase flow (v_{sl}) is the volumetric flow rate of liquid phase (Q_l) divided by the pipe cross-sectional area taken by the liquid phase flow (A_l).

$$v_{sl} = \frac{Q_l}{A_l} = \frac{Q_l}{(1 - \alpha)A} \quad (32)$$

The definition of the average velocity of gas phase flow (v_{sg}) is the volumetric flow rate of gas phase (Q_g) divided by the pipe cross-sectional area taken by the gas phase flow (A_g).

$$v_{sg} = \frac{Q_g}{A_g} = \frac{Q_g}{\alpha A} \quad (33)$$

To characterize a two-phase flow, the slip ratio (S) is often employed in the place of void fraction. Its definition is the ratio of the average velocity of gas phase flow (v_g) to the average velocity of liquid phase flow (v_l). The void fraction (α) relates to the slip ratio (S) as the following:

$$S = \frac{v_g}{v_l} = \frac{Q_g / \alpha A}{Q_l / (1 - \alpha)A} = \frac{Q_g(1 - \alpha)}{Q_l \alpha} \quad (34)$$

$$S = \frac{v_g}{v_l} = \frac{G x / \alpha A \rho_g}{G (1 - x) / (1 - \alpha)A \rho_l} = \frac{\rho_l x(1 - \alpha)}{\rho_g \alpha(1 - x)} \quad (35)$$

For the same velocity of phases ($S = 1$), the mixture density is defined as

$$\rho_m = \alpha\rho_g + (1 - \alpha)\rho_l \quad (36)$$

The average density of the material flowing in the tube is estimated by observing the definition of density. The definition of the density of any material is ($\rho = m/V$) and accordingly, for the flowing material it is:

$$\rho = \frac{\dot{m}}{Q} \quad (37)$$

$$\therefore \rho_{average} = \frac{1}{\frac{x}{\rho_g} + \frac{(1-x)}{\rho_l}} \quad (38)$$

Then, the average specific volume of the flow is

$$V_{average} = \frac{1}{\rho_{average}} = \frac{x}{\rho_g} + \frac{(1-x)}{\rho_l} = x V_g + (1-x)V_l \quad (39)$$

The relationship between x and α is

$$x = \frac{\dot{m}_g}{\dot{m}_l + \dot{m}_g} = \frac{\rho_g V_g \alpha A}{\rho_l V_l (1 - \alpha)A + \rho_g V_g \alpha A} = \frac{\rho_g V_g \alpha}{\rho_l V_l (1 - \alpha) + \rho_g V_g \alpha} \quad (40)$$

If the slip is one ($S = 1$), hence, Equation (40) turns into

$$x = \frac{\rho_g \alpha}{\rho_l (1 - \alpha) + \rho_g \alpha} \quad (41)$$

**The equations 16 to 41 were obtained from [5].*

Homogeneous Models

The complexity of the flow should be mentioned before proceeding to the homogeneous models. The assumption that the flow is continuous is valid for fluid basic equations. However, now, the assumption is valid only for small segments (chunks). Moreover, such segments are not defined. Rather, they result from the conditions imposed on the flow. In addition, various flow regimes exemplify configurations of the continuous flow of different segments. Before, it was considered that it is possible to neglect various flow regimes in regard to pressure loss, which is not right for the heat transfer. To resolve it, the most appropriate is to use approximation [25]. (See Equation 31), the average velocity is

$$v_m = \frac{Q_l + Q_g}{A} = v_{sl} + v_{sg} = v_m \quad (42)$$

The continuity equation is met as

$$\dot{m} = \rho_m v_m A = \rho_m Q \quad (43)$$

Under what conditions Equation (43) is correct?

Under construction.

The approximation of governing momentum equation is the following:

$$\dot{m} \frac{dv_m}{dx} = -A \frac{dP}{dx} S \tau_w - A \rho_m g \sin\theta \quad (44)$$

Whereas modifying Equation (43) is the following

$$-\frac{dP}{dx} = -\frac{S}{A} \tau_w - \frac{\dot{m}}{A} \frac{dv_m}{dx} + \rho_m g \sin\theta \quad (45)$$

The approximation of the energy equation is the following:

$$\frac{dq}{dx} - \frac{dw}{dx} = \dot{m} \frac{d}{dx} \left(h_m + \frac{v_m^2}{2} + g x \sin\theta \right) \quad (46)$$

2.5.1 Pressure Loss Components

Body force (gravitation), acceleration, and friction loss impact the pressure loss in a tube flowing upward in an incline angle (θ). The losses are mutually dependent and non-linear. To illustrate, the gravitation force leads to the reduction of the pressure. Accordingly, the density changes and as a result, acceleration takes part. Nevertheless, it is possible to neglect this dependency for small distances (dx). Accordingly, from Equation (47), the total pressure loss is as the following:

$$\frac{dP}{dx} = \overbrace{\frac{dP}{dx}}^{\text{friction}} \Big|_f + \overbrace{\frac{dP}{dx}}^{\text{acceleration}} \Big|_a + \overbrace{\frac{dP}{dx}}^{\text{gravity}} \Big|_g \quad (47)$$

2.5.1.1 Friction Pressure Loss

Calculating the frictional pressure loss for a conduit is the following:

$$-\frac{dP}{dx} \Big|_f = \frac{S}{A} \tau_w \quad (48)$$

The frictional pressure loss in the pipe is calculated as the following when S is the perimeter of the fluid:

$$-\frac{dP}{dx} \Big|_f = \frac{4 \tau_w}{D} \quad (49)$$

To estimate the wall shear stress:

$$\tau_w = f \frac{\rho_m v_m^2}{2} \quad (50)$$

To measure the friction factor for a single flow, the average velocity relates directly to the wall shear stress. The relationship of the wall shear stress and average velocity of two and more phases has not been established by available experimental data. Nor, the measurement of the friction factor for the “averaged” viscosity of the two-phase flow has

been conducted. Accordingly, the data developed and measured for the single flow were employed.

The friction factor was acquired by using the following correlation

$$f = C \left(\frac{\rho_m v_m D}{\mu_m} \right)^{-n} \quad (51)$$

Where C and n are constants dependant on the flow regimes (laminar or turbulent flow). In a case of laminar flow $C = 16$ and $n = 1$. In a case of turbulent flow $C = 0.079$ and $n = 0.25$.

Regarding homogeneous models, several suggestions for the average viscosity have been proposed. To illustrate, Duckler proposed the following:

$$\mu_m = \frac{\mu_g Q_g}{Q_l + Q_g} + \frac{\mu_l Q_l}{Q_l + Q_g} \quad (52)$$

However, not in all cases Duckler's linear formula gives an adequate approximation. Therefore, Cichilli proposed an equation comparable to the Equation (52) taking average viscosity as

$$\mu_{average} = \frac{1}{\frac{x}{\mu_g} + \frac{(1-x)}{\mu_l}} \quad (53)$$

Besides, the average viscosity is dependant on the mass fraction as in the following:

$$\mu_m = x \mu_g + (1 - x) \mu_l \quad (54)$$

It is possible to estimate the friction loss by using this formula

2.5.1.2 Gravity Pressure Loss

It is possible to estimate the gravitational pressure loss by

$$\left. \frac{dP}{dx} \right|_g = \rho_m g \sin\theta \quad (55)$$

The change of density throughout the flow is shown as a function of density. The density in Equation (55) is the static density, namely without movement.

2.5.1.3 Acceleration Pressure Loss

It is possible to estimate the acceleration pressure loss by:

$$-\left. \frac{dP}{dx} \right|_a = \dot{m} \frac{dv_m}{dx} \quad (56)$$

The positive or negative acceleration pressure loss is caused by change of cross section and of density. It is possible to write the Equation (56) as the following:

$$-\left. \frac{dP}{dx} \right|_a = \dot{m} \frac{dv_m}{dx} \left(\frac{\dot{m}}{A \rho_m} \right) \quad (57)$$

Furthermore, explicitly, Equation (57) becomes

$$-\left. \frac{dP}{dx} \right|_a = \dot{m}^2 \left[\overbrace{\frac{1}{A} \frac{d}{dx} \left(\frac{1}{\rho_m} \right)}^{\text{Pressure loss due to density change}} + \overbrace{\frac{1}{\rho_m A^2} \frac{dA}{dx}}^{\text{Pressure loss due to area change}} \right] \quad (58)$$

There are several four special cases. First, the cross section is constant, $dA/dx = 0$. Second, the mass flow rates of liquid and gas is constant, the derivative of X is zero, $dX/dx = 0$. Third, constant density of one phase only is constant, $d\rho_l/dx = 0$. Lastly, in both phases, densities are constant.

The acceleration pressure losses throughout pipelines and wellbores in most cases are very little. Therefore, are ignored during the pressure loss calculations. As a result, the total pressure loss in pipeline or wellbore can be explained as the sum of the friction and gravitational pressure losses.

2.5.1.4 Total Pressure Loss

Integration is needed to calculate the total pressure between two points, (*a* and *b*) as the following

$$\Delta P_{total} = \overbrace{\Delta P_{ab f}}^{friction} + \overbrace{\Delta P_{ab g}}^{gravity} \quad (59)$$

2.6 Newtonian Pressure Drop Calculations

2.6.1 Pressure Drop in a Single-Phase Flow

Several correlations are employed to precisely calculate the pressure drop in a single-phase flow in a wellbore or pipeline or wellbore, such as:

- Weymouth Correlation
- Panhandle Correlation
- Blasius Correlation
- Darcy-Weisbach Correlation
- Fanning Correlation

Typically, flows in wellbores and pipelines in the field and industry are turbulent. This study used the Fanning correlation for calculating the pressure loss for both single phase and two-phase flows in horizontal orientation.

Darcy-Weisbach Correlation

The Fanning and Darcy friction factors are commonly used. Terms the Moody friction factor and the Darcy–Weisbach friction factor are also used when referring to the Darcy friction factor. To prevent errors in fluid flow calculation results and pressure loss, it is essential to know which friction factor is used in a chart or following Equation (60).

The distinction between the two factors is that the Fanning friction factor is four times smaller than the Darcy friction factor. As apart from it, they are two same, it is possible to apply conversion factor 4 and to use them interchangeably.

$$f = 4f_F \quad (60)$$

To determine the Darcy friction, it is possible to read it from Moody Chart or to apply the adequate friction factor correlation. Also, it is important to underline that the Darcy friction factor is a dimensionless number.

Hence, the pipe diameter and the pipe roughness employed to compute the friction factor have to be dimensionally consistent. More precisely, both diameter and roughness have

to be measured either in inches or in mm. Which method is used to determine the friction factor depends on the flow regime of the fluid, as the Reynolds Number determines it. The Darcy equation is used to describe the Darcy friction factor for laminar flow ($Re < 2100, f = 64/Re$).

$$h_f = f \frac{L}{D} \frac{v^2}{2g} \quad (\text{Head loss}) \quad (61)$$

$$\Delta P = 2f \frac{\rho v^2 L}{D} \quad (62)$$

2.6.2 Pressure Drop in a Multiphase Flow

Single phase pressure loss calculations and multiphase pressure loss calculations are not the same. Hence, correlations must be modified to be applied to multiphase cases. What is more, pressure drop calculations are more complex for multiple phases, as properties of all fluids need to be considered, as well as interactions between phases. As mixture properties need to be used, it is required to determine the gas and liquid in-situ volume fractions through the pipe need to be determined (Welling an Associates, 1999). The frictional and hydrostatic pressure losses are modified to compute the pressure loss in a multiphase flow in correlations. The correlations* are:

- Duns & Ros Correlation
- Hasan & Kabir Correlation
- Ghajar & Bhagwat Correlation
- Dukler et al. Correlation
- Beggs and Brill Correlation
- Lockhart-Martinelli (L-M) Correlation

* *Further information about some of those correlations are in Appendix A.*

Lockhart Martinelli Model

This method is based on the assumption that individual phases flow separately. However, the model of Lockhart and Martinelli assumes that the separated pressure losses are mutually independent. Parameters in this model are the ratio of the pressure loss of two phases and pressure of a single phase.

The Reynolds Number Re for each phase on the basis of the actual flow rate of the individual phase [25].

$$Re_g = \frac{GxD}{\mu_G} \quad (63)$$

$$Re_l = \frac{G(1-x)D}{\mu_l} \quad (64)$$

Darcy friction factor f for each phase

$$f_l = \begin{cases} \frac{16}{Re_l}, & Re_l < 1000 \\ \frac{0.046}{Re_l^{0.2}}, & Re_l > 2000 \\ \omega \frac{16}{Re_l} + (1 - \omega) \frac{0.046}{Re_l^{0.2}}, & 1000 < Re_l < 2000 \end{cases} \quad (65)$$

$$f_g = \begin{cases} \frac{16}{Re_g}, & Re_g < 1000 \\ \frac{0.046}{Re_g^{0.2}}, & Re_g > 2000 \\ \omega \frac{16}{Re_g} + (1 - \omega) \frac{0.046}{Re_g^{0.2}}, & 1000 < Re_g < 2000 \end{cases} \quad (66)$$

Where $\omega = (Re_l - 1000)/(2000 - 1000)$ which results in a linear interpolation for the transitional Reynolds number region

Frictional pressure drop on the basis of the actual flow rate of each phase

$$-\left(\frac{dP}{dz}\right)_l = \frac{2f_l G^2 (1-x)^n v_l}{D} \quad (67)$$

$$-\left(\frac{dP}{dz}\right)_g = \frac{2f_g G^2 x^n v_g}{D} \quad (68)$$

Lockhart-Martinelli parameter

$$X = \sqrt{\left(\frac{dP}{dz}\right)_l / \left(\frac{dP}{dz}\right)_g} \quad (69)$$

L-M Constant C based on the flow Re of each phase (1500 is used as the transitional Re to assure continuity)

$$C = \begin{cases} 20 & Re_l > 1500 \text{ and } Re_g > 1500 \\ 12 & Re_l < 1500 \text{ and } Re_g > 1500 \\ 10 & Re_l > 1500 \text{ and } Re_g < 1500 \\ 5 & Re_l < 1500 \text{ and } Re_g < 1500 \end{cases} \quad (70)$$

Two-phase multipliers for each phase

Gas multiplier

$$\phi_g = 1 + CX + X^2 \quad (71)$$

Liquid multiplier

$$\phi_l = 1 + \frac{C}{X} + \frac{1}{X^2} \quad (72)$$

Discover gradient for a given value of X

$$-\left(\frac{dP}{dz}\right)_{f,2\phi} = \begin{cases} -\left(\frac{dP}{dz}\right)_g \phi_g, & -\left(\frac{dP}{dz}\right)_g \phi_g > -\left(\frac{dP}{dz}\right)_l \phi_l \\ -\left(\frac{dP}{dz}\right)_l \phi_l, & -\left(\frac{dP}{dz}\right)_g \phi_g < -\left(\frac{dP}{dz}\right)_l \phi_l \end{cases} \quad (73)$$

It has been established that the Lockhart-Martinelli correlation is appropriate for two-phase flows at low and moderate pressures. However, it is recommended to use the modified models of Martinelli and Nelson (1948) and Thom (1964) if applied at higher pressures [26].

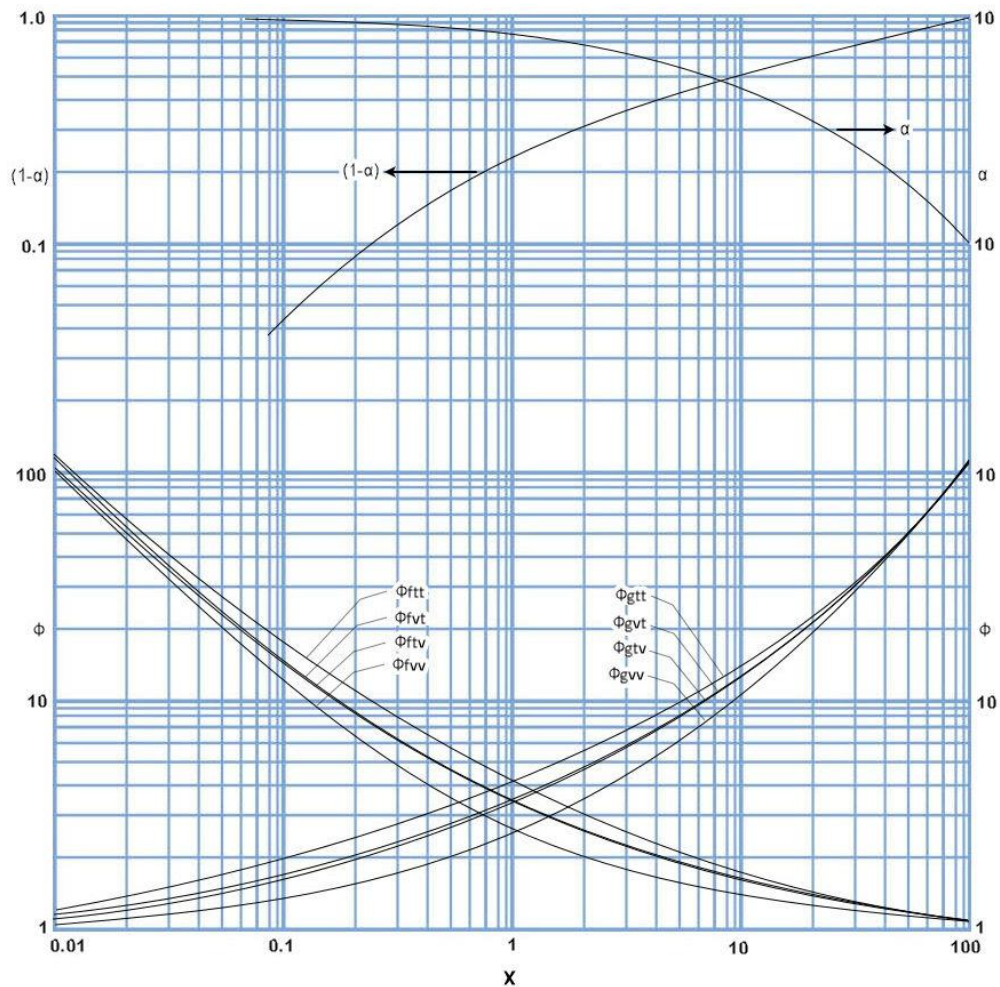


Figure 21 - Correlations for void fraction and frictional pressure drop (Adapted from Lockhart and Martinelli, 1949 [26])

2.7 Non-Newtonian Pressure Drop Calculations

In general, non-Newtonian fluids change viscosities when the fluid is exposed to shear rate and shear stress. Hence, calculating pressure loss in a Newtonian fluid (i.e. Water) is straightforward, because its viscosity is constant under shear strain and shear stress, whereas it is not possible in a case of non-Newtonian fluids. To precisely predict the pressure loss in any non-Newtonian fluid, it is critical to carry out a rheology test of the fluid to detect if it is time-independent or a time-dependent fluid and to find out if it is shear thickening or shear thinning.

2.7.1 Pressure Drop in a Single-Phase Flow

Herschel-Bulkley Model

Herschel-Bulkley fluids is a three-parameter rheological model whose mathematical formula is the following (Maglione, 1996) [27]:

$$\tau = \tau_0 + K\gamma^n \quad (74)$$

The Herschel-Bulkley rheological model is more widely used than the Power-law or Bingham models as it provides more precise models of rheological behavior with available proper experimental data. There are drilling fluids conforming to the Herschel-Bulkley fluid model. In this case, it is necessary to have a minimum stress to start the flow. Afterward, as shear is increasing, the stress is decreasing. Commonly, drilling muds are non-Newtonian fluids, which means that simultaneously with the rise in shear rate, viscosity is decreasing.

The Reynolds number (Re) is generated from the Newtonian Reynolds number to represent the flow consistency (K) and behavior index (n) [28]:

$$Re = \frac{\rho v^{2-n} D^n}{(\tau_0/8)(D/v)^n + K((3m+1)/(4m))^n 8^{n-1}}, \quad m = \frac{nK(8v/D)}{\tau_0 + K(8v/D)^n} \quad (75)$$

If $Re < 2100$, the flow is laminar, accordingly, the Darcy friction factor is calculated as follows:

$$f = \frac{64}{Re} \quad (76)$$

if $Re > 4000$, the flow is turbulent, accordingly, the friction factor is determined iteratively by considering the flow behavior index using the following relationship [29]:

$$\sqrt{f} = 0.8685n^{0.25} \ln \left(\frac{2n}{3n+1} Re \sqrt{f} \right) + \frac{2.4082}{n^{0.75}} (1-n) - \frac{0.2}{n^{1.2}} \quad (77)$$

Now, it is possible to determine the pressure loss using friction factor and the Reynolds number calculated previously.

$$\Delta P = 2f \frac{\rho v^2 L}{D} \quad (78)$$

Power-Law Model

The Power Law describes the flow of pseudoplastic drilling fluids and shear thinning. This model encompasses fluids in which the rheogram, when plotted on a log-log graph, is a straight line without an intercept. Accordingly, a real power law fluid cannot exhibit a yield stress (Chukwu, 2011). A fluid whose viscosity decreases as the shear rate increases and the two-parameter rheological model of a pseudoclastic fluid are used to describe Power-Law fluids. Mathematically, [30]:

$$\tau = K\gamma^{n-1} \quad (79)$$

The Reynolds number (Re) used in a power-law fluid is a modified form of the conventional Reynolds number of Newtonian fluid to account for behavior index (n) and flow consistency (K) expressed as follows:

$$Re = \frac{D^n v^{2-n}}{8^{n-1} K \left(\frac{3n+1}{4n} \right)^n} \quad (80)$$

If $Re < 2100$,

$$f = \frac{64}{Re} \quad (81)$$

If $Re > 4000$,

$$\frac{1}{\sqrt{f}} = \frac{4.0}{n^{0.75}} \log \left(Re f^{(1-\frac{n}{2})} \right) - \frac{0.4}{n^{1.2}} \quad (82)$$

When considering minor losses, the equivalent length L_e as a result of pipe fittings is calculated as follows:

$$L_e = \frac{KD}{4f} \quad (83)$$

Accordingly, the entire length L_T is

$$L_T = L + L_e \quad (84)$$

The pressure loss can be detected using friction factor, the Reynolds number, and total length calculated previously.

$$\Delta P = 2f \frac{\rho v^2 L}{D} \quad (85)$$

2.7.2 Pressure Drop in a Multiphase Flow

According to the theory, xanthan gum is a time dependent shear thinning fluid. It perfectly fits the Herschel-Bulkley Model, known also as a Power Law Model. In addition, at higher shear strain and stress, xanthan gum follows the Herschel-Bulkley Model. Accordingly, the models are employed to detect and compare pressure predictions at various shear strain and shear stress. In the original forms, the Power-law and Herschel-Bulkley solely apply to a one phase non-Newtonian fluid. However, it is possible to modify them by adding a second phase (air) to the non-Newtonian flow. Then, they consider modifying fluid mixture properties. Accordingly, to adequately predict the pressure loss in a two-phase (liquid and air) non-Newtonian flow, the fundamental fluid parameters that require the modification are the following:

- Viscosity of the two-phase mixture
- Density of the two-phase mixture
- Velocity of the two-phase mixture

The Beggs and Brill correlation is a method employed to efficiently modify the fluid parameters by using volume fraction and flow rate. It is expressed by C_g for air and by C_l for liquid.

The entire flow rate of the mixture is expressed by Q_T . It is the sum of the flow rates of liquid Q_l . And air Q_g and expressed as the following:

$$Q_T = Q_l + Q_g \quad (86)$$

$$\therefore v_T = v_l + v_g \quad (87)$$

The flow rate/volume fraction of air and liquid is calculated as follows:

$$C_l = \frac{Q_l}{Q_T}; \quad C_g = \frac{Q_g}{Q_T} \quad (88)$$

The mixture viscosity and density is a measure of the in-situ viscosity. Accordingly, the density of the mixture must be determined and defined as following:

$$\mu_m = C_l \mu_l + C_g \mu_g \quad (89)$$

$$\rho_m = C_l \rho_l + C_g \rho_g \quad (90)$$

In the power-law model and the Herschel-Bulkley the single-phase parameters replace these mixture parameters. Accordingly, it is possible to apply them and predict the pressure loss in a two phase (liquid-air) non-Newtonian flow.

Lockhart Martinelli Model

The Reynolds numbers (Re_g & Re_l) were modified in this model only for the non-Newtonian model [31].

$$Re_g = \frac{D^n x v^{2-n}}{8^{n-1} K \left(\frac{3n+1}{4n} \right)^n} \quad (91)$$

$$Re_l = \frac{D^n (1-x) v^{2-n}}{8^{n-1} K \left(\frac{3n+1}{4n} \right)^n} \quad (92)$$

For the friction factor f for each phase, check Equation (65) and (66).

The following correlations* were employed to detect the two-phase non-Newtonian pressure drop:

- Dziubinski- Chhabra.
- Ruiz-Viera et al.
- Chhabra et al.
- Dziubinski et al.
- Farooqi and Richardson

**Further information about some of those correlations are in Appendix A.*

3 Experimental Setup

3.1 Process Flow Loop

The flow loop refers to a 65-meter pipe closed-loop system. A polyvinylchloride pipe (PVC) is used to pump the liquid from the tank. To visualize the flow, there are installed transparent horizontal pipe sections. Different temperature and pressure sensors are used to measure the liquid and gas flow rates as illustrated in Figure 22 and Figure 23 in more details. This flow loop is employed to produce the two-phase flow. It is done by mixing liquid from the liquid line and air flow from the air line. The air injection pipe comprises of two sizes - DN 25 (1 in) and DN 15 (0.5 in) needed for various air flow volumes. Control valves are employed for compressing air flow and throttling the liquid. In this way, the flow regimes are created, and the flow conditions controlled. Data acquisition system measures process parameters.

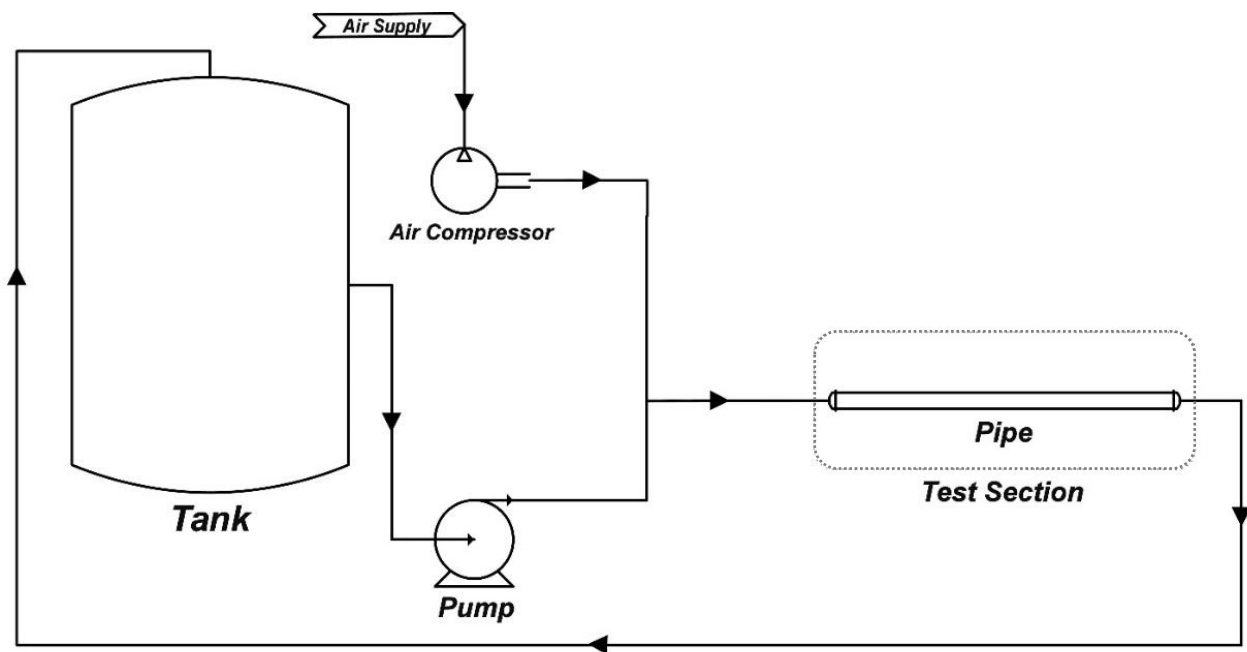


Figure 22 - Simplified Diagram of Process Flow Loop

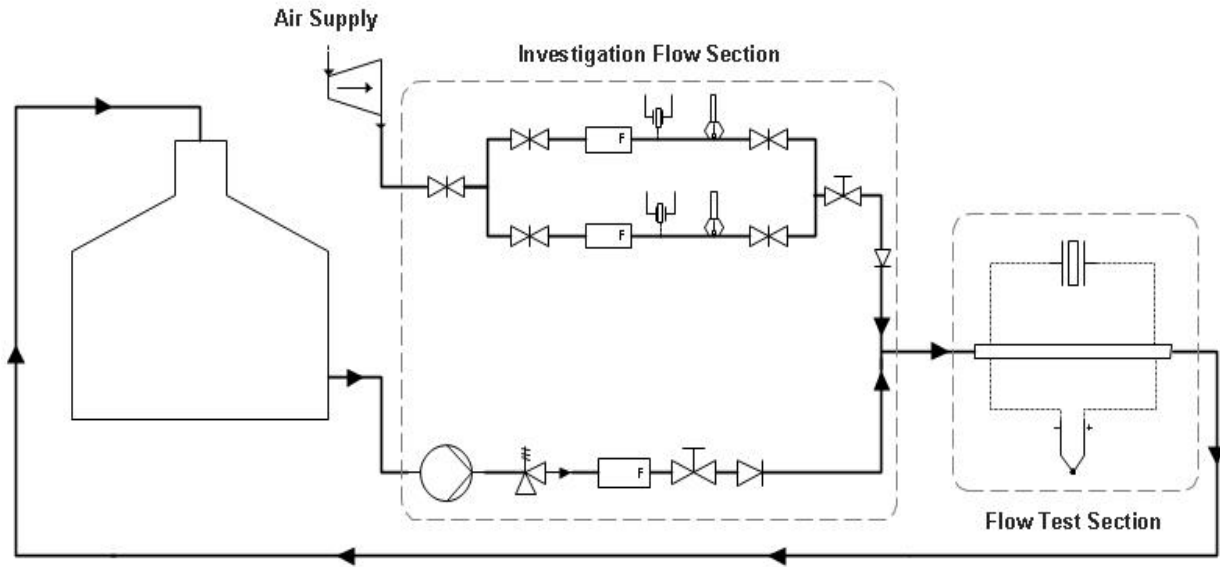
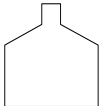


Figure 23 - Schematic of The Flow Loop

Table 1 - P&ID Legend

P&ID Legend		
<u>Valves</u>	<u>Instruments</u>	<u>Equipment</u>
	 F	 Air compressor
	 Pressure sensor	 Centrifugal pump
	 Thermocouple	 Tank
	 dP cell sensor	
	 Manometer	

3.2 Flow Loop Equipment

3.2.1 Storage Tank

The flow loop includes a 1000L PVC tank for the liquid attached to the circulation pump by using a 4-inch pipe as seen in Figure 24.



Figure 24 - Storage Tank of The Flow Loop

3.2.2 Pump

A Goulds pump with a DN 80 outlet and a DN 100 inlet uses the flow loop to generate the needed volume flow rates. To function properly, the 5 HP motor of the pump needs three voltage phases. The electric panels in the fluids laboratory were used to obtain 460 V. The pump is made out of 316 stainless steel, and accordingly, it prevents the corrosion of the pump. As can be seen from Figure 25, 25SH2J5F0 A0400053 is the model number of the pump. A TB Wood's inverter including into the pump is in charge of controlling the power supplied and the fluid flow in the pipe system. The pump can be operated at a slow or fast pace, depending on the frequency. The operator controls the speed of the pump and consequently the liquid flow rate through the converter attached to the computer. The inverter attached to the wall beside the pump is shown in Figure 25. When the frequency is set to 60 Hz, the pump runs at the highest speed and a respective flow rate is around 1000 L/min. The pump is likely to be damaged if it is operated at frequencies higher than 75 Hz. The flow rate of around 200 L/min occurs at the 45 Hz, which is the lowest speed.



Figure 25 - Goulds Pump and TB Wood Inverter

3.2.3 Liquid Flow Meter

Flow meters are monitoring the flow rates of the fluids located in the flow loop. It is necessary to have separate meters in the air and liquid flow, placed in the lines just before the point of joining of the streams. As illustrated by Figure 26, an Omega FTB-730 turbine flow meter is placed into the liquid DN80 pipe. Its accuracy is accuracy of $\pm 1\%$ of the full scale (FS) and its measures flow rates between 3 and 400 GPM (0.68 - 90.85 m³/h). A solid-state Hall-effect sensor electronically detects small magnets found in the flow meter's rotor. Ruby bearings and journal-type sapphire are used by the turbine rotor to maximize lifespan and minimize friction. The body of the meter is made out of PVC. Also, it has 150 Class American National Standards Institute (ANSI) ends that are flanged. They are directly attached to the liquid line [32]. Omega provides the key factor of 9.69 of the flow meter (pulses per gallon).

The display of the flow meter is a transmitter/indicator based a microcontroller. It shows the entire flow input signal and the current flow rate. As illustrated by Figure 26, the total flow is presented in liter and the current flow rate in L/min. The flow meter has a display which is a microcontroller-based indicator/transmitter that displays the current flow rate and additionally provides the total flow output signal.



Figure 26 - Omega FTB-730 Turbine Flow Meter

3.2.4 Gas Flow Meter

To ensure that the entire range of air flow in the air lines of the flow loop is covered, the turbine flow meters were employed. The FLR6750D was installed in the DN 25 pipe to cover flow rates from 5 to 50 SCFM (8.50 to 84.95 m³/h). Besides, the Omega FLR6725D was installed in the DN 15 pipe for flow rates from 2 to 25 SCFM (3.40 to 42.48 m³/h). The primary line that supplies air, illustrated by Figure 27, has two branches. Their diameters are different in order to fit the flow meters. One flowmeter is shown in Figure 28. Each branched part has the valves at the beginning, so that air is managed through the right meter on the basis of the required gas flow. Furthermore, a signal conditioner is attached to each flow meter. In this way, meters are connected to the Data Acquisition System. Besides, each flow meter has a display to show the flow rate. A Hall Sensor is measuring the flow, as it records the pulses per minute. It can be opened by a screw and set to the basic mode.

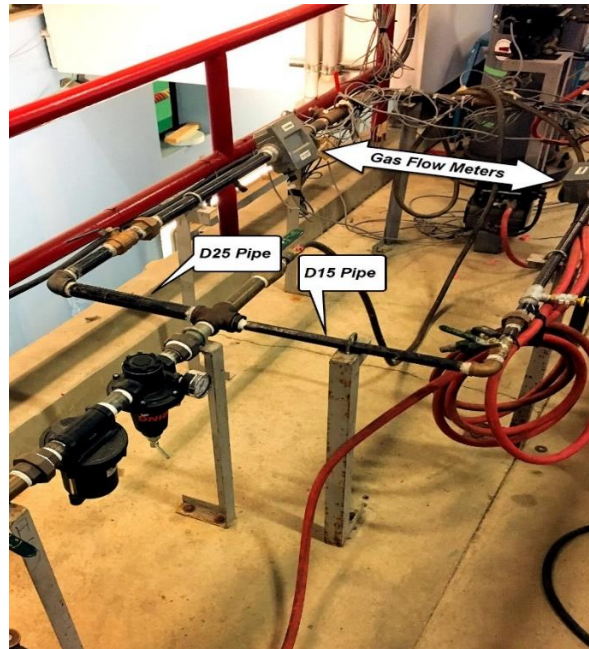


Figure 27 - Branched Air Pipeline and Gas Flow Meters



Figure 28 - Omega FLR6750D Gas Flow Meter [33]

3.2.5 Pressure Sensor

There are four Omega PX603 series cable style pressure transducers in the flow loop, compatible with gas and liquid. In the air lines, two models of PX603-200G5V were used for 0 to 200 psi (0 to 1378.95 kPa). In the liquid line, the model PX603-100G5V was used for 0 to 100 psi (0 - 689.48 kPa). Transducers are attached to the data acquisition system and they create a 1-5 V output signal. Each transducer has a DN 8 (1/4 in) male National Pipe Thread Taper (NPT) fitting. It is required for the installation into the flow loop. The Omega installed pressure transducer from Omega is presented in Figure 29. To estimate the pressure gradients, the pressure should be measured in when the test sections begins and when it ends.

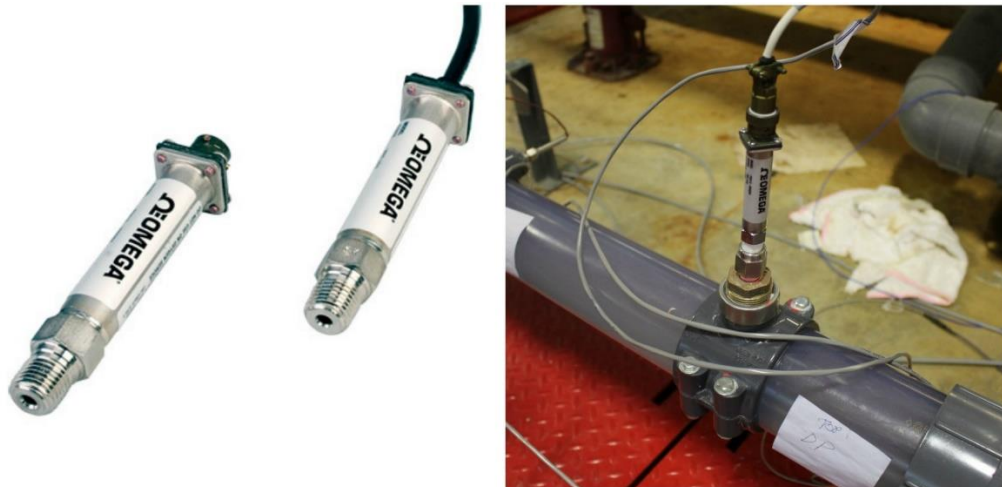


Figure 29 - Omega Pressure Sensor PX603 [34]

3.2.6 Differential Pressure (dP Cell) Sensor

Omega PX409 Wet/Wet 5 psi Differential Pressure Range, 0 To 5 Vdc Output, 2 m (6ft) Cable Termination [35]. It was employed in the experiment to estimate the differential pressure. It has a full scale of 5 psi (34.473kPa) and an accuracy of +/- 0.008. With this accuracy, the error is around 28 Pa. The setup of the differential pressure sensor PX409 is shown in Figure 30 and Figure 31.



Table 2 - Specifications of Omega PX409 Sensor [36]

Model:	PX409-005DWU5V
Application:	Wet/Wet, Uni-directional
Range:	5 psi differential pressure
Input Voltage:	10-30 VDC
Output Voltage:	0-5 VDC
Termination:	2 m (6ft) cable
Accuracy:	0.08%
Tolerance:	+/- 27.58 Pa

Figure 30 - Omega PX409 Sensor [35]



Figure 31 - Omega PX409 Sensor Setup

3.2.7 Manometer

Figure 32 illustrates the Comark C9555 pressure meter. It is both very fast and accurate. Also, it includes twin inputs for gauge pressure measurement. This device was employed to compare its measurements with those of the dP cell sensor measurements. In general, applications include calibration of other instruments, service and maintenance, process pressures, laboratories and clean rooms, air conditioning filters, and boiler flue draft [37].



Figure 32 - Comark C9555 Manometer

Table 3 - Specifications of Comark C9555 Manometer [38]

Model	Comark C9555 Pressure Meter
Maximum Over-Range Pressure	90 PSI / 6200mBar
Accuracy at 23°C	±0. 2% of full scale
Repeatability at +23°C	±0. 1% of full scale
Mean Temperature Coefficient of Reading	Better than 0.1% per °C
Operating Temperature	0 to 40°C
Operating Humidity	10 to 90% RH non-condensing
Environmental Protection	IP67 BS EN 60529 IEC 529
Protection Levels	ATEX certified to Ex II 1 g EEx ia IIC T4 Baseefa 03 ATEX 0079
Connectors	1/8" BSP female
Battery Type	6F22 MN1604, PP3 VT3 UCAR 9V
Battery Life	90 hours

3.2.8 Thermocouples

There are four thermocouples the flow loop. The temperature transducer belongs to the Omega TC-(*) -NPT Series, or more precisely T-type thermocouples of pipe plug probe style. It expands 1/2 in from the end of the 1/4 NPT pipe plug. The thermocouple-grade lead wires are made of stainless steel over braided with stripped leads and insulated with fiberglass. They are 20 American Wire Gauge (AWG). A hex section of 0.56 in (22mm) over flats 0.23 in (5.8 mm) wide serves to constrict mounting threads on the pipe connection clamp. One used temperature sensor is illustrated in Figure 33. In relation to the temperature, they generate a multi-volt signal.

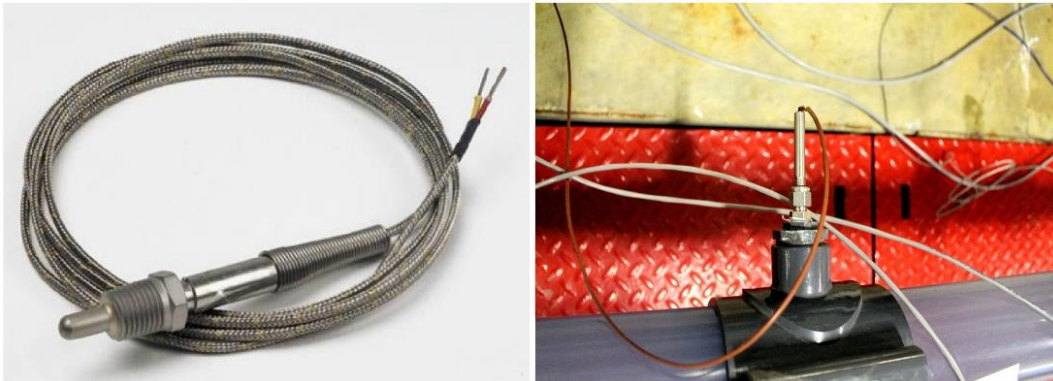


Figure 33 - Omega TC-(*)-NPT Sensor [39]

It is necessary to have an additional wire to attach thermocouples to the DAQ board. It must be created out of different metals, not the same as the Omega. For installing the transducers, it is necessary to use fittings for PVC liquid lines, the steel air lines, and both pipelines. The pressure transducers and thermocouples are installed in air lines by tees with DN 8 bushings. Clamp-it saddles are used to mount the transducers to the PVC pipe. It uses O-ring to seal it around the pipe. Then, a bushing is placed into a socket. Also, there is a hole in the pipe necessary for measuring the pressure within the pipe [39].

3.3 Flow Loop Valves

3.3.1 Pneumatic Ball Valves

There are two electro-pneumatic ball control valves. One is installed into the air lines, and the other in the liquid line as represented in Figure 34. They must be installed promptly before joining the compressed air and liquid lines. A 1-inch valve is used to control the gas flow in the air line, whereas a 3-inch valve is in charge of controlling the liquid flow in the PVC pipe. Both are connected to VRC VE700 electro-pneumatic positioners and Bettis pneumatic actuators.

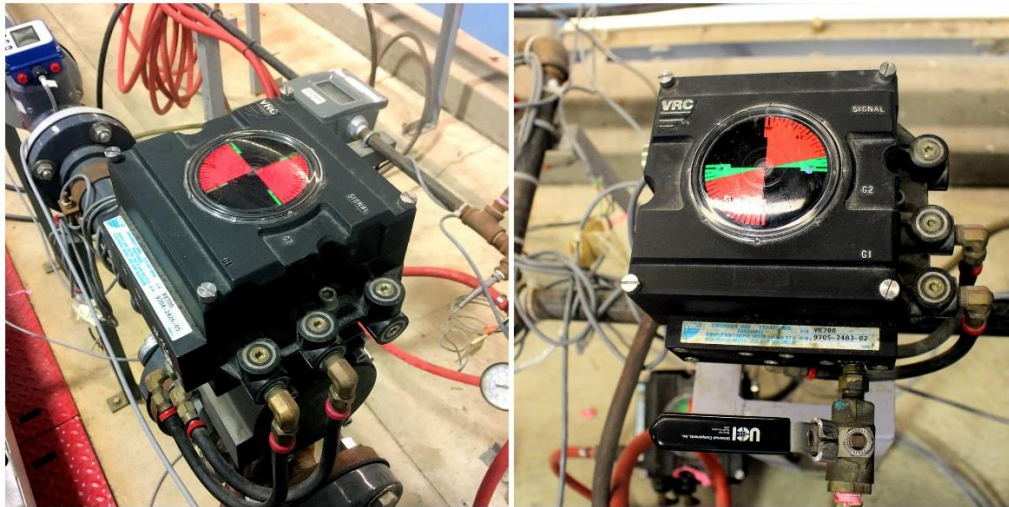


Figure 34 - Installed Control Valves for The Liquid Flow (on The Left) and The Air Flow (on The Right)

3.3.2 Pressure Relief Valve

First, the pump is installed in the flow loop and then a DN 40 Jaybell pressure relief valve. The function of the valve is to make sure that the pump does not surpass the pressure rate of the PVC piping. Aquatrol, Inc in Elburn, IL manufactured the valve (series 69). It is made according to the industry standards for liquid by-pass and relief. It is designed and produced for commercial and industrial heavy-duty use. Its single-piece bonnet serves for removing leakage while simultaneously permitting simple cleaning. It is possible to adjust the pressure on the sealed hex-cap [40]. Figure 35 illustrates the installed pressure relief valve.



Figure 35 - Jaybell Pressure Relief Valve

The pressure of the relief valves is set to 100 psi on the basis of different flow-rates in gallon per minute (GPM) versus set pressure and seat size. The valve opens when the pressure is higher than 100 psi (690 kPa), and then the liquid is let to get into the drain. Hence, the valve is configured at 690 kPa. Accordingly, the working pressure rating of the pipe of 130 psi (900 kPa), is also the maximum pressure in the pipe. The pressure set for other components is 150 psi (1030 kPa).

3.3.3 Pressure Regulator

TOPRING (52.360) produced an air pressure regulator with a gauge, which is installed on the system. Its design is high slow; it includes a T-handle for pressure adjustment and the ability to keep continual downstream pressure. Its maximum pressure is 300 psi, whereas maximum air flow is 400 SCFM at 100 psi. The body and the spring cage are made out of Zinc. The pressure regulator represents a specialized control valve for reducing the upstream supply pressure level to a determined constant downstream pressure. It is done despite changes in flow through the valve and variations in the upstream pressure. It is important to underline that if the pneumatic equipment used at a higher-pressure level than recommended, the energy for generating the pressure is wasted. In addition, it may result in a safety hazard and the early wearing out of the equipment. Also, the pressure should be as recommended to save the air pipes from rust and corrosion resulting from dirt and water found in the air flow pipes. Hence, it is critical to precisely control air pressure so that air-powered equipment can operate efficiently.

3.3.4 Air Filter

An air filter, in addition to the air pressure regulator installed in the system. TOPRING is the manufacturer as well and its model number is 52.160-filter 1 Manual Zinc HIFLO. It has a high flow design, and its function is to remove water through centrifugal force and contaminants down to 40 microns in size. It can also conduct an automatic drain. Zinc was used to make the body, whereas the bowl is made out of zinc with a sight gauge. To compress air, it is necessary to filter contaminants created during the compression cycle. There can be billions of contaminating particles in compressed air. Particles are particularly harmful to the compressed air system at high speed and high concentration. As a result of cooling and compression of air, a certain amount of water vapor is condensed as free water. Consequently, pneumatic components and tools become rusted, lubricants destroyed, while frozen air lines occur in periods of low temperature. The function of the air filter is to remove water, dirt, contaminants, and other particles in the flow. Also, it makes sure that just the required phases go through the flow as needed, as the experiment requires, and that the system operates in a safe, economic, and efficient manner for a long time as shown in Figure 36.



Figure 36 - TOPRING Air Filter 52.160 and TOPRING Pressure Regulator 52.360

3.3.5 Check Valves

Check valves have a critical function in the flow loop system. Two kinds of check valves are installed in the system - air and water check valves as it can be seen in Figure 37. Their purpose is the prevention of backflow within the system. Spears Manufacturing produced the water check valve, which prevents back flow of water and air from entering the pump. The function of the air check valve is to keep air flows in the right direction and not to allow water to get into the compressed air system.

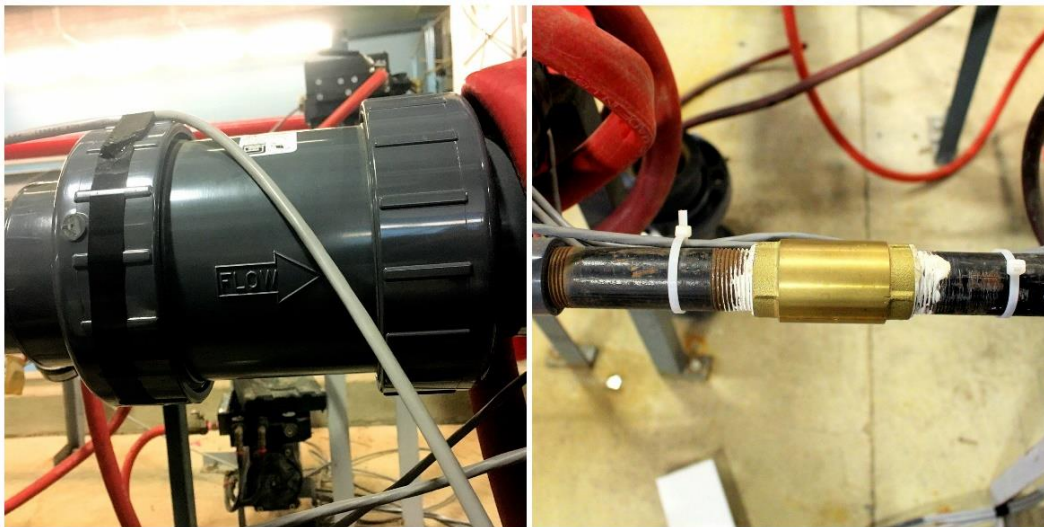


Figure 37 - Liquid Ball Check Valve (on The Left) and Air Check Valve

3.4 Data Acquisition System – NI cDAQ-9178

The NI cDAQ-9178 represents an 8-slot NI CompactDAQ USB chassis. It works with mixed-measurement test systems that are portable and small. The cDAQ-9178 can be combined with maximum of eight NI C Series I/O modules for having customized counter/timer measurement system, digital I/O, analog output, analog input. Modules can conduct different sensor measurements as they are equipped with microphones, flow meters, accelerometers, torque cells, load and pressure transducers, strain gages, RTDs, and thermocouples. NI CompactDAQ systems combine digital signals, current, and voltage with sensor measurements. As a result, they produced customized mixed-measurement systems. They include one simple USB cable that can be connected to a netbook, laptop, or PC. The cDAQ-9178 has built-in four 32-bit general-purpose counter/timers. The counters can be accessed through installed, hardware-timed digital modules NI 9402 and NI 9401 for applications involving a period or frequency measurement, pulse train generation, event counting, PWM, and quadrature encoders [41].

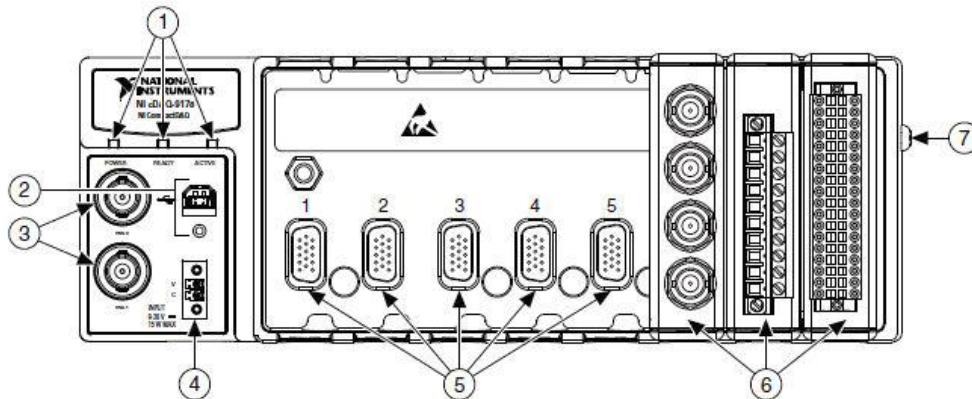


Figure 38 - NI cDAQ-9178 Chassis [41]

-
- 1 POWER, READY, and ACTIVE LEDs
 - 2 USB Connector with Strain Relief
 - 3 TRIG 0 (PFI 0) and TRIG 1 (PFI 1) BNC Connectors
 - 4 Power Connector
 - 5 Module Slots
 - 6 Installed C Series Modules
 - 7 Chassis Grounding Screw
-

The following is included into NI-DAQmx driver software (Table 4):

- LabVIEW SignalExpress LE for simple data-logging applications
- NI Measurement & Automation Explorer (MAX) for system configuration and test
- DAQ Assistant code generation for NI LabVIEW, LabWindowsTM/CVI, and Measurement Studio
- API for LabVIEW, ANSI C/C++, C#, and Visual Basic .NET

Example programs for all supported languages

Table 4 - NI cDAQ-9178 Specifications [41]

General	
Product Name	cDAQ-9178
Form Factor	CompactDAQ, USB
Product Type	Chassis
Part Number	781156-01
Operating System/Target	Windows
LabVIEW RT Support	No
Operating Relative Humidity	10 percent, 90 percent
Chassis	
Number of Slots	8
Total Available Power	15 W
Built-In Trigger	Yes
Counter/Timers	
Counters	4
Resolution	32 bit
Bus Interface	
USB Specification	USB 2.0 Hi-Speed
High-Performance Data Streams	7
Types Available	Analog Output, Analog Input, Digital Output, Counter/Timer Input, Digital Input
Shock and Vibration	
Operational Shock	30 g
Random Operating Frequency Range	5Hz, 500Hz
Random Vibration	0.3 g
Physical Specifications	
Length	25.4 cm
Width	8.81 cm
Height	5.89 cm
Weight	878 g
Minimum Operating Temperature	-20 °C
Maximum Operating Temperature	55 °C
Maximum Altitude	5000 m

NI cDAQ-9178 comes with:

- Power supply by Mean Well, MDR-100-24
- NI 9219 universal analog input, 24-bit, 100 S/s/ch, 4 ch Module
- NI 9218 dynamic universal simultaneous analog input, 51 kS/s, 2 ch.
- Power supply by Mean Well, MDR-100-12



Figure 39 - NI cDAQ-9178 Setup

When using the DAQ system, the user is able to decide and to control which amount of fluid will enter the system and circulate through it. The screen displays the numeric values of the flow rate for all active sensor inputs. As shown in Figure 39, the SignalExpress software monitor displays flow rates, pressure signals, and temperature signals of the system.

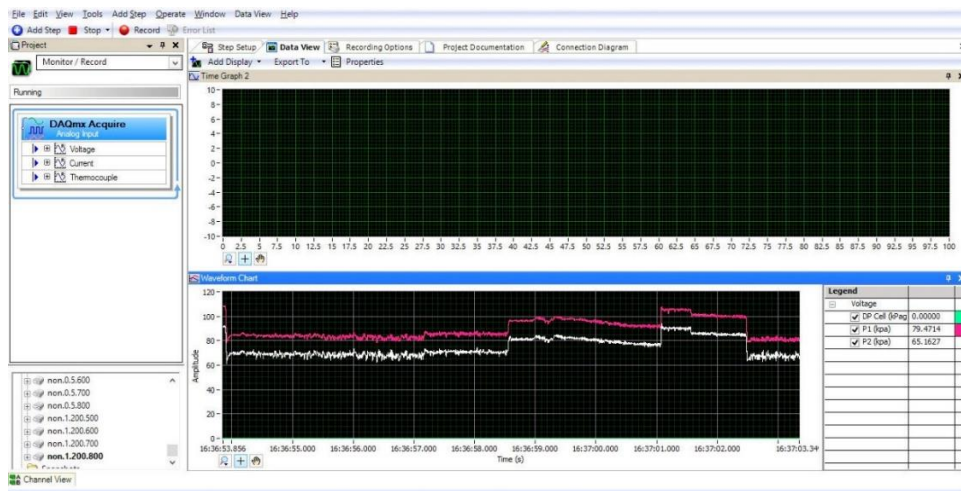


Figure 40 - SignalExpress Interface Signals Monitoring

The DAQ system can be observed from Figure 40. Its function is to collect input signals from the meters and sensors. What is more, it emits the signals to the control valves in the air line and liquid (Figure 41).

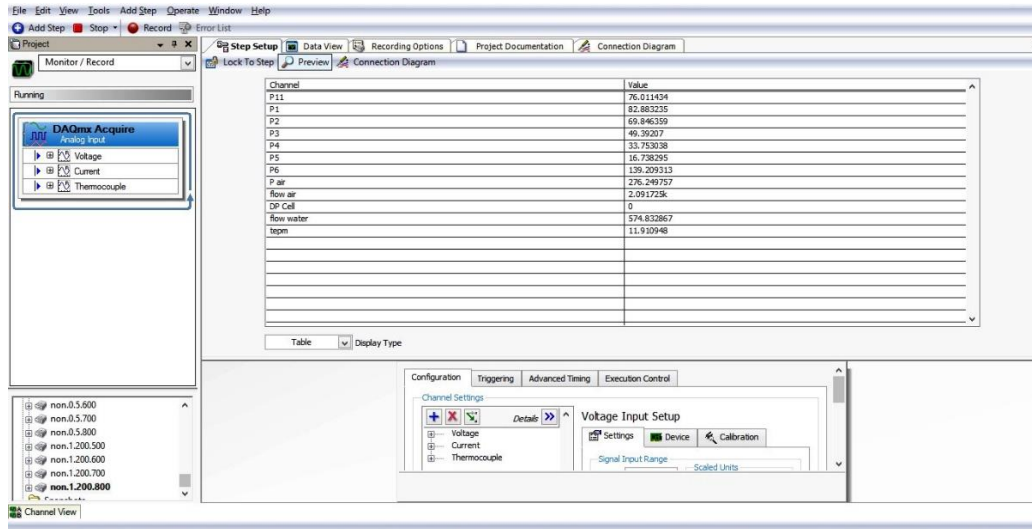


Figure 41 - SignalExpress Signal outputs Interface

3.5 Mega Speed MS55K - High Speed Camera

The Mega Speed MS55K Digital Camera System is a high speed digital camera. Its performance is high when used in different scientific and industrial imaging applications, packaging, and machine visions. Its main advantages are high quality of images, robust design, easy connectivity, and small form factor. A software package includes systems if control of different functions, such as set-up commands, loading and saving files, single frame advance, reverse, forward, playback rate, trigger type, shutter speed, and frame rate. It is also possible download, save and re-arm sequences and to automatically flow the capture as defined by user. Thanks to the fact that the Mega Speed Digital Camera System is compact, it can be smoothly placed and integrated into various kinds of imaging environments. It includes the universal "C" mount, which is located to the front of the camera body. Accordingly, it is simple to connect it to all "C" mount lenses. As a result, end users are able to use their lenses.

The Standard Mega Speed Digital Camera System is user-friendly and flexible as can be seen in Figure 42. Through a Personal Computer Interface slot (PCI), it can be connected to all 500MHz computers. Its turn key packages include lightening, power supply, software, camera cables, and a pre-set computer [42]. Table 5 provides the specifications of Mega Speed MS55K camera.



Figure 42 - Mega Speed MS55K - High Speed Camera

Table 5 - Mega Speed MS55K Specifications [42]

Mega Speed MS55K	
Maximum image size is 1280 x 1024 with recording speeds of 2000 fps at full resolution.	Available with 4 GB up to 32 GB on board memory storage.
“C” mount or “F” mount optical interface.	The high-speed image files are recorded in a circular buffer ready to be downloaded after the high-speed capture ends.
Outputs live pre-view images back to the control PC while recording to the cameras internal high-speed RAM.	Gig E ready.
Maximum CAT 6 cable length is 300 ft. from the camera to the control PC.	Available with fibre optic interface for PC connections out to 60 KM.
Can be used in most “stand-alone armed” applications without a control PC connection.	Typical uses are high speed applications from 25 fps to 3000 fps.
Maximum camera speed is 100,000 fps at reduced resolutions.	The minimum image size is 32 x 8.

Pictures were taken, and videos of the flow regimes were recorded by using the reflector light and the Mega Speed MS55K Digital Camera System. The purpose was to obtain improved visualization through the flow loop.



Figure 43 - Mega Speed MS55K Visualization

The High-Speed Imaging Software is a user-friendly image capture program, yet with a high capacity. It is used for rapid identification, diagnosis, and solving of problems through taking videos. The transformation of images to the PC occurs in a real time. Alternatively, images can be kept on board camera RAM as shown in Figure 43 and Figure 44.

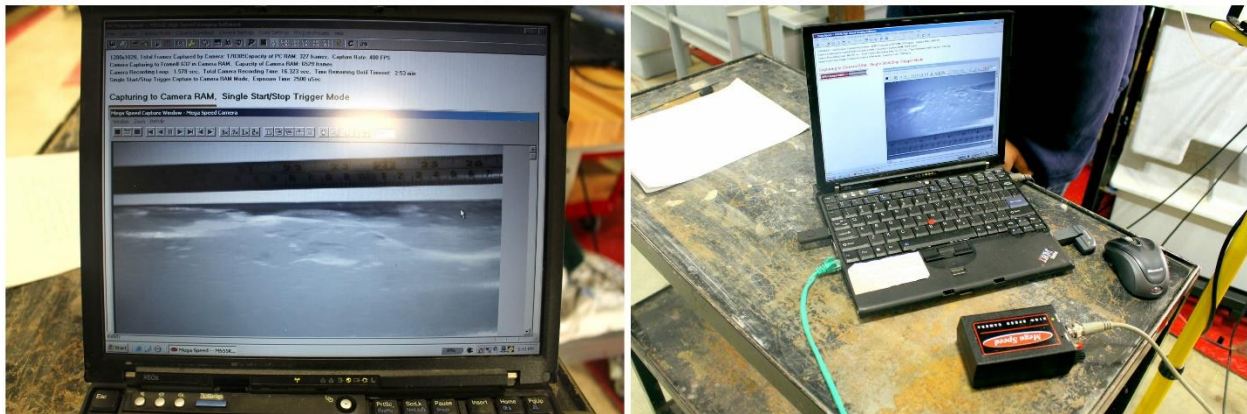


Figure 44 - Mega Speed MS55K High-Speed Imaging Software

3.6 Rheology Measurement Equipment

The following equipment and apparatus were required to carry out the rheology measurement experiment were:

An Electronic Weighing Scale: the mass of xanthan gum that should be added per each liter of water was measured by this scale (Figure 45).

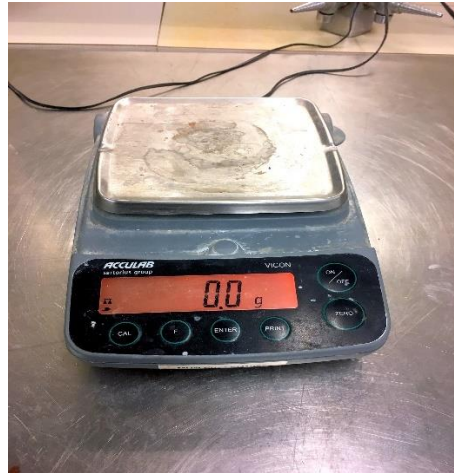


Figure 45 - Acculab Vicon Scale

Graduated Beakers: It measured the volume of water that should be added to the xanthan to make precise concentrations as seen in Figure 46.

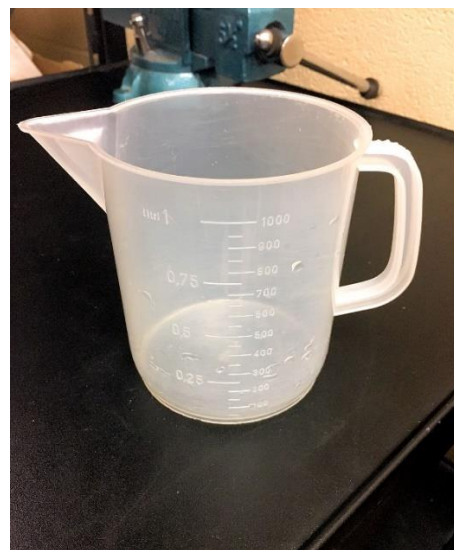


Figure 46 - Graduated Beaker

Marsh Funnel: Viscosity is quickly tested by it (Figure 47).



Figure 47 - Marsh Funnel Viscometer

Density Mud Balance: the mud balance is shown in Figure 48. The specific gravity of the xanthan gum solution was estimated by using it.

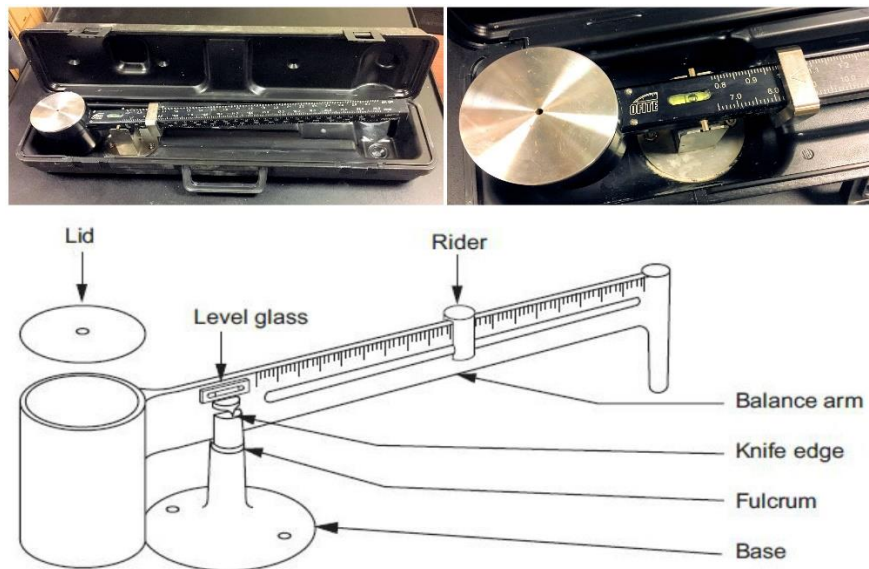


Figure 48 - Density Mud Balance

High-Speed Mixer: The xanthan gum solution was mixed uniformly and evenly using the high-speed mixer which is can be seen in Figure 49.



Figure 49 - High-Speed Multi Mixer

Rotary Viscometer: Figure 50 bellow shows this decide. The viscosity of the xanthan gum solution at different speeds is determined by the rotary viscometer.



Figure 50 - Rotational Viscometer

4 Experimental Procedure

4.1 Rheology Determination of Non-Newtonian Test Fluid

The experiment, with respecting all required safety procedures, was conducted in the geo-mechanic laboratory of the Memorial University in two days in the following way:

1. The electronic weighing scale was used to measure the following masses of xanthan gum: 2.5g, 2g, 1.5g, 1g, and 0.5g.
2. Each mass was then put in a separate beaker (1L), which was then filled with water. The water and xanthan gum mixed and then the process of settling lasted one day.
3. When the water and xanthan gum settled, they were mixed again, and then the density mud balance was used to measure the density of each xanthan gum concentration.
4. The preliminary test of estimation of viscosity trends in all xanthan gum concentrations was done by the marsh funnel. Each liter of xanthan gum solution was drained through the marsh funnel. The time required to drain was recorded. Accordingly, it is possible to relatively estimate the viscosity by:

$$\mu = \rho(t - 25) \quad (93)$$

Where:

μ = Viscosity (cp)

ρ = Density of Xanthan gum (g/cm³)

t = Time to drain 1 US Quart (~1L)

5. Lastly, the rotary viscometer is used to estimate the viscosity of each xanthan gum solution. Various rotary speeds provide various dials. All were recorded.

The OFITE 8-Speed Model 800 Viscometer (Figure 51) of the rotary viscometer was used. It includes a bob and a rotor for stirring the xanthan gum solution in order to produce a shearing effect. Also, to create a dial read, it is necessary to attach the bob to spring, as presented in Figure 51. As the theory suggests, there is a tendency of non-Newtonian

fluids to vary in viscosity once the fluid is under the exposure of a shear strain or a shear rate resulting in a shear stress. Eight shear rates are produced by using the eight following speeds of the rotary viscometer: 600 rpm, 300 rpm, 200 rpm, 100, rpm, 60 rpm, 30 rpm, 6 rpm, and 3 rpm (gel). While carrying out the test, the highest rpm was used to take the reading. The reason is that with the highest rpm the viscosity does not skew because of the strength of the gel when on a low rpm. When this kind of viscometer is used, the rotor rotating at a constant rate causes the shear rate. The constant rate is given in rpm - revolutions per minute. The following relationship is used to determine the shear rate:

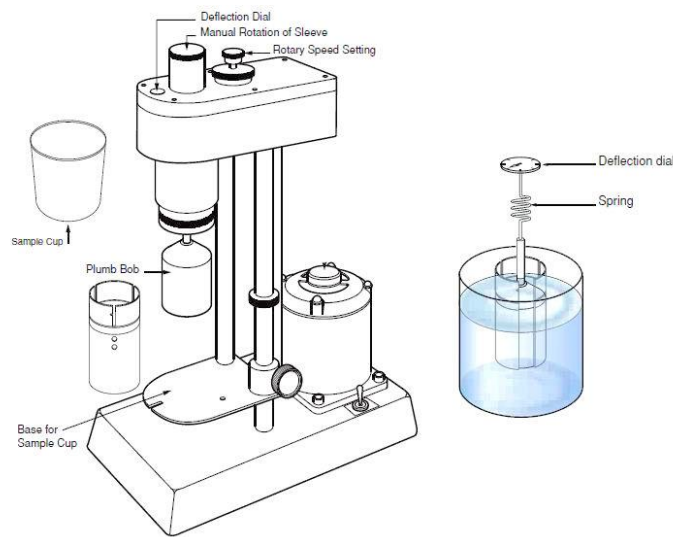


Figure 51 - OFITE 8-Speed Model 800 Viscometer [43]

$$\gamma = rpm * 1.7034 \quad (94)$$

Where:

τ = Shear stress (lb/100 ft²)

To convert, lb/100ft² to Pascals (Pa), τ should be multiplied by 0.478803.

First, the dial reads for all speeds were recorded. Then, the conversion mentioned above was used to convert it to shear rate and shear stress. Shear stress was plotted against the shear rate. In general, the viscosity of the xanthan gum solution at various shear rates and rpm is acquired through the slope of shear stress-shear rate curve.

Deriving from the shear stress-shear rate graph, the rheology of the xanthan gum solution is related to Herschel-Bulkley model and in particular to Shear Thinning (Pseudo-plastic). The following equation is used to calculate the Plastic Viscosity μ_p :

$$\mu_p (cP) = Dial\ Read\ at\ 600\ rpm - Dial\ Read\ at\ 30\ rpm \quad (95)$$

From the graph, the viscosity of the fluid is noted from the slope of the curve. The linear part of the curve serves to estimate the plastic viscosity of the fluid. In addition, the plot shows that the following equation is used to read off the presence of Yield Strength from the intercept of the curve:

$$Y_B (Pa) = (Dial\ Read\ at\ 300 - \mu_p) * 0.478803 \quad (96)$$

The true yield strength is given as:

$$Y_T = \frac{3}{4} * Y_B \quad (97)$$

To detect the range of xanthan gum concentrations which result in the exhibition of a non-Newtonian rheology, while at the same time being adequate for application in the process flow loop because of the constraints of the current pump in the system, the viscosity test was carried out. Any two values of shear stress and shear rate can serve to calculate K (consistency index) and n (flow behavior index). It is common to acquire 3 rpm, 300 rpm, and 600 rpm from all tests. They are used to detect K and n [43].

$$n = 0.5 \log \frac{\theta_{300}}{\theta_3} \quad (98)$$

$$K = \frac{5.11 * \theta_{300}}{511^n} \quad (99)$$

Where,

θ_{300} = reading at 300 rpm

θ_3 = reading at 3 rpm

4.2 Flow Test Experimental Procedure

Different pressure drop estimations, namely single-phase Newtonian flow of water and air, two-phase Newtonian flow of water and air, single phase non-Newtonian flow with xanthan gum solution of 1g/L and 2g/L, and two-phase non-Newtonian flow xanthan solution of 1g/L and 2g/L with air were carried out by using the flow loop. Various frequencies and operating pressures were applied.

4.2.1 Newtonian Procedure

1. Different frequencies (60Hz, 50Hz, and 40Hz) were used for running the flow loop in both single-phase and two-phase flow measurements.
2. Then, before collecting pressure loss readings, the completely operational data acquisition system was established.
3. After turning on the pump, and opening the water valve, the flow loop started to run at the selected flow rate until the steady state of the system was reached.
4. In the case of the single-phase flow measurements, flow rates of the opened air flow valve were at 2000, 1800, 1400, 1000, 600, and 200 L/min and flow rates of the opened water flow valve were at 1200, 1000, 800, 600, 400, and 200 L/min
5. In the case of two-phase flow measurements, flow rates of the opened water flow valve were at 1200, 1000, 800, 600, 400, and 200 L/min and they mixed with air, while the air flow rate was constant. It was repeated for three times for the air flow rates at 2000, 1000, and 200 L/min.
6. At each flow, once the steady state flow reached, pressure loss readings can be collected.
7. The observation and recording of flow regimes were carried out by the high-speed camera for all rates of air-water flow.
8. After turning off the pump, the flow stabilized, and then a baseline pressure reading was collected.
9. After turning on the pump, and opening the water valve, the flow loop started to run at the selected flow rate until the steady state of the system was reached.
10. The next step was opening the air flow valve. In this way, the air was mixed with water. The rates of air flow were 2000, 1800, 1400, 1000, 600, and 200 L/min.

The air mixed with water at all mentioned flow rates. However, the rate of the water flow did not change. This procedure was done for all rates of water flow (1000, 600, and 200 L/min).

11. At each flow, once the steady state flow reached, pressure loss readings can be collected.
12. The observation and recording of flow regimes were carried out by the high-speed camera for all rates of air-water flow.
13. After turning off the pump, the flow stabilized, and then a baseline pressure reading was collected.
14. The evaluation of the pressure drop was carried out by the Manometer and the DP cell sensor. In total, 864 pressure drop readings were obtained.

4.2.2 Non-Newtonian Procedure

1. The first four steps of the Newtonian procedure were carried out in the Non-Newtonian test.
2. To match the volume of the whole system and the concentration calculation, the measurement of the height of the water in the tank was done.
3. Before turning on the pump, the collection of initial pressure drop readings was carried out. The pressure readings are called in this case baseline pressure reading. They were used to detect the real pressure drop.
4. Using a step ladder, 1Kg of xanthan gum was placed into the tank. As a result, around 1Kg/1000L (1g/L) xanthan gum solution was made.
5. After turning on the pump and opening the water valve (xanthan gum solution), the flow loop started to run at the selected flow rate until the steady state of the system was reached. Then, the collection of pressure loss readings took part. They were then exported and saved an excel file.
6. To measure the Non-Newtonian single-phase pressure drop, the fifth step was carried out for 1Kg/1000L xanthan gum solution flow as follows: at 1000, 800, 600, 400, and 200 L/min.

7. The next step was opening the air flow valve. In this way, the air was mixed with xanthan gum solution. The rates of air flow were 2000, 1800, 1400, 1000, 600, and 200 L/min. The air mixed with the solution at all mentioned rates of rate flow. However, the rate of the solution flow did not change. This procedure was done for all rates of xanthan gum solution flow (1000, 600, and 200 L/min).
8. At each flow, once the steady state flow reached, pressure loss readings can be collected.
9. The observation and recording of flow regimes were carried out by the high-speed camera for all rates of air-xanthan gum solution flow.
10. After turning on the pump and opening the water valve (xanthan gum solution), the flow loop started to run at the selected flow rate until the steady state of the system was reached.
11. The next step was opening the air flow valve. In this way, the air was mixed with xanthan gum solution. The rates of air flow were 2000, 1800, 1400, 1000, 600, and 200 L/min. The air mixed with the solution at all mentioned rates of rate flow. However, the rate of the solution flow did not change. This procedure was done for all rates of xanthan gum solution flow (1000, 600, and 200 L/min).
12. Each flow reached steady state before prior to collection of pressure loss readings.
13. The observation and recording of flow regimes were carried out by the high-speed camera for all rates of air-xanthan gum solution flow.
14. Using the step ladder again, additional 1Kg of xanthan gum to the tank to create around 2Kg/L (2g/L) of xanthan gum solution.
15. All steps from the fifth to fourteenth were conducted again, this time with the 2Kg/L xanthan gum solution.
16. The tank was sprayed and washed with the hose, and the xanthan gum solution was flushed out of the flow loop pipes with air.
17. The evaluation of the pressure drop was carried out by the Manometer and the DP cell sensor. In total, 864 pressure drop readings were obtained.

Precautions

- To avoid cavitation of the pump, in particular in a case when the xanthan gum solution is pumped, the pump was operated until 60Hz.
- Before data collection, all introduced concentrations of xanthan gum flowed between half an hour and one hour.
- Adequate personal protective equipment was always worn during the experiment.
- No tools were employed without the approval of the technician.
- To ensure that solution does not spill pipe leak checks were routinely conducted.
- Following each experiment session, the adequate housekeeping was done.

5 Flow Test Results and Analysis

5.1 Lab Test Fluid Rheology

The test fluid sample was taken after completing each flow testing state in the process flow loop. Subsequently, the analysis was performed to identify the viscous properties. The table below summarizes the results of the measurements:

Table 6 - Experiment Sample Concentration = 1 g/L

RPM	Dial	Shear Rate, $\dot{\gamma}$ (1/sec)	Shear Stress, τ (Pa)	Plastic Viscosity, μ_p (cP)	Yield Point, Y_B (Pa)	True Yield Point, Y_T (Pa)	Parameters
3	1	5.1102	0.51088	3	2.394015	1.795511	K = 0.07053 (Pa. s ⁿ) n = 0.91362 $\rho = 996.956$ (kg/m ³) ($\rho_w = 988.568$ (kg/m ³))
6	2	10.2204	1.02177	3	2.394015	1.795511	
30	2.5	51.102	1.27721	3	2.394015	1.795511	
60	3.5	102.204	1.78809	3	2.394015	1.795511	
100	4	170.34	2.04353	3	2.394015	1.795511	
200	6.5	340.68	3.32074	3	2.394015	1.795511	
300	8	511.02	4.08706	3	2.394015	1.795511	
600	11	1022.04	5.61971	3	2.394015	1.795511	

Table 7 - Experiment Sample Concentration = 2 g/L

RPM	Dial	Shear Rate, $\dot{\gamma}$ (1/sec)	Shear Stress, τ (Pa)	Plastic Viscosity, μ_p (cP)	Yield Point, Y_B (Pa)	True Yield Point, Y_T (Pa)	Parameters
3	4	5.1102	2.04353	6.5	4.9316709	3.698754	K = 0.08552 (Pa. s ⁿ) n = 0.71837 $\rho = 1001.749$ (kg/m ³) ($\rho_w = 988.568$ (kg/m ³))
6	4.5	10.2204	2.29897	6.5	4.9316709	3.698754	
30	7	51.102	3.57618	6.5	4.9316709	3.698754	
60	8.5	102.204	4.3425	6.5	4.9316709	3.698754	
100	10	170.34	5.10883	6.5	4.9316709	3.698754	
200	13	340.68	6.64148	6.5	4.9316709	3.698754	
300	16	511.02	8.17412	6.5	4.9316709	3.698754	
600	22.5	1022.04	11.49486	6.5	4.9316709	3.698754	

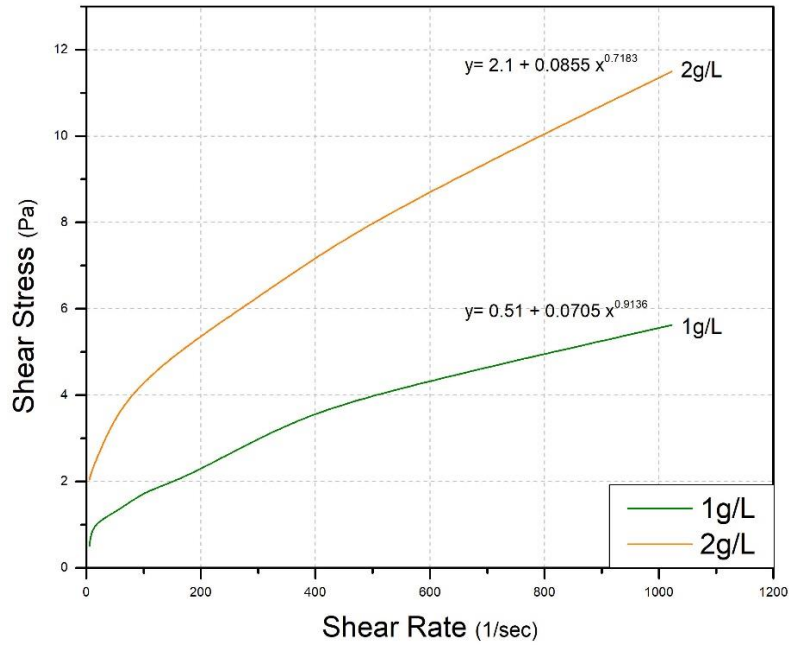


Figure 52 - Rheogram for Experiment Sample Concentrations

Figure 52 presented above illustrates the shear stress versus shear rate relationships of the test fluids. It indicates the shear stress increases at a higher rate when there is a higher concentration of Xanthan gum in the solution.

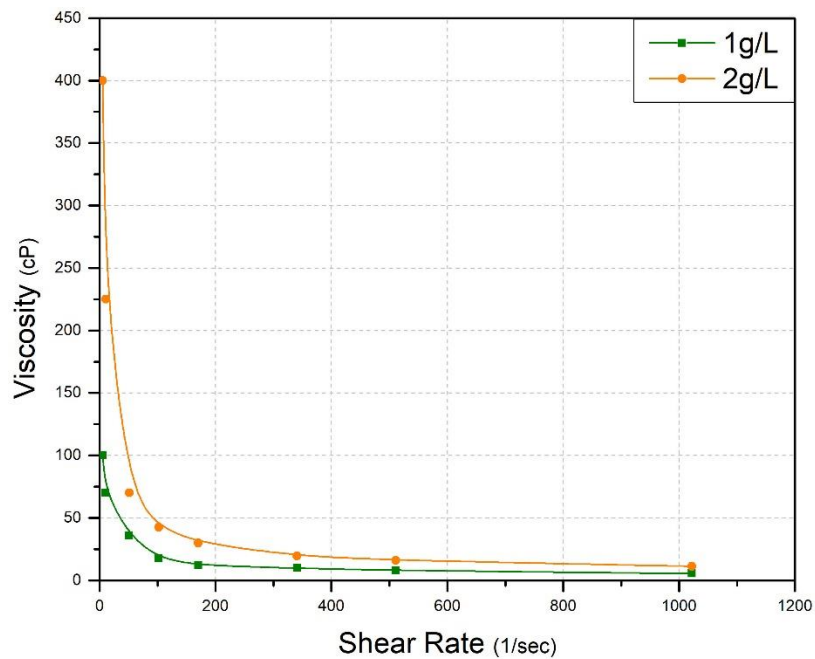


Figure 53 - Effect of Shear Rate on Viscosity of Xanthan Gum Concentrations

The impact of shear rate on the viscosity of xanthan gum solution concentrations (2g/L and 1g/L) is presented in Figure 53. With the rise in the shear rate, the viscosity significantly decreases. With the following values, 0.07053 and 0.08552 (Pa. sⁿ), which correspond to 1g/L and 2g/L respectively, the consistency index (*K*) increases with the concentration of solutions. With the values 0.91362 and 0.71837, which correspond to 1g/L and 2g/L respectively, the flow index (*n*) drops.

5.2 Pressure Drop Measurements

Three operating pressures, namely 15 psi (40Hz), 20 psi (50Hz), and 25 psi (60Hz), were used to perform experiments. Operating the setup at 20 psi (50Hz) is the optimum condition of the flow loop because the best results of flow regime tests and the pressure drop were obtained in this case.

5.2.1 Single-Phase Flow

5.2.1.1 Newtonian Pressure Drop

- **Water Flow**

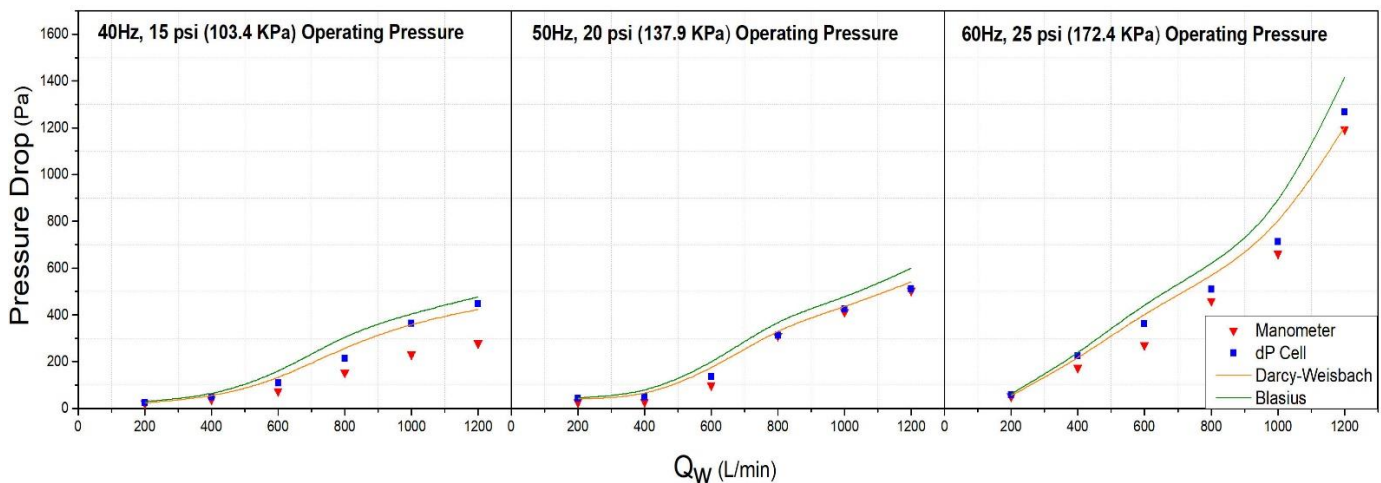


Figure 54 - Single-Phase Water Flow - Experimental and Correlations Pressure Drop Results

- **Air Flow**

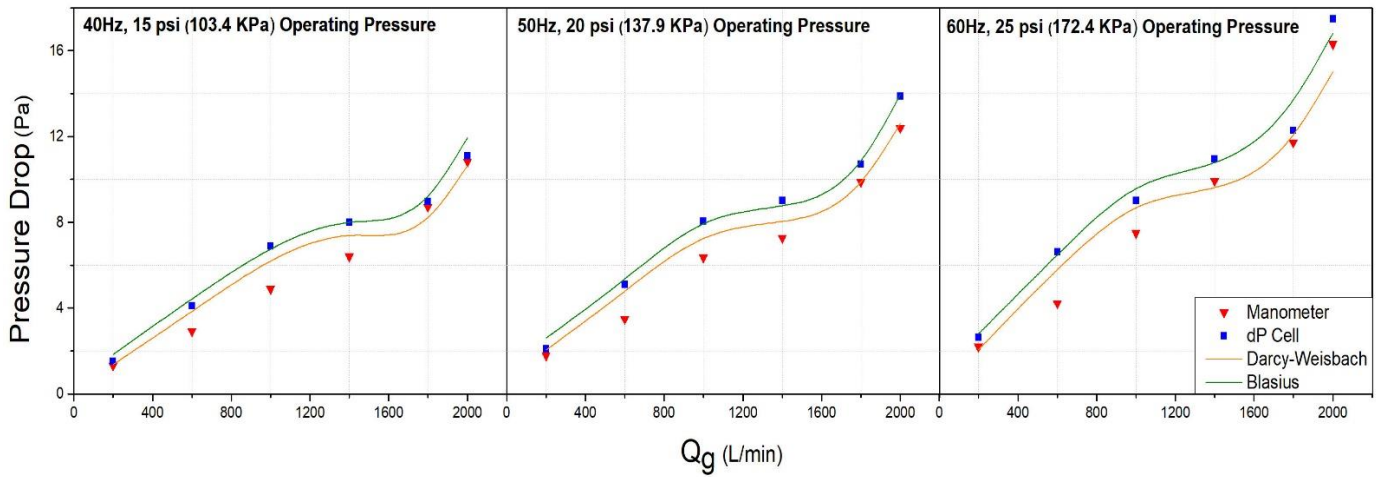


Figure 55 - Single-Phase Air Flow - Experimental and Correlations Pressure Drop Results

The review of Figures 54 and 55 reveals that the rise in the operating pressure and the flow rates for single-phase flow results in the pressure drop increase. Moreover, a significant agreement with the experimental results was demonstrated by the empirical models. A closer match was exhibited by Darcy-Weisbach correlation, in particular regarding the manometer results and the dP (Differential Pressure) cell sensor. When the flow rates are identical, the air flow results in significantly fewer pressure drops than in a case of the water flow in horizontal single-phase flow.

5.2.1.2 Non-Newtonian Pressure Drop

- **1g/L Xanthan Gum Solution**

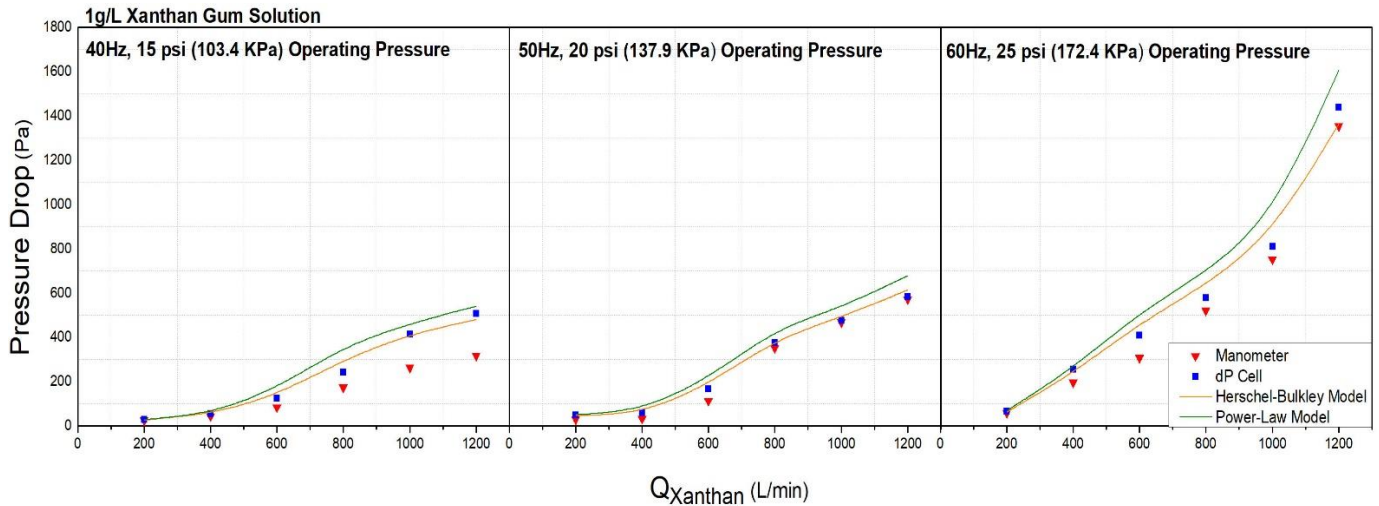


Figure 56 - 1g/L Xanthan Gum Solution - Experimental and Correlations Pressure Drop Results

- **2g/L Xanthan Gum Solution**

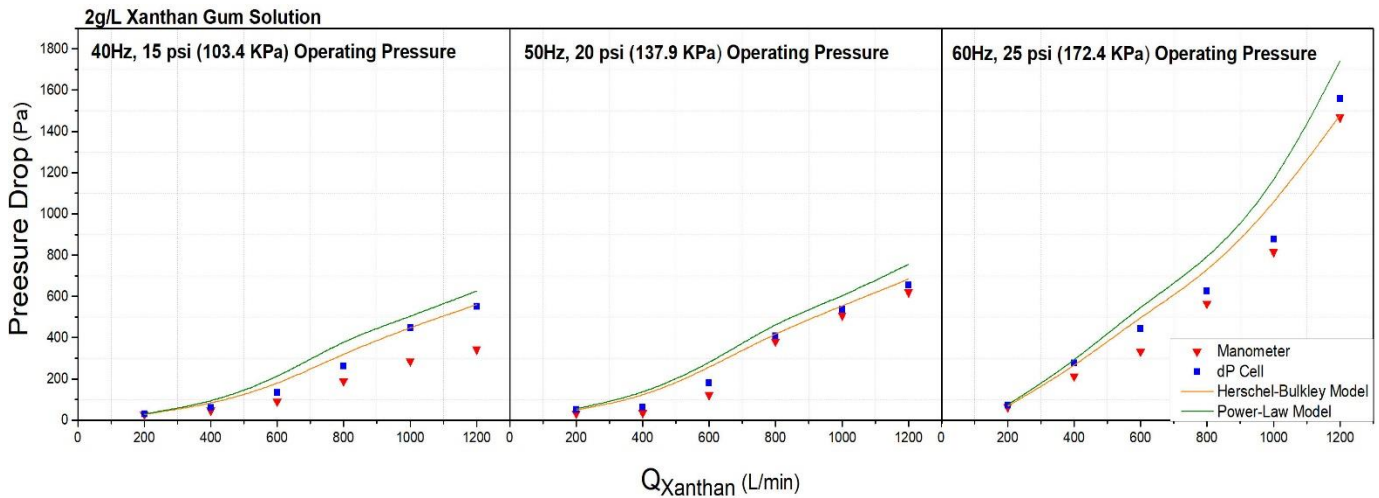


Figure 57 - 2g/L Xanthan Gum Solution - Experimental and Correlations Pressure Drop Results

As demonstrated in Figures 56 and 57 that pressure drop rises with rising operating pressure and the flow rates for single-phase flow. A satisfactory agreement with the experimental results was presented by the empirical models. The best approach in regard to the experimental results of used xanthan gum solution concentrations is the Herschel-

Bulkley model. Also, more pressure drops with the 2g/L. Therefore, at a higher viscosity and higher concentration, xanthan gum solutions can lead to an additional decrease in pressure in horizontal single-phase flow.

5.2.2 Single-Phase Pressure Drop vs Reynolds Number

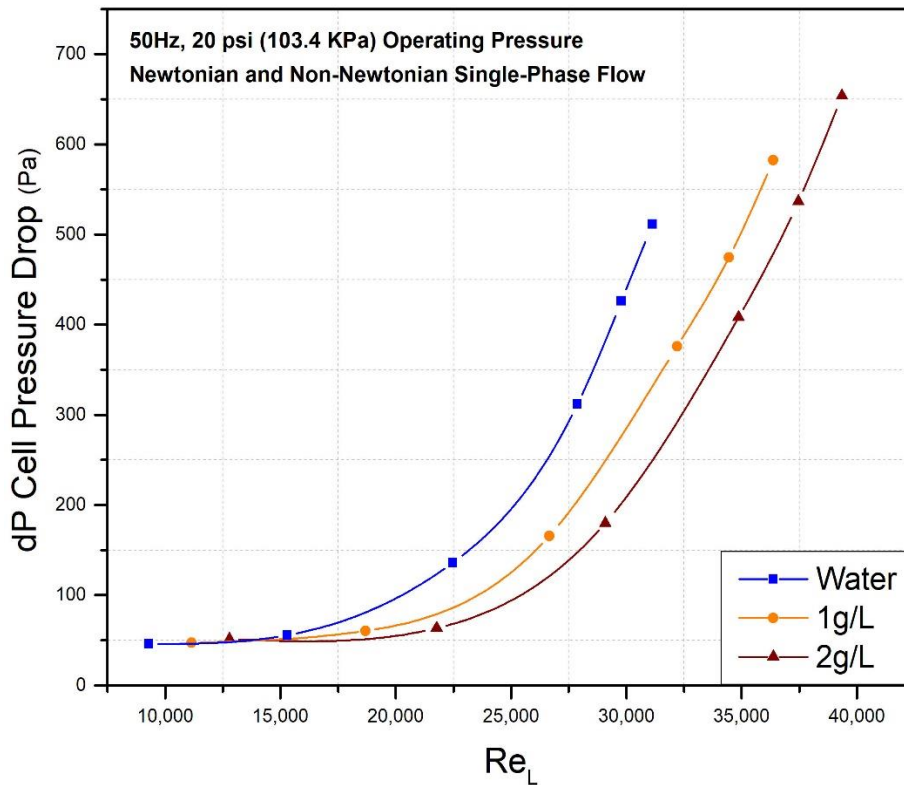


Figure 58 - Single-Phase Pressure Drop vs Reynolds Number

The relation between Reynolds number and pressure drop for Newtonian and non-Newtonian single-phase flow at operating pressure of 20 psi (50Hz) is shown in Figure 58. It was demonstrated that the pressure drop rises promptly with the increase in Reynolds number. The highest growth of the pressure drop against Reynolds number occurs with 2g/L concentration as compared to 1g/L and water case. The reason is more considerable pressure drop generated by the 2g/L xanthan gum solution single-phase flow throughout the pipeline.

5.2.3 Two-Phase Flow

5.2.3.1 Newtonian Pressure Drop

Figure 59 illustrates the effect of modifying the air flow rates on the pressure drop when water flow rates are constant. It is evident that the increase in the operating pressure and the air flow rate contribute to the pressure drop for horizontal Newtonian two-phase flow. Commonly, the experimental results fit in the range of different empirical models. Here, Lockhart-Martinelli matches the most accurately obtained experimental results.

- *Water Flow, $Q_g = 200, 1000 \text{ \& 2000 (L/min)}$*

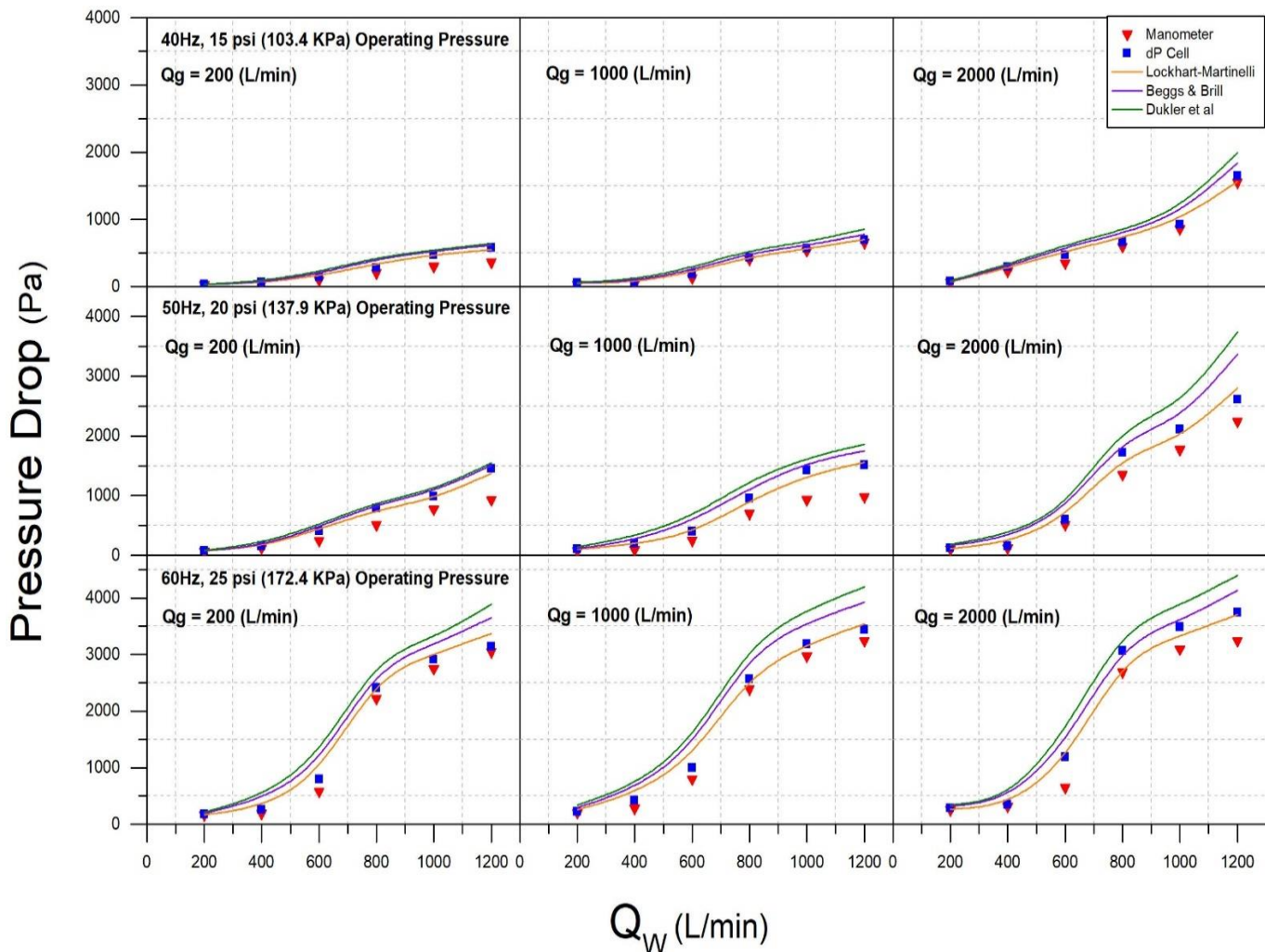


Figure 59 - 2-P Water and Air Flow - Experimental and Correlations Pressure Drop Results

Figure 60 illustrates that the pressure drop rises together with the rise in operating pressure and the water flow rates when air flow rates are constant in horizontal Newtonian two-phase flow. Furthermore, the best approach is the Lockhart-Martinelli model, and the empirical correlations exhibit a close match with the manometer results and the dP (Differential Pressure) cell sensor.

- **Air Flow, $Q_w = 200, 600 \text{ \& 1200 (L/min)}$**

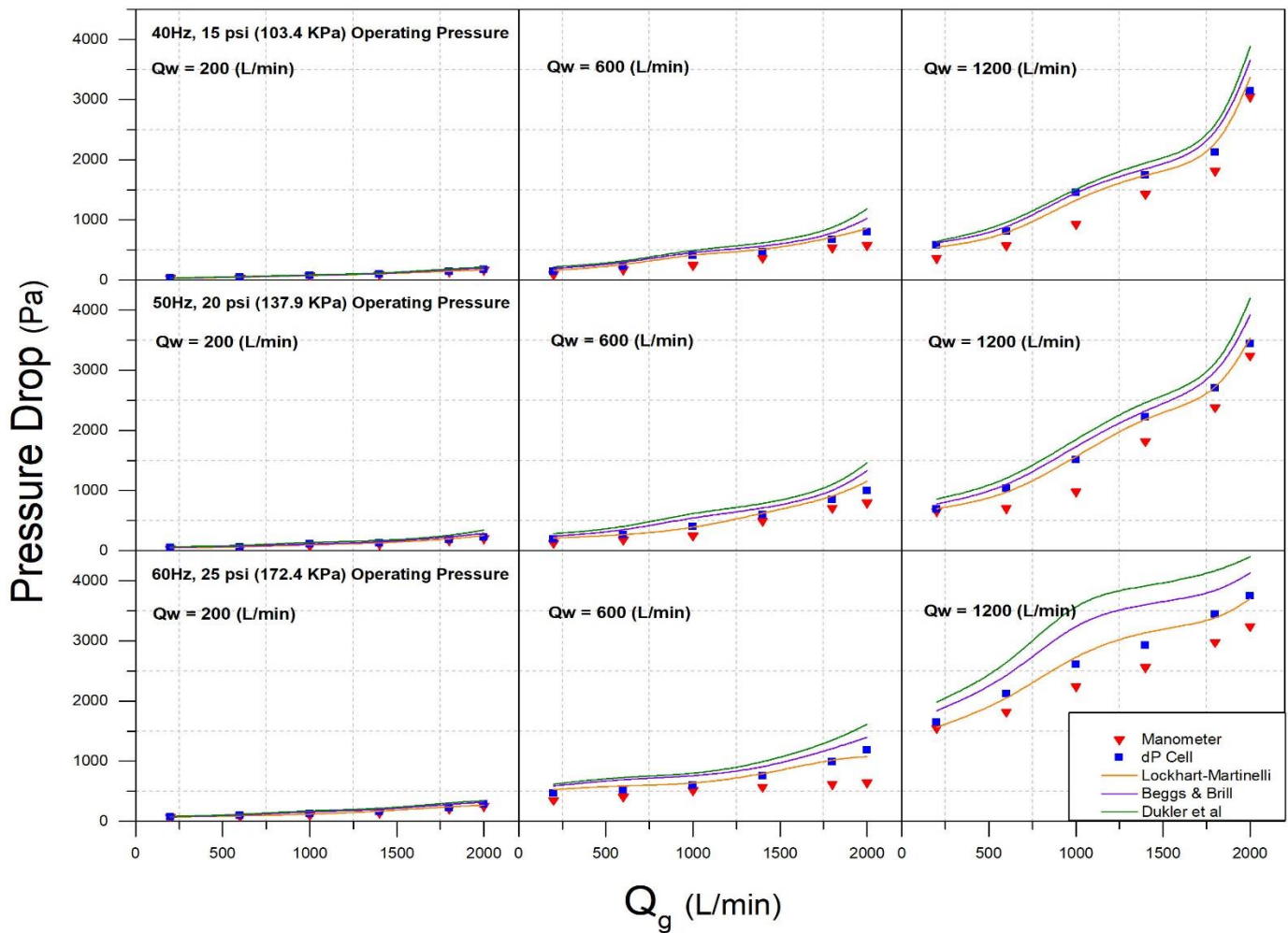


Figure 60 - 2-P Air and Water Flow - Experimental and Correlations Pressure Drop Results

5.2.3.2 Non-Newtonian Pressure Drop

- 1g/L Xanthan Gum Solution Flow, $Q_g = 200, 1000 \text{ \& 2000 (L/min)}$

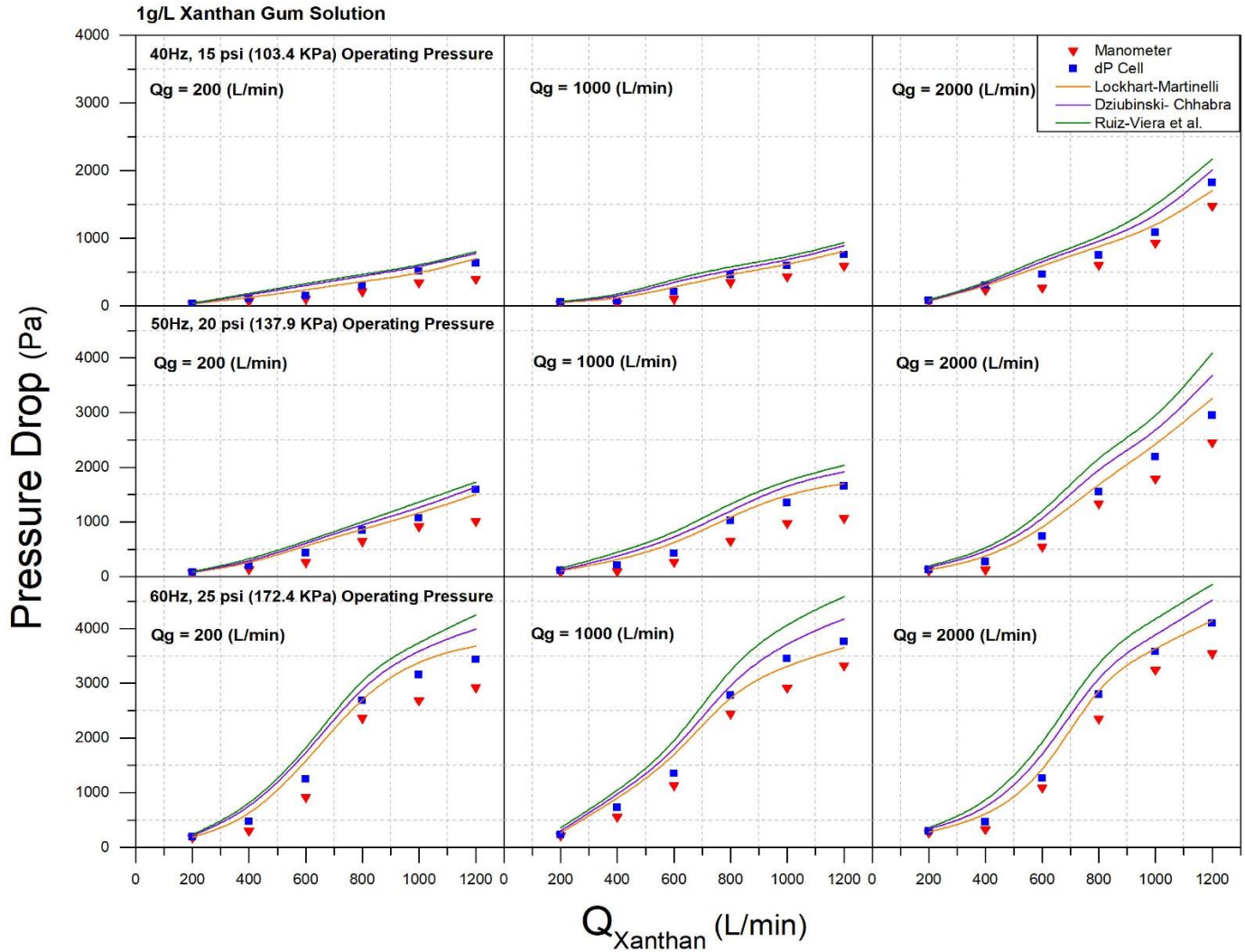


Figure 61 - Two-Phase 1g/L Xanthan Gum Solution and Air Flow - Experimental and Correlations Pressure Drop Results

- Air Flow, 1g/L $Q_{xanthan} = 200, 600 \text{ \& } 1200 \text{ (L/min)}$

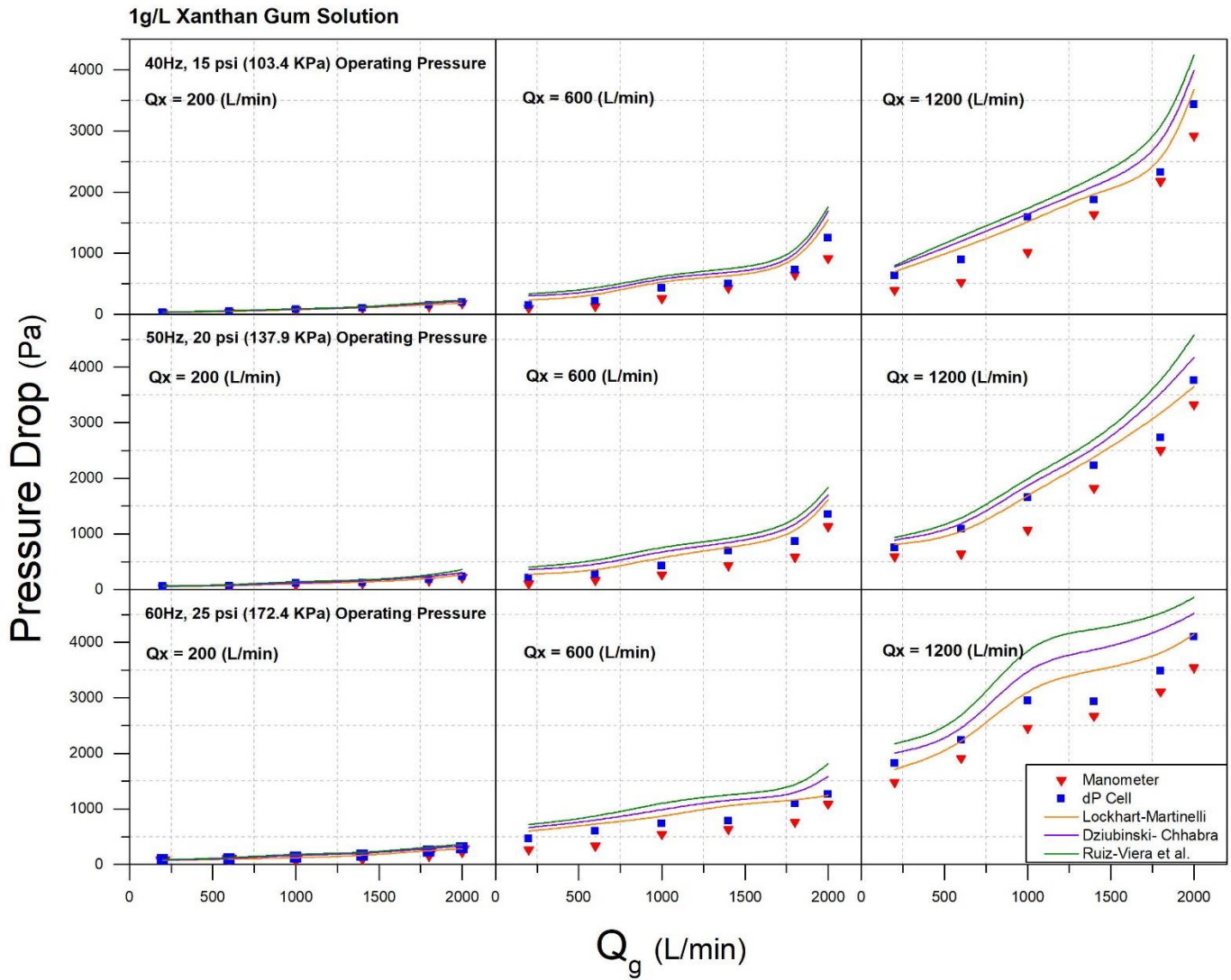


Figure 62 - Two-Phase Air Flow and 1g/L Xanthan Gum Solution - Experimental and Correlations Pressure Drop Results

- 2g/L Xanthan Gum Solution Flow, $Q_g = 200, 1000 \text{ \& 2000 (L/min)}$

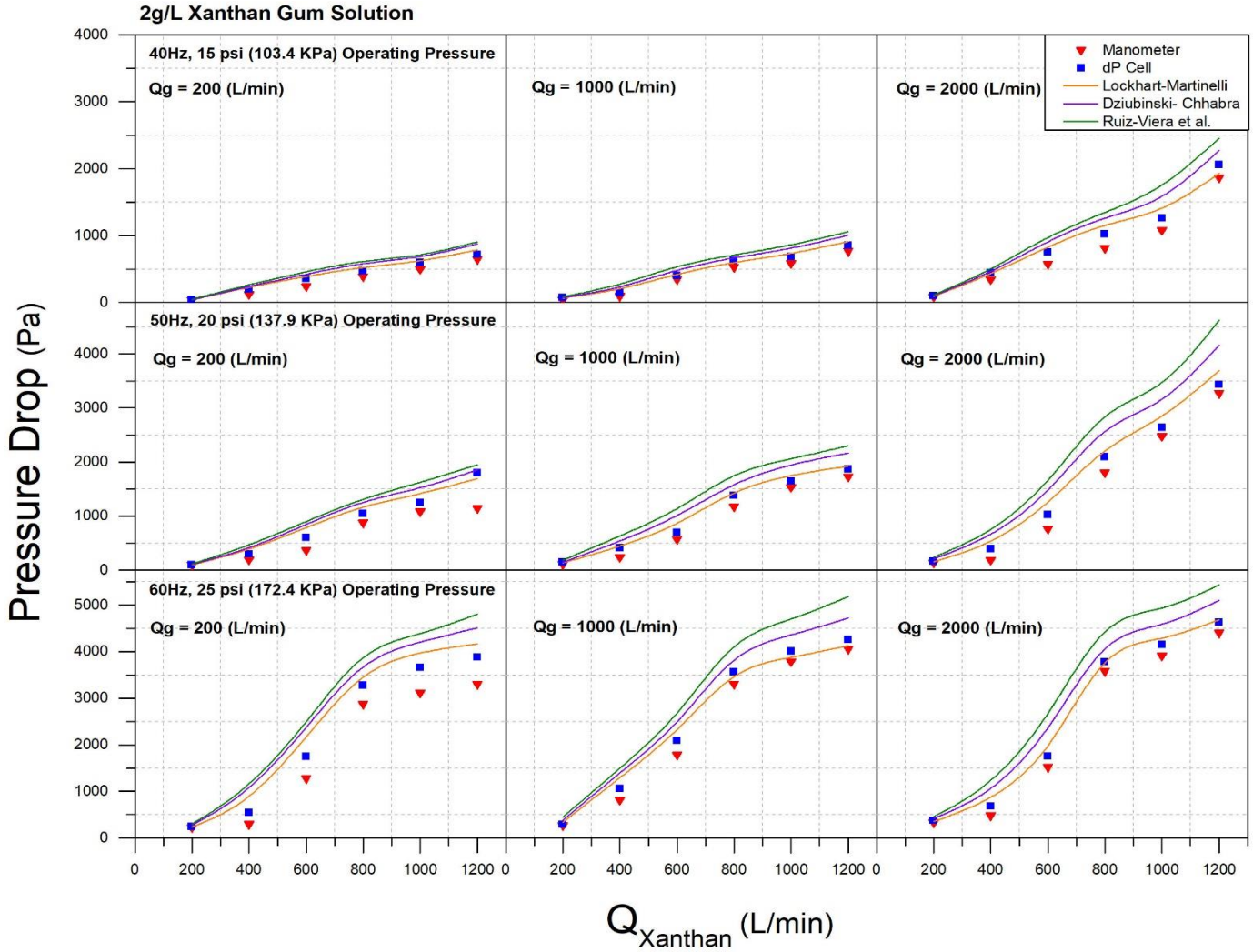


Figure 63 - Two-Phase 2g/L Xanthan Gum Solution and Air Flow - Experimental and Correlations Pressure Drop Results

- Air Flow, 2g/L $Q_{xanthan} = 200, 600 \text{ \& } 1200 \text{ (L/min)}$

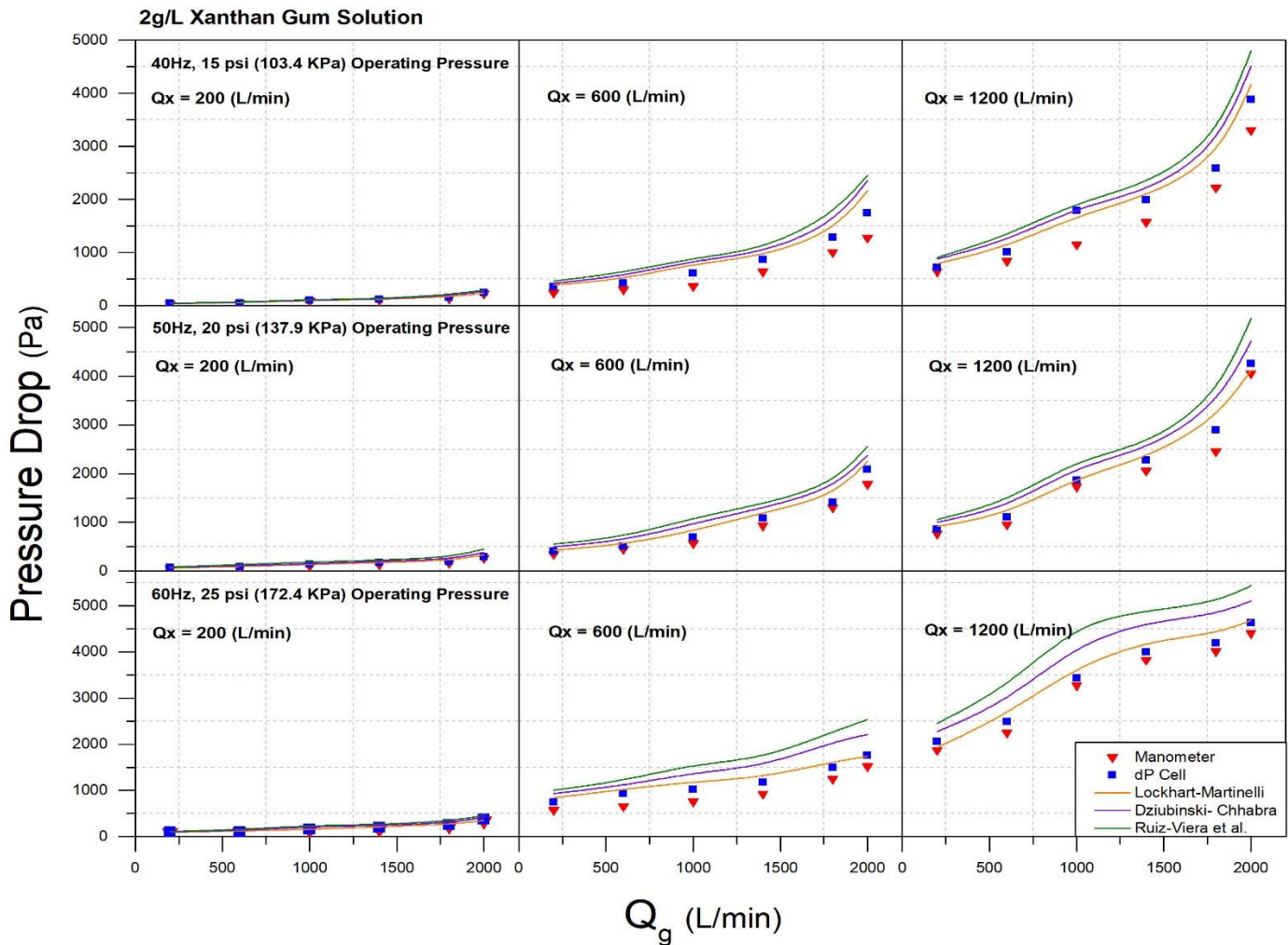


Figure 64 - Two-Phase Air Flow and 2g/L Xanthan Gum Solution - Experimental and Correlations Pressure Drop Results

Figures 61 and 63 show that as the amount of air rises in horizontal non-Newtonian two-phase flow, also the pressure drop rises when xanthan gum solution flow rates are constant. Moreover, it is observed that the highest values of the pressured drop are reached at the operating pressure of 25 psi (60Hz). In addition, in comparison to the case of the 1g/L xanthan gum concentration, the 2g/L xanthan gum concentration flows cause the highest growth of pressure drop. Hence, xanthan gum solutions generate an additional pressure drop in horizontal non-Newtonian two-phase flow at a higher viscosity and higher concentration. According to the empirical correlations, there is satisfactory

matching with the experimental results. The Lockhart-Martinelli model exhibits the most accurate match with the manometer results and the dP (Differential Pressure) cell sensor.

The review of Figures 62 and 64 shows the growth in the pressure drop along with the rise in the operating pressure and xanthan gum solution flow rates when air flow rates are constant in the horizontal non-Newtonian two-phase flow. Furthermore, in comparison to the 1g/L concentration case, the case of 2g/L concentration represents the most important development of the pressure drop. According to the empirical correlations, there is satisfactory matching with the experimental results. The Lockhart-Martinelli model exhibits the most accurate match with the obtained empirical results.

5.2.4 Two-Phase Pressure Drop versus Reynolds Number

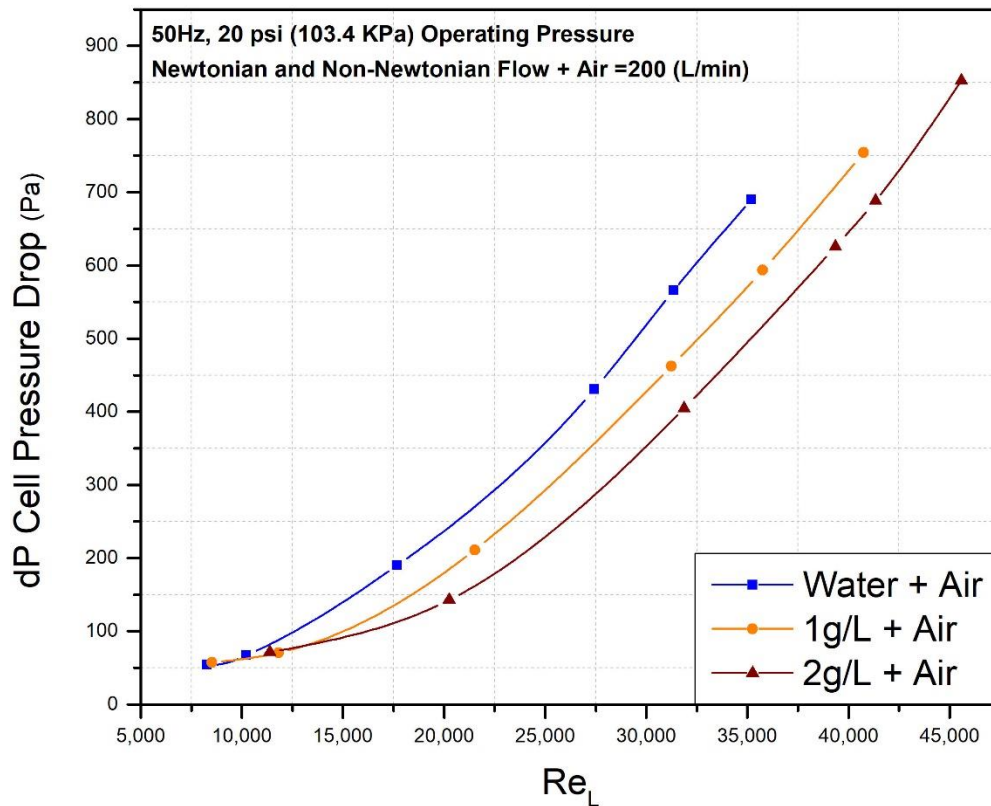


Figure 65 - Two-Phase Pressure Drop vs Reynolds Number

Figure 65 illustrates the relation between Reynolds number and pressure drop for Newtonian and non-Newtonian two-phase flow with operating pressure at 20 psi (50Hz). It was observed that with the rise in Reynolds number the pressure drop rises significantly.

Moreover, in comparison to 1g/L concentration and water cases, 2g/L concentration causes the highest values of the pressure drop against Reynolds number. The reason is that the 2g/L xanthan gum solution two-phase flow results in the highest pressure drop in a horizontal pipeline.

5.2.5 Phase Pressure Drop Comparisons

5.2.5.1 Newtonian Experimental Pressure Drop Comparison

- **Single Phase versus Two Phase**

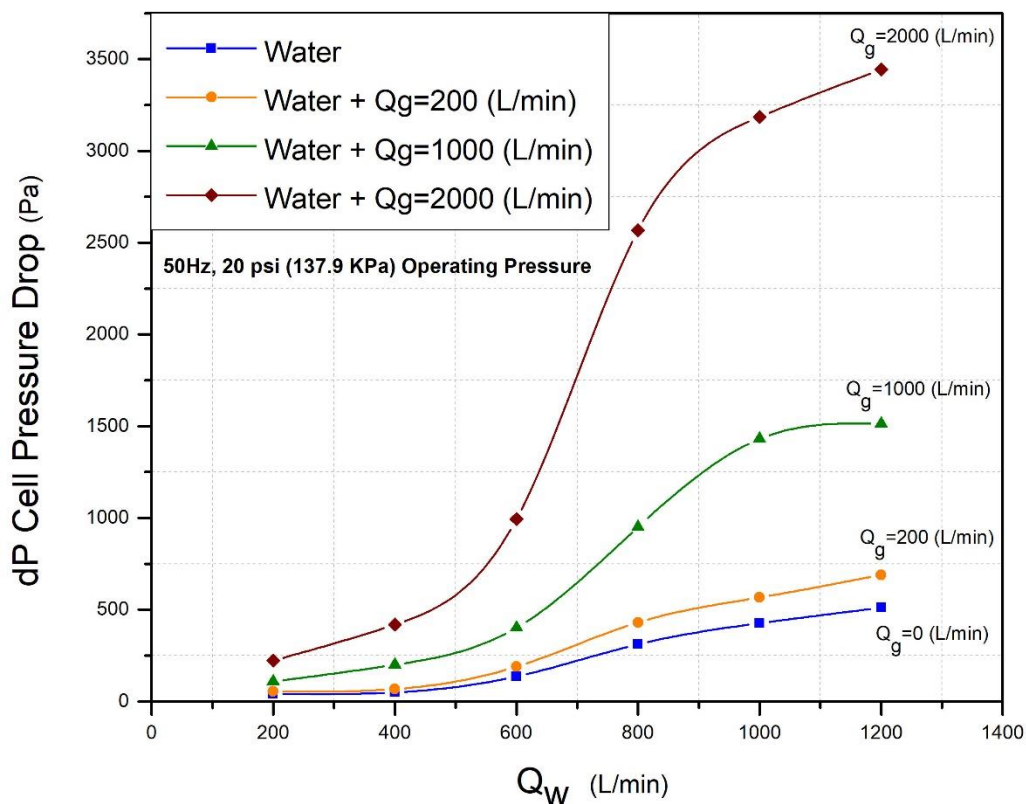


Figure 66 - Newtonian Experimental Pressure Drop Comparison - Single Phase vs Two Phase

Figure 66 shows the growth of the dP cell pressure drop during the transition from single-phase to two-phase flow when operating pressure is at 20 psi (50Hz). It is observed that with the rise in the air flow rate the pressure drop rises as well. Hence, in comparison to Newtonian single-phase flow, Newtonian two-phase flow generates more pressure drop through a horizontal pipeline.

5.2.5.2 Non-Newtonian Experimental Pressure Drop Comparison

- *Single Phase versus Two Phase*

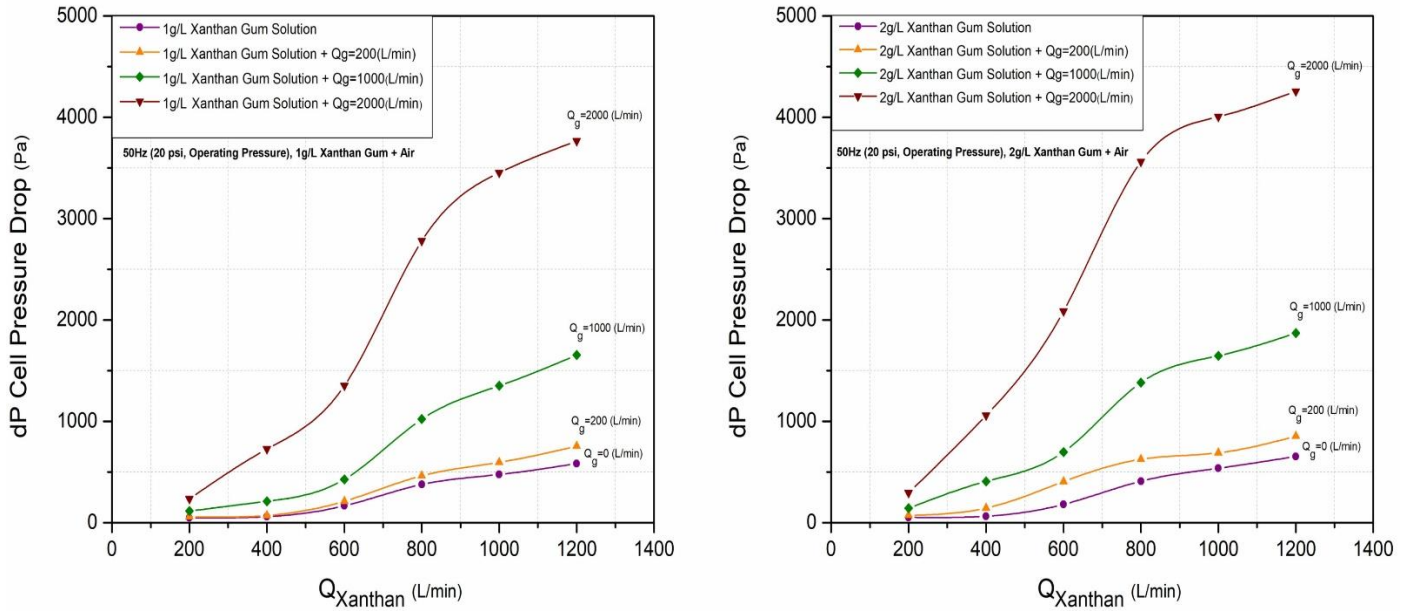


Figure 67 - Non-Newtonian Experimental Pressure Drop Comparison - Single Phase vs Two Phase

Figure 67 illustrates that with the increase in the air flow rate, the dP cell pressure increases as well during the transition from single-phase to two-phase flow when operating pressure is at 20 psi (50Hz). Moreover, in comparison to the single-phase case, the two-phase flow of 2g/L and 1g/L xanthan gum solution concentrations result in a greater growth of the pressure drop. As a consequence, in a comparison to non-Newtonian single-phase flow, non-Newtonian two-phase flow generates a larger pressure drop in a horizontal pipe.

5.2.5.3 Newtonian and Non-Newtonian Experimental Pressure Drop Comparison

- *Single Phase versus Two Phase*

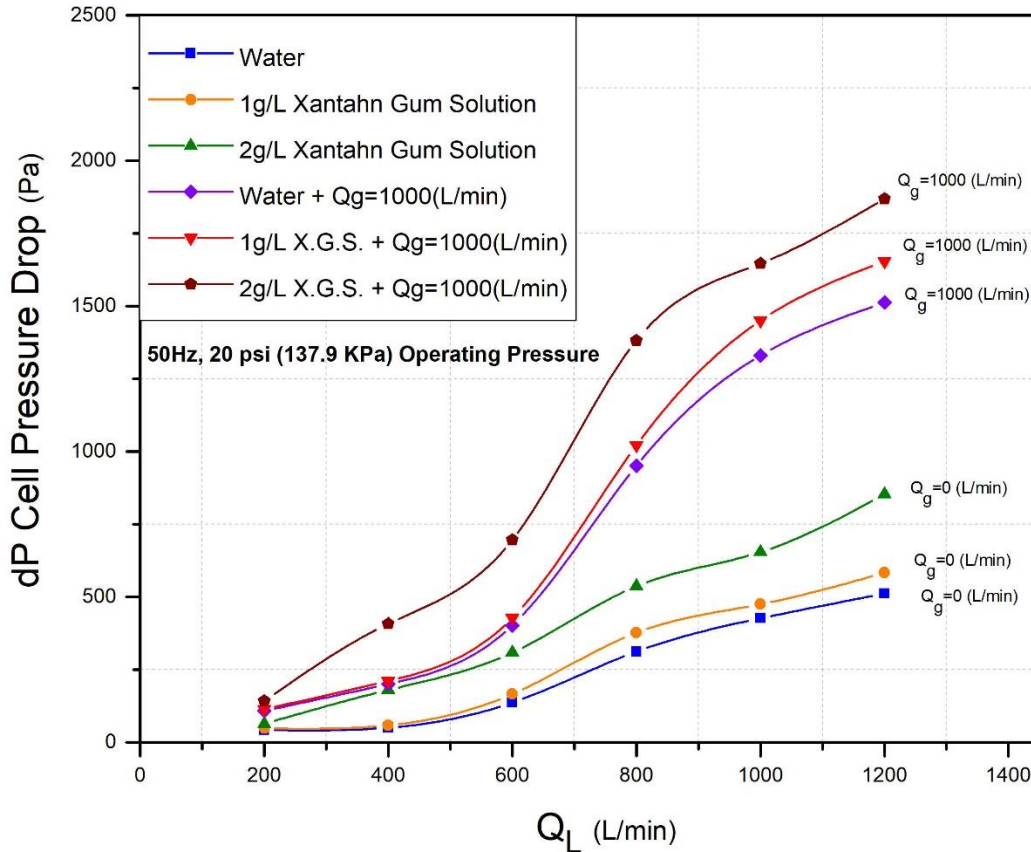


Figure 68 - Newtonian and Non-Newtonian Experimental Pressure Drop Comparison - Single Phase vs Two Phase

Figure 68 illustrates the comparison of the dP cell pressure drop when operating pressure is at 20 psi (50Hz) between single-phase flow and two-phase flow of Newtonian and non-Newtonian fluids. It is observed that the rise in the air flow rate increases the pressure drop. Furthermore, water single-phase flow produces the lowest pressure drop and two-phase flow of 2g/L xanthan gum solution concentration results in the largest pressure drop. Hence, in a horizontal flow, a higher viscosity and higher air flow rate cause the greater pressure drop.

5.3 Flow Regime Visualizations

The operating pressure of 20 psi (50Hz) was used to perform the flow regimes experiments for Newtonian and 1g/L-concentration non-Newtonian flow.

5.3.1 Newtonian Flow Regimes

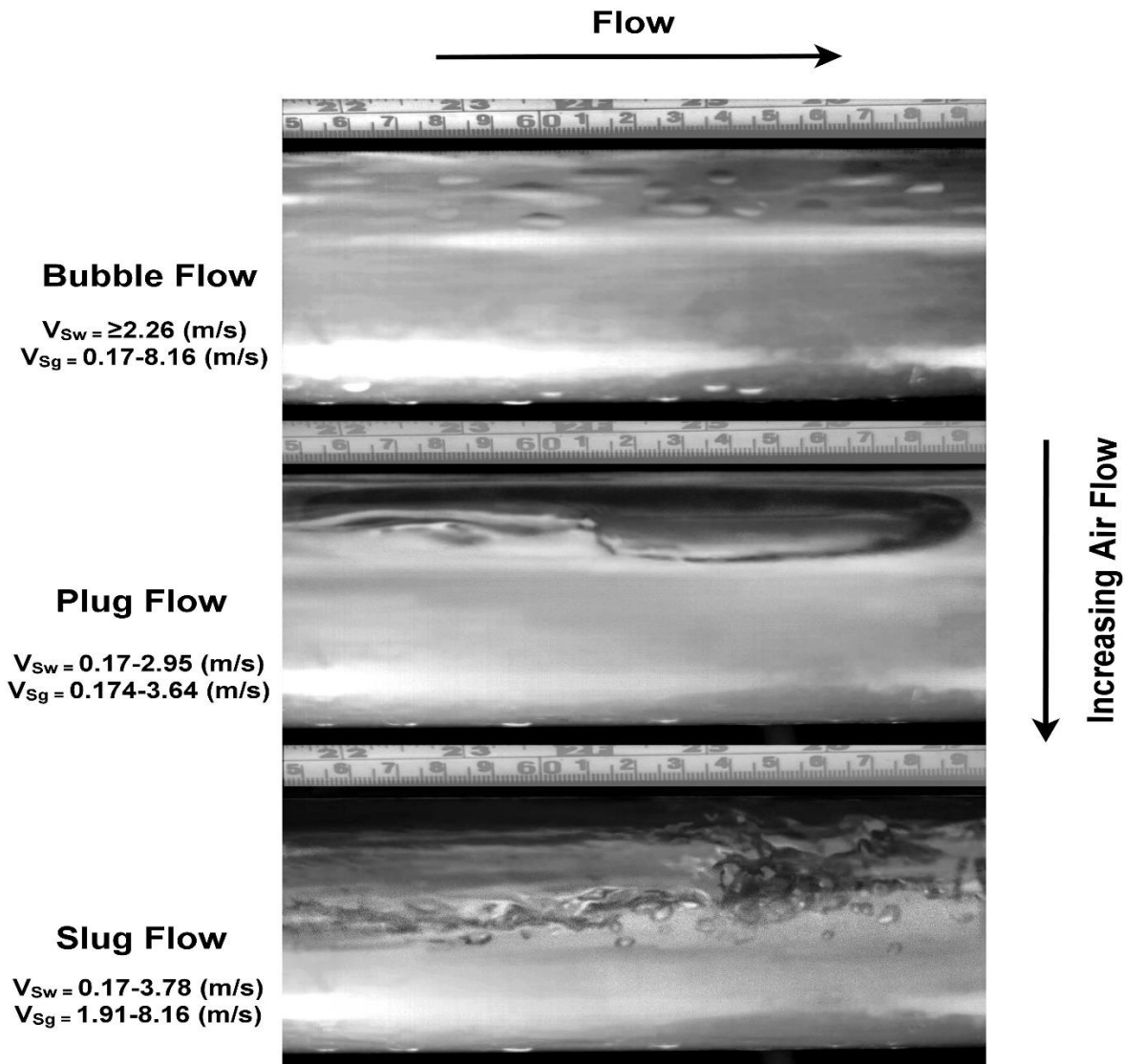


Figure 69 - Newtonian Flow Regimes Visualized by High-Speed Camera Mega Speed MS55K

The flow regime images presented in Figure 69 taken by the high-speed camera, Mega Speed MS55K. They correspond to three Newtonian flow regimes used in this study. The sequential visualization shows bubble, plug, and slug flow with the rise in the air flow rate.

5.3.2 Non-Newtonian Flow Regimes

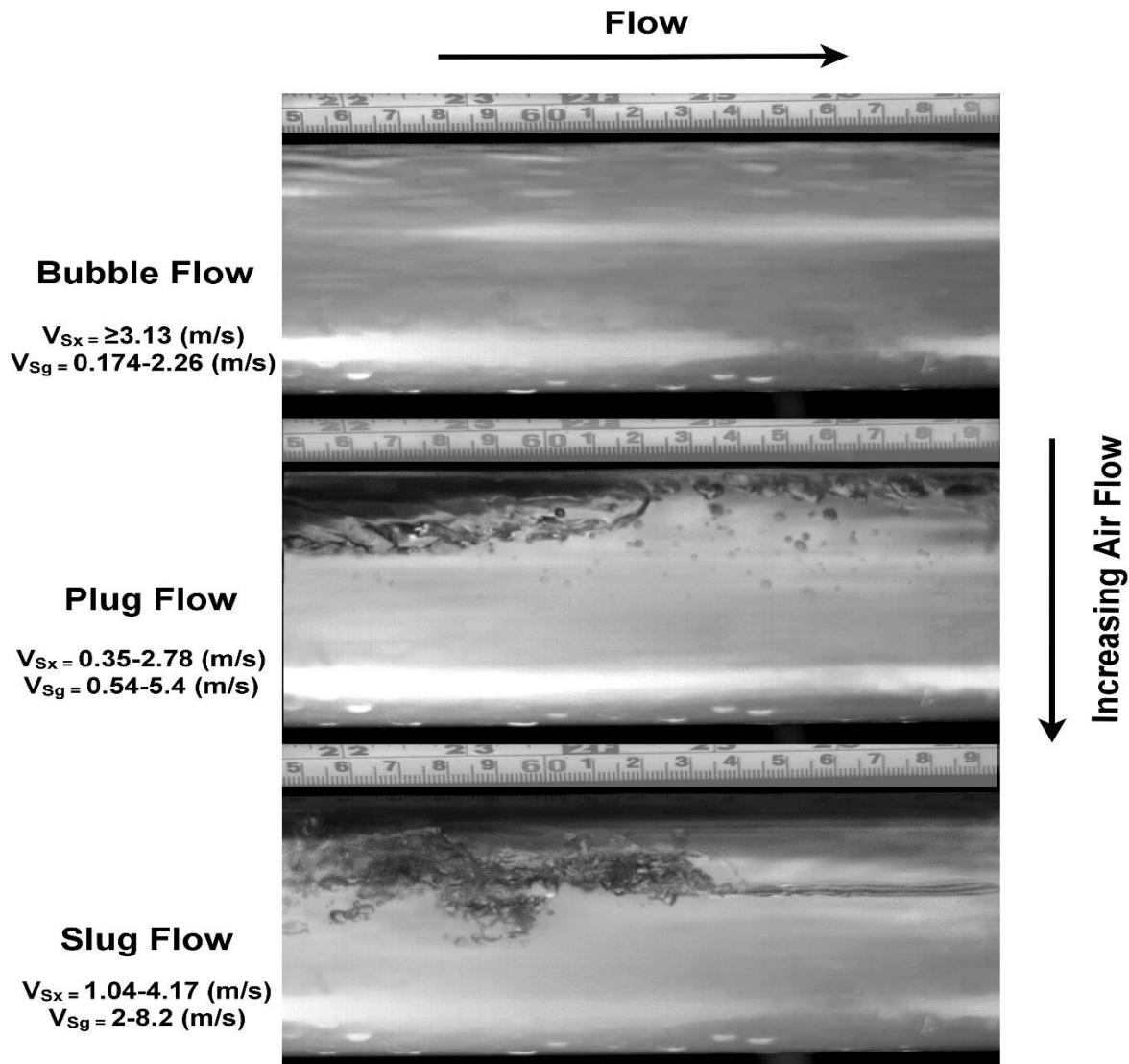


Figure 70 - Non-Newtonian Flow Regimes Visualized by High-Speed Camera Mega Speed MS55K

Figure 70 shows standard bubble, plug and slug flow regimes of 1g/L-concentration non-Newtonian flow. They were taken with the high-speed camera. It was not possible to visualize the 2g/L xanthan gum solution flow because of a murky flow caused by the more considerable amount of xanthan gum powder.

Non-Newtonian flow required more amounts of air to produce bubble flow, plug flow, and slug flow regime comparing to Newtonian flow case.

5.3.3 Flow Regime Maps

The experimental results were employed to generate maps of flow regime for the non-Newtonian and Newtonian horizontal flow. Subsequently, the results were compared with the maps of two-phase flow in horizontal pipes regimes proposed by (Taitel and Duckler (1976) [21] and Mandhane (1974) [20]) which used the gas and liquid superficial velocities.

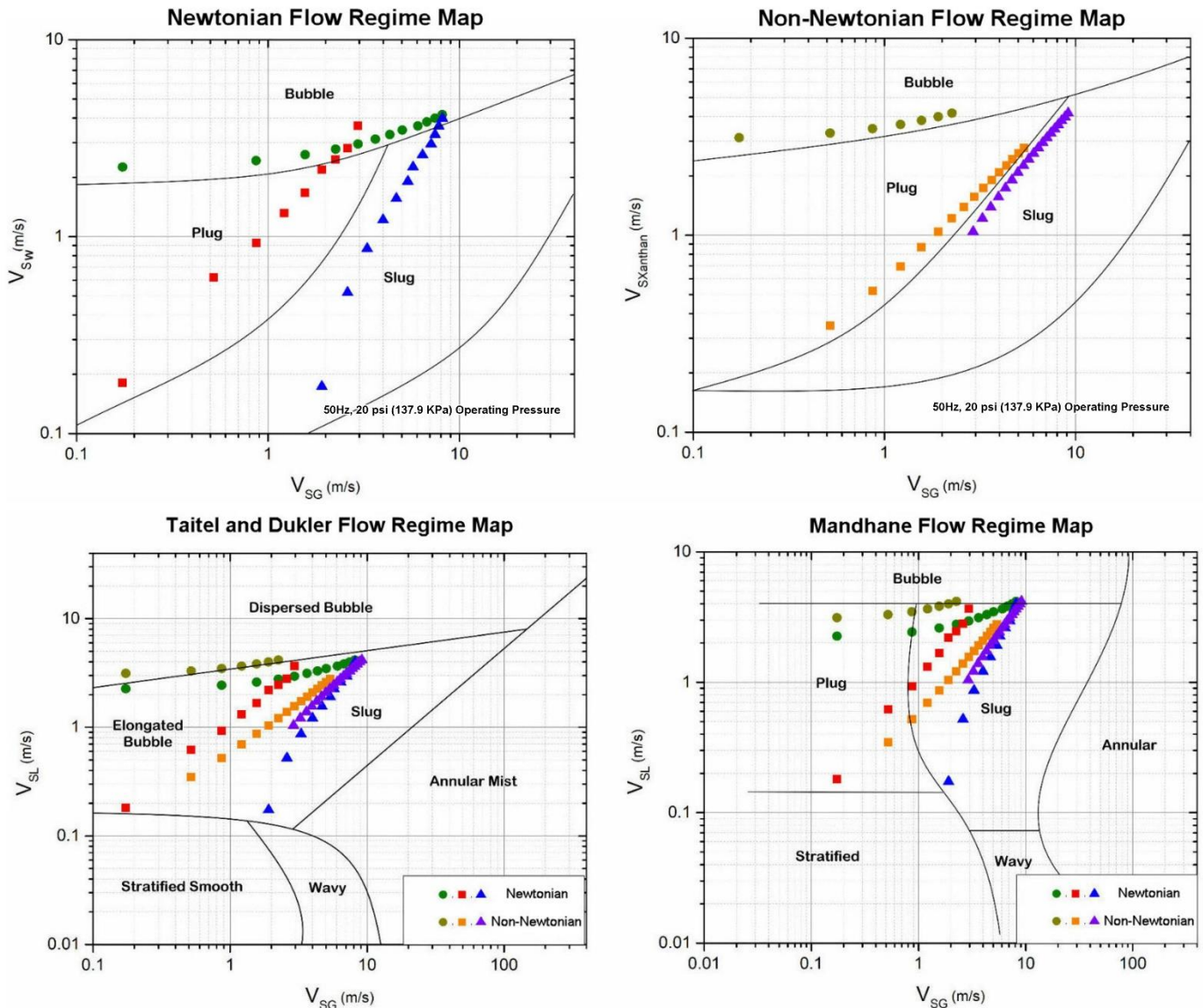


Figure 71 - Comparison Taitel and Duckler (1976) and Mandhane (1974) Flow Regime Maps with Flow Regimes Visualizations Through a 3 in (76.2 mm)-ID Horizontal Pipe.

In Figure 71, the experimentally observed flow structures in a horizontal pipe of diameter 76.2 mm were compared the empirical map presented by Mandhane et al. (1974) and the theoretical map presented by Taitel et al. (1976). Accordingly, the graph shows slug flow data, plug (elongated bubble), and the data for the bubble. Thus, maps of Mandhane (1974) and Taitel and Duckler (1976) predicted the majority of the points in the given flow regime accurately. Moreover, the flow patterns were observed at the moment of varying the flow rates of each phase to determine the limits of particular flow regime areas.

The experimental setup of the flow loop provides slug, plug, and bubble flow regimes. Because of specific pipeline dimensions and air and liquid flow range, this flow loop setup cannot provide adequate annular, wavy, or stratified flow regimes as demonstrated in Table 8.

Table 8 - Comparison Flow Regime Area Limits of The Experimental Results with Literature review

Author	Fluids	Pipe Diameter	Coordinate Parameters	Dispersed Bubble		Elongated Bubbly (Plug)		Stratified		Wavy		Slug		Annular Mist	
				V _{SL}	V _{SG}	V _{SL}	V _{SG}	V _{SL}	V _{SG}	V _{SL}	V _{SG}	V _{SL}	V _{SG}	V _{SL}	V _{SG}
Taitel et al. 1976 [20]	Air-Water	26 mm	V _{SL} , V _{SG} (m/s)	≥1.8	≥90	-	-	0.01-0.22	0.01-4.3	0.01-0.13	1.75-18	0.22-5.2	0.01-90	0.01-5.5	≥2.4
Mandhane et al. 1974 [21]	Air-Water	25.4 mm	V _{SL} , V _{SG} (m/s)	≥4.2	0.1-156	0.17-4.2	0.1-0.97	0.01-0.17	0.1-2.6	0.01-0.089	2.75-112	0.089-4.2	0.97-158	≥0.01	≥112
Weisman et al. 1979 [44]	Air-Water	12.7-50.8 mm	V _{SG} , V _{SL} (m/s)	≥2	0.1-700	0.25-2	0.1-9.2	0.01-0.178	0.1-2.9	0.01-0.196	0.194-9	0.25-2	0.1-9.2	≥0.01	≥6
Griffith 1984 [45]	Air-Water	25.4 mm	V _{SL} , V _{SG} (m/s)	≥2.45	0.1-170	0.168-2.45	0.1-0.98	0.01-0.165	0.1-1.48	0.01-0.155	3.6-16.5	0.168-6.65	0.98-170	≥0.01	≥2.8
Newtonian Exp.	Air-Water	76.2 mm	V _{SL} , V _{SG} (m/s)	≥2.26	0.17-8.16	0.17-2.95	0.174-3.64	-	-	-	-	0.17-3.78	1.91-8.16	-	-
Non-Newtonian Exp.	Air-Xanthan Gum Solution	76.2 mm	V _{SX} , V _{SG} (m/s)	≥3.13	0.174-2.26	0.35-2.78	0.57-5.4	-	-	-	-	1.04-4.17	2-8.2	-	-

6 Discussions

During this experimental study, different sources of errors were noted. All of them adversely impact the study results. Based on origin, these error sources are categorized as follows:

1. *Measurements*

- The accuracy of flow meters used to measure air flow is not known. Moreover, air measurement of 2000 [L/min] exceeded 1400 [L/min], which is the maximum recommended by the manufacturer.
- The accuracy of a flow meter used to measure liquid flow is not known. Moreover, the accuracy of the specific turbine flow meter used to measure a non-Newtonian flow was not confirmed.
- A newly installed differential sensor (dP cell) was used to measure pressure. It had factory calibration. Its output was a reading of around -15 [kPa] at no flow conditions, and it was regarded as a baseline. Hence, it was measured prior and following each test run to measure fluctuation. Nevertheless, there was no confirmation of the validity of this approach.
- According to manometer pressure drop results, the device is not precise enough to measure the small range of flow rates accurately in which the measurements were carried out.
- The average of 50 Hz over 10 seconds was used to take pressure readings. A frequency-independent reading did not confirm this sampling rate, nor it was validated by calculation.
- No adjustment was made to the differential pressure, which resulted in noise. It accounts for a significant standard deviation in the data sets of the sample.

2. Procedure

- There is a possibility that the experimental results were gathered before the system reached equilibrium in the process.
- It was observed that Xanthan gum rheology was time-independent during lab scale tests. However, slight, gradual changes in xanthan gum solution properties were noticed.
- It was necessary to complete all tests with xanthan gum in five hours to avoid damage to the flow loop equipment. There was no set mixing regimen was established. It probably negatively influenced the possibility of other researchers to replicate the results.
- As can be observed from flow regime images, the light source was not adequate. Hence, reflections on the slug and bubble surface at the interface between water and air discompose the picture.

3. Calculation Errors

- As outlined before, three operating pressures were used to perform the experiment. As it is impossible to ensure consistency of the flow rates because of the design of the flow loop setup and the frequency difference, inaccuracies in the flow rate reading were noticed. To illustrate, the reading of 200 (L/min) implies possible fluctuation in the range of the 190-220 (L/min). Exact values were used to make calculations, resulting in minor deviations.
- It was necessary to modify Reynold's number in the Lockhart-Martinelli model for a non-Newtonian pressure drop calculations. It did not include the viscosities of each phase. Hence, inaccurate estimations of the non-Newtonian pressure losses are possible.
- The basis of Xanthan gum concentrations (1g/L and 2 g/L) was a volumetric calculation of the process flow loop. Subsequently, the viscosity measured during the lab testing was compared with the viscosity of each sample. It

was discovered that the volume of the actual system was greater than an approximate calculation of 1 m³.

7 Conclusions

- In each experiment, intervals of 200 (L/min) were used to modify the liquid flow rate from the minimum of 200 (L/min) to the maximum of 1200 (L/min). Intervals of 400 (L/min) were used to modify the air flow rate from the minimum of 200 (L/min) to the maximum of 2000 (L/min). To detect the data trends, the pressure drop was plotted over the air and liquid flow rates. It was concluded that the empirical results are reliable because the validation of the experimental results proved good predictions and a reasonable approximation.
- It was found that the single-phase pressure drop rises along with the rise in the flow rate in non-Newtonian and Newtonian flow tests. It was noticed that the two-phase pressure drop rises with the rise in the air flow rate (air superficial velocity) for air-water two-phase flow. It happens because air phase disturbs the flow and extra pressure loss happens in the mixture of air-water flow. Moreover, the experiment explained the impact of the rising xanthan gum solution concentrations and the flow rates on the pressure drop of xanthan gum solution/air flow. It was definitely observed that the non-Newtonian pressure drop increases with the rise in xanthan gum solution concentration. A higher viscosity liquid establishes extra frictional shear forces along the pipe leading to a more substantial pressure drop.
- Lockhart-Martinelli model exhibits the best match with two-phase experimental results due to the presumption of considering each phase flow individually and an accurate representation of various parameters.

- The study accomplished flow regime visualizations for Newtonian and non-Newtonian flow. Slug flow, plug flow, and bubble flow were observed in spite of the fact that the flow loop is not adequate in providing annular, wavy, or stratified flow regimes. It was influenced by the flow rates of the fluids, their physical properties, and the setup design (pipe diameter). For increasing the quality of further recordings, it is recommended to use a laser as a light source as its narrow wavelength spectrum would not lead to reflections on slugs and bubbles. In order for the flow loop to produce more flow patterns, two things should happen: reduce the pipe diameter (20-26 mm) and upgrade the setup to inject larger amounts of air.
- The study undertook a technical evaluation to check if it is feasible to add solid particles to the current system (Appendix B). The chosen solid particle for use in the process flow loop was polystyrene microspheres particles (25nm to 750 μ m in diameter, 1.06 g/cm³ density).

References

- [1] Xu, J. Y., Gao, M. C., & Zhang, J. (2014). Pressure Drop Models for Gas/Non-Newtonian Power-Law Fluids Flow in Horizontal Pipes. *Chemical Engineering & Technology*, 37(4), 717-722.
- [2] Majumder, S. K., Ghosh, S., Mitra, A. K., & Kundu, G. (2010). Gas-Newtonian and gas-non-Newtonian slug flow in vertical pipe, Part I: Gas holdup characteristics. *International Journal of Chemical Reactor Engineering*, 8(1).
- [3] *An Overview of Heat Transfer Phenomena*, Two-Phase Flow by M. M. Awad, ISBN 978-953-51-0827-6, (11), 252-254.
- [4] http://www.mne.psu.edu/cimbala/learning/fluid/cv_momentum/home.htm. Retrieved October 10, 2016
- [5] <http://www.homeintheearth.com/tag/equations/>. Retrieved October 13, 2016
- [6] <http://www.whatispiping.com/what-is-fluid-flow>. Retrieved October 13, 2016
- [7] <http://uorepc-nitk.vlabs.ac.in/exp1/index.html>. Retrieved October 13, 2016
- [8] <http://motaharname.persianguig.com/document/%D9%85%DA%A9%D8%A7%D9%86%DB%8C%DA%A9%20%D8%B3%DB%8C%D8%A7%D9%84%D8%A7%D8%AA/>. Retrieved October 14, 2016
- [9] *An Overview of Heat Transfer Phenomena* Edited by Salim N. Kazi, ISBN 978-953-51-0827-6, 538 pages, Publisher: InTech, Chapters published October 31, 2012 under CC BY 3.0 license
- [10] Pietro Asinari, PhD Spring 2007, *Multiphase Flows: Basic Physics and Engineering Modeling*, TOP – UIC Program: The Master of Science Degree of the University of Illinois at the ‘Politecnico di Torino’
- [11] Bar-Meir, Genick, “Basics of Fluid Mechanics”, Last modified: Version 0.3.4.0 October 17, 2016, www.potto.org/downloads.php
- [12] Crowe, C. T. (Ed.). (2005). *Multiphase flow handbook* (Vol. 59). CRC press.
- [13] de Oliveira, L. A., Cunha Filho, J. S., Faccini, J. L. H., & Su, J. (2010). Visualization of Two-Phase Gas-Liquid Flow Regimes in Horizontal and Slightly-Inclined Circular Tubes. In *Proceedings of 13th Brazilian Congress of Thermal Sciences and Engineering (ENCIT 2010)*. Holland, F., & Bragg, R. (1995). *Fluid Flow for Chemical and Process Engineers*. Butterworth-Heinemann.

- [14] Two-phase-flow regimes, Halldor Palsson, University of Iceland, Accessed, October 19, 2016, www.researchgate.net
- [15] Morshed, M., Amin, A., Rahman, M. A., & Imtiaz, S. (2016, July). Experimental and computational analysis of pressure response in a multiphase flow loop. In M. Ali, M. A. S. Akanda, & A. M. Morshed (Eds.), *AIP Conference Proceedings* (Vol. 1754, No. 1, p. 040010). AIP Publishing.
- [16] Hubbard M.G. & Dukler A.E., 1966, The characterization of flow regimes for horizontal two-phase flow, *Proc. Heat Transfer and Fluid Mech. Institute*. Stanford University Press -M. Saad & J.A. Moller eds.
- [17] Gazley, C., *Intertacial Shear and Stability in Two-Phase Flow*, PhD theses, Univ. Del., Newark (1949).
- [18] Taitel, Y., & Dukler, A. E. (1976). A model for predicting flow regime transitions in horizontal and near horizontal gas-liquid flow. *AIChE Journal*, 22(1), 47-55
- [19] Mandhane, J. M., Gregory, G. A., & Aziz, K. (1974). A flow pattern map for gas—liquid flow in horizontal pipes. *International Journal of Multiphase Flow*, 1(4), 537-553.
- [20] <http://www.rheosense.com/applications/viscosity/newtonian-non-newtonian>. Retrieved October 20, 2016
- [21] R. S. Schulkes, " Pipe Flow with Radial Inflow: Experimental and Modeling Work," *Journal of Fluids Engineering*, pp. 121, 106-111, 1999.
- [22] H. Asheim, "Flow Resistance Correlation for Complete Wellbore," *Journal of Petroleum Science and Engineering*, pp. 8,97-104, 1992.
- [23] Björn, A., Karlsson, A., Svensson, B. H., Ejlertsson, J., & de La Monja, P. S. (2012). *Rheological characterization*. INTECH Open Access Publisher
- [24] Zhong, L., Oostrom, M., Truex, M. J., Vermeul, V. R., & Szecsody, J. E. (2013). Rheological behavior of xanthan gum solution related to shear thinning fluid delivery for subsurface remediation. *Journal of hazardous materials*, 244, 160-170.
- [25] Heywood, N. I., & Charles, M. E. (1979). The stratified flow of gas and non-Newtonian liquid in horizontal pipes. *International Journal of Multiphase Flow*, 5(5), 341-352.
- [26] https://neutrium.net/fluid_flow/pressure-loss-in-pipe/. Retrieved November 2, 2016

- [27] <http://achp.sourceforge.net/ACHPComponents/FluidCorrelations.html>. Retrieved November 3, 2016
- [28] Madlener, K., Frey, B., & Ciezki, H. K. (2009). Generalized reynolds number for non-newtonian fluids. In *Progress in Propulsion Physics* (Vol. 1, pp. 237-250). EDP Sciences.
- [29] Pereira, A. S., & Pinho, F. T. (2002). Turbulent pipe flow of thixotropic fluids. *International journal of heat and fluid flow*, 23(1), 36-51.
- [30] White, F. M., Fluid Mechanics, McGraw-Hill Education, 7th edition, February 2010, ISBN: 978-0077422417.
- [31] Omosebi, A. O., & Adenuga, K. A. (2012, January). Pressure drop versus flow rate profiles for power-law and Herschel-Bulkley fluids. In *Nigeria Annual International Conference and Exhibition*. Society of Petroleum Engineers.
- [32] <http://www.omega.ca/shop/pptsc.asp?ref=PXM409-WWDIF&nav=>. Retrieved November 9, 2016
- [33] http://www.omega.ca/pptst_eng/FLR-D.html. Retrieved November 9, 2016
- [34] <http://www.omega.com/pptst/PX603.html>. Retrieved November 9, 2016
- [35] <https://www.electronicsdatasheets.com/manufacturers/newport-electronics/inc/parts/px409005dwu5v>. Retrieved November 9, 2016
- [36] <http://www.omega.com/pptst/PX409-WWDIF.html>. Retrieved November 9, 2016
- [37] <http://cuthbertsonlaird.co.uk/comark-indicators/415-comark-c9555-0-30-psi-manometer.html>. Retrieved November 10, 2016
- [38] <https://www.testex.co.uk/comark-c9555-sil-pressure-meter-range-0-to-2000mbar>. Retrieved November 10, 2016
- [39] <http://www.omega.co.uk/pptst/TC-NPT.html>. Retrieved November 9, 2016
- [40] <https://www.jjdowns.com/>. Retrieved November 12, 2016
- [41] www.rcmt.cvut.cz/soubor/f-at/70d22ce0.../NI_cDAQ-9178-specification-eng.pdf. Retrieved November 12, 2016
- [42] <http://megaspeedusa.com/pc-connected/ms55k/>. Retrieved November 15, 2016

- [43] <http://petroleumsupport.com/drilling-fluid-test-on-field/>. Retrieved November 16, 2016
- [44] Abdulmouti, H. (2014). Bubbly Two-Phase Flow: Part I-Characteristics, Structures, Behaviors and Flow Patterns. *American Journal of Fluid Dynamics*, 4(4), 194-240.
- [45] Griffith, P. (1984). Multiphase flow in pipes. *Journal of Petroleum Technology*, 36(03), 361-367.
- [46] Fox, W., Pritchard, P., McDonald, A., *Introduction to Fluid Mechanics. Seventh Edition*, John Wiley & Sons, 2010, 754 pp.
- [47] D. Chisholm, " International Journal of Heat and Mass Transfer," *International Journal of Heat and Mass Transfer*, p. 1767, 1967.
- [48] H.M. Mekisso, *Comparison of frictional pressure drop correlations for isothermal two-phase horizontal flow*, Bachelor of Science in Engineering, Bahir Dar University, Bahir Dar, Ethiopia 2004, 2(2), 33-34
- [49] Dziubinski, M., and R. P. Chhabra. "Predicting 2-Phase Pressure-Drop for The Flow of Gas-Non-Newtonian Liquid-Mixtures in Horizontal Pipes." *International Journal of Engineering Fluid Mechanics* 2.1 (1989): 63-78.
- [50] Farooqi, S. I., & Richardson, J. F. (1982). Horizontal flow of air and liquid (Newtonian and non-Newtonian) in a smooth pipe. Pt. 2: average pressure drop [water, water/glycerol, water/glycerol/kaolin]. *Transactions of the Institution of Chemical Engineers*, 60, 323-33.
- [51] Ruiz-Viera, M. J., Delgado, M. A., Franco, J. M., Sánchez, M. C., & Gallegos, C. (2006). On the drag reduction for the two-phase horizontal pipe flow of highly viscous non-Newtonian liquid/air mixtures: Case of lubricating grease. *International Journal of Multiphase Flow*, 32(2), 232-247.
- [52] Kay, J. M.; Nedderman, R. M., *Fluidmechanics and Transfer Processes. Cambridge University Press* 1985. XVIII, 602 S. 8(8.3), 223.
- [53] Don W. Green, Robert H. Perry (2007), *Perry's Chemical Engineers' Handbook*, Eighth Edition, *McGraw Hill professional*, Department of Chemical Engineering at the University of Oklahoma, 6: 1375.
- [54] Efstathios Michaelides, Clayton T. Crowe, John D. Schwarzkopf (2005), *Multiphase Flow Handbook*, Second Edition, *Mechanical and Aerospace Engineering*, 5: 457.

Appendix A: Pressure Drop Correlations

- **Single-Phase Flow**

Blasius Correlation (1912)

The simplest equation for solving the Darcy friction factor is the Blasius equation. However, it is only valid for smooth pipes, because it does not include the term for pipe roughness. Nevertheless, due to its simplicity, it is also occasionally employed in rough pipes. The Blasius equation is valid up to the Reynolds number 10^5 [46]. The Blasius equation is the following

$$f = \frac{0.316}{Re^{0.25}} \quad 3,000 > Re > 100,000 \quad (100)$$

Hence,

$$\Delta P = f \frac{L}{D} \frac{\rho v^2}{2} \quad (101)$$

- **Two-Phase Flow**

Beggs and Brill's Correlation (1973)

Beggs and Brill's multiphase correlation is similar to the majority of pressure loss correlations, as it deals with both the hydrostatic pressure difference and the friction pressure drop. Nevertheless, it takes into account the flow regime patterns for the gas-liquid mixture, liquid, and gas rates. The patterns are categorized as Transition, Distributed, Intermittent, and Segregated. The liquid holdup, and accordingly, the in-situ density of the gas-liquid mixture is subsequently computed on the basis of the adequate flow regime to determine the hydrostatic pressure difference (Kaushal, 2012). The Fanning friction factor and the input gas-liquid ratio are used to calculate a two-phase friction factor. Subsequently, input gas-liquid mixture properties are used to calculate the friction pressure drop. A detailed procedure is outlined below.

The first step is a calculation of the superficial velocity of each phase (liquid and gas). The superficial velocity refers to the volumetric flow rate of the phase divided by the cross-sectional area of the pipe.

$$v_{sl} = \frac{Q_l}{A} \quad (102)$$

$$v_{sg} = \frac{Q_g}{A} \quad (103)$$

The velocity of the gas-liquid mixture flow (multiphase) is the following:

$$v_m = v_{sl} + v_{sg} \quad (104)$$

In Beggs and Brill Correlation, the input volume fractions of liquid C_l and gas C_g are crucial parameters, defined as follows:

$$C_l = \frac{Q_l}{Q_l + Q_g} \quad (105)$$

$$C_g = \frac{Q_g}{Q_l + Q_g} \quad (106)$$

Comparable to the mixture velocity, density and viscosity that are measures of the in-situ density and viscosity of the mixture need to be detected. They are defined as follows:

$$\mu_m = \mu_l E_L(0) + \mu_g (1 - E_L(0)) \quad (107)$$

$$\rho_m = \rho_l E_L(0) + \rho_g (1 - E_L(0)) \quad (108)$$

Nevertheless, the assumption for calculating the no-slip (*NS*) density and viscosity is that both phases move at the same in-situ velocity, defined in the following way:

$$\mu_{NS} = \mu_l C_l + \mu_g(1 - C_l) \quad (109)$$

$$\rho_{NS} = \rho_l C_l + \rho_g(1 - C_l) \quad (110)$$

Flow Pattern Map

As mentioned previously, Beggs and Brill's correlation need a determination of a flow pattern. Transitions lines from L_1^* to L_4^* are employed to modify the correlation, defined in the following way:

$$L_1^* = 316 C_l^{0.302} \quad (111)$$

$$L_2^* = 0.000925 C_l^{-2.4684} \quad (112)$$

$$L_3^* = 0.1 C_l^{-1.4516} \quad (113)$$

$$L_4^* = 0.5 C_l^{-6.738} \quad (114)$$

Froude Mixture Number is a parameter without a dimension also employed to define the flow pattern in the following way:

$$Fr_m = \frac{v_m^2}{gD} \quad (115)$$

A representative flow pattern map or the following conditions are used to readily determine the flow type [47]:

Segregated/Stratified Flow

$$C_l < 0.01 \ \& \ Fr_m < L_1^* \ \text{or} \ C_l \geq 0.01 \ \& \ Fr_m < L_2^* \quad (116)$$

Intermittent/Slug Flow

$$0.01 \leq C_l < 0.4 \text{ \& } L_3^* \leq Fr_m < L_1^* \text{ or } C_l \geq 0.4 \text{ \& } L_3^* < Fr_m \leq L_4^* \quad (117)$$

Distributed Flow

$$C_l < 0.4 \text{ \& } Fr_m \geq L_4^* \text{ or } C_l \geq 0.4 \text{ \& } Fr_m > L_4^* \quad (118)$$

For Transition Flow

$$L_2^* < Fr_m < L_3^* \quad (119)$$

After the determination of the flow type, the next step is to calculate the liquid holdup. According to Beggs and Brill, there are two parts of the liquid holdup calculation. The first step is to determine the liquid holdup for horizontal flow $E_L(0)$. The second step is to modify this holdup for inclined flow to give $E_L(\theta)$ [47].

$E_L(0)$ must be $\geq C_l$, and accordingly, when $E_L(0)$ is smaller than C_l , $E_L(0)$ is assigned a value of C_l .

Subsequently, the liquid holdup $E_L(0)$ is computed for various flow patterns, as presented below.

Segregated/Stratified Flow

$$E_L(0) = \frac{0.98 C_l^{0.4846}}{Fr_m^{0.0868}} \quad (120)$$

Intermittent/Slug Flow

$$E_L(0) = \frac{0.845 C_l^{0.5351}}{Fr_m^{0.0173}} \quad (121)$$

Distributed Flow

$$E_L(0) = \frac{1.065 C_l^{0.5824}}{Fr_m^{0.0609}} \quad (122)$$

For Transition Flow

$$E_L(0)_{transition} = A E_L(0)_{segregated} + B E_L(0)_{intermittent} \quad (123)$$

Where:

$$A = \frac{L_3^* - Fr_m}{L_3^* - L_2^*}, \quad B = 1 - A \quad (124)$$

When the horizontal in situ liquid volume fraction is computed, the next step is to obtain the actual liquid volume fraction by multiplying $E_L(0)$ by an inclination factor, $B(\theta)$.

$$E_L(\theta) = B(\theta) * E_L(0) \quad (125)$$

Where:

$$B(\theta) = 1 + \beta[\sin(1.8 \theta) - \frac{1}{3} \sin^3(1.8 \theta)] \quad (126)$$

β is a function of the mixture Froude Number (Fr_m), the liquid velocity number (N_{vl}), the direction of inclination of the pipe (uphill flow or downhill flow), and flow type.

Uphill Flow

Segregated/Stratified Flow

$$\beta = (1 - C_l) \ln \left[\frac{0.011 N_{vl}^{3.539}}{C_l^{3.768} Fr_m^{1.614}} \right] \quad (127)$$

Intermittent/Slug Flow

$$\beta = (1 - C_l) \ln \left[\frac{2.96 C_l^{3.768} Fr_m^{1.614}}{N_{vl}^{0.4473}} \right] \quad (128)$$

For Distributed

$$\beta = 0 \quad (129)$$

Downhill Flow

All flow types are defined as

$$\beta = (1 - C_l) \ln \left[\frac{4.7 N_{vl}^{0.1244}}{C_l^{0.3692} Fr_m^{0.5056}} \right] \quad (130)$$

The value of β is in all cases greater than zero. Accordingly, if a negative value is computed for β , a value of zero is assigned to β .

The liquid velocity number (N_{vl}) is a a number without a dimension necessary for computing of β and it is defined in the following way:

$$N_{vl} = 1.938 v_{sl} \left(\frac{\rho_l}{g\sigma} \right)^{0.25} \quad (131)$$

Hydrostatic Pressure Loss

When the liquid holdup ($E_L(\theta)$) is computed, it is employed to compute the mixture density (ρ_m). Subsequently, the mixture density is employed to compute the pressure change occurring because of the hydrostatic pressure loss in the wellbore or pipe.

$$\Delta P_H = \rho_m g \Delta h \quad (132)$$

Frictional Pressure Loss

The first step in computing the pressure drop because of the friction is to compute the empirical parameter S . The value of S is determined by the following conditions:

$$y = \ln \frac{C_l}{E_l^2} \quad (133)$$

If, $1 < y < 1.2$, then

$$S = \ln(2.2 y - 1.2) \quad (134)$$

If not,

$$S = \frac{y}{-0.0523 + 3.1 y - 0.872 y^2 + 0.0185 y^4} \quad (135)$$

The second step is to compute the no-slip frictional factor. Here, the Chen friction equation is employed to compute the no-slip frictional factor using no-slip viscosity, no-slip density, and no-slip Reynolds number.

$$Re_{NS} = \frac{\rho_{NS} v_m D}{\mu_{NS}} \quad (136)$$

$$\frac{1}{\sqrt{f_{NS}}} = -0.4 \log \left[0.2698 \left(\frac{k}{D} \right) - \frac{5.0452}{Re_{NS}} \log \left\{ 0.3539 \left(\frac{k}{D} \right)^{1.1098} + \frac{5.8506}{Re_{NS}^{0.8981}} \right\} \right] \quad (137)$$

A ratio of friction factors is defined in the following way:

$$\frac{f_{tp}}{f_{NS}} = e^S \quad (138)$$

The last step is to calculate the expression for the pressure drop occurring because of friction following solving the ratio above to obtain the two-phase friction factor f_{tp} .

$$\Delta P_f = \frac{2 f_{tp} v_m^2 \rho_{NS} L}{D} \quad (139)$$

Dukler et al. Correlation (1964)

The basis of those two methods to compute the two-phase pressure frictional drop is the similarity analysis. Equations to compute friction factor and Reynolds number were suggested by using an analogy between single-phase and two-phase flows. As there are two cases, two types of correlations are used. First, it is assumed that the slip velocity is zero and accordingly, equations for a homogeneous flow are as follows [48].

Case I

$$\mu_{NS} = \mu_l C_l + \mu_g (1 - C_l) \quad (140)$$

$$\rho_{NS} = \rho_l C_l + \rho_g (1 - C_l) \quad (141)$$

Where:

$$C_l = \frac{Q_l}{Q_l + Q_g} = \frac{1}{1 + \left(\frac{x}{1-x}\right) \frac{\rho_l}{\rho_g}} \quad (142)$$

$$Re_{NS} = \frac{\rho_{NS} v_m D}{\mu_{NS}} \quad (143)$$

$$f = 0.0014 + \frac{0.125}{Re_{NS}^{0.32}} \quad (144)$$

$$\Delta P_{tp} = \frac{2 f_{tp} v_m^2 \rho_{NS} D}{\mu_{NS}} \quad (145)$$

According to the second case, a slip can happen during the flow. Hence, the proposal is an equation on the basis of the homogeneous (non-slip) model.

Case II

$$\mu_{tp} = \mu_l C_l + \mu_g (1 - C_l) \quad (146)$$

$$\rho_{tp} = \rho_l \left(\frac{C_l^2}{1 - \alpha} \right) + \rho_g \left(\frac{1 - C_l}{\alpha} \right) \quad (147)$$

$$Re_{tp} = \frac{\rho_{tp} v_{tp} D}{\mu_{tp}} \quad (148)$$

$$\frac{f_{tp}}{f_0} = 1.0 + \frac{-\ln C_l}{S} \quad (149)$$

Where:

$$f_0 = 0.0014 + \frac{0.125}{Re_{tp}^{0.32}} \quad (150)$$

$$S = 1.281 - 0.478(-\ln C_l) + 0.444(-\ln C_l)^2 - 0.094(-\ln C_l)^3 + 0.00843(-\ln C_l)^4 \quad (151)$$

$$\Delta P_{tp} = \frac{2 f_{tp} v_{tp}^2 \rho_{tp} D}{\mu_{tp}} \quad (152)$$

Dziubinski- Chhabra Correlation (1995)

Dziubinski and Chhabra [49] empirically modified the dimensionless pressure drop following the correlation of Lockhart and Martinelli. They introduced into the correlation the correction factor of Farooqi and Richardson (J) [50]. Hence, the frictional pressure drop of two-phase horizontal flow is deduced in the following way:

$$\left(\frac{dP}{dl}\right)_{tp} = \left(\frac{dP}{dl}\right)_l \left(J + \frac{C_0}{X} + \frac{J}{X^2}\right) \quad (153)$$

Where:

$$C_0 = \begin{cases} 20 & Re_l > 1500 \text{ and } Re_g > 1500 \\ 12 & Re_l < 1500 \text{ and } Re_g > 1500 \\ 10 & Re_l > 1500 \text{ and } Re_g < 1500 \\ 5 & Re_l < 1500 \text{ and } Re_g < 1500 \end{cases} \quad (154)$$

$$Re_g = \frac{D^n x v^{2-n}}{8^{n-1} K \left(\frac{3n+1}{4n}\right)^n} \quad (155)$$

$$Re_l = \frac{D^n(1-x)v^{2-n}}{8^{n-1}K\left(\frac{3n+1}{4n}\right)^n} \quad (156)$$

Lockhart-Martinelli parameter

$$X = \sqrt{\left(\frac{dP}{dl}\right)_g / \left(\frac{dP}{dl}\right)_l} \quad (157)$$

Farooqi and Richardson correction factor

$$J = \left(\frac{v_{sl}}{v_{sg}}\right)^{1-n} \quad (158)$$

Ruiz-Viera et al. Correlation (2005)

In this model, it is assumed that liquid and air are built discrete flat-ended plugs filling the whole cross-section of the pipe. It implies negligible pressure gradient along air plugs, no-slip velocity between phases, the short plugs length in comparison to the total length of pipeline and pressure gradient along liquid plugs equivalent to the one in conventional pipeline functioning at the same velocity [51]. The two-phase pressure drop is written in the following way:

$$-\frac{\Delta P_{tp}}{L} = \frac{2 f_{tp} v_m^2 \rho_l \lambda_l}{D} \quad (159)$$

Where: f_{tp} refers to the two-phase Fanning friction factor. Thus, the mixture velocity is provided by

$$v_m = v_{sg} + v_{sl} \quad (160)$$

with v_{sl} and v_{sg} being the superficial velocities of liquid and gas, respectively. They are taken as volumetric flux divided by pipe cross-sectional area of diameter D . In addition, ρ_l refers to the liquid density, whereas the input volume fraction of liquid is as follows:

$$\lambda_l = \frac{v_{sl}}{v_{sg}} \quad (161)$$

The rheological model describing the flow behavior of the liquid should be considered for the estimation of f_{tp} . Taking into account the power-law model,

$$\tau = k \gamma^n \quad (162)$$

where τ is shear stress, γ shear rate, n the flow index, in relation to the slope of the shear-thinning region, and k the consistency coefficient, the standard expression (Chhabra et al., 1983; Heywood and Richardson, 1978) for the two-phase generalized Reynolds number is the following:

$$Re'_{tp} = \frac{8D^n \rho_l v^{2-n}}{K \left(\frac{3n+1}{4n}\right)^n 2^{3n}} \quad (163)$$

More complex expressions should be proposed for other phenomenological models, including the Sisko model (Turian et al., 1998):

$$\tau = \eta_\infty \gamma + m \gamma^n \quad (164)$$

$$Re_{tp} = \frac{\rho_l v_m D}{\eta_\infty} + \frac{G(n, X)}{(1+X)} \quad (165)$$

Where η_∞ is the high shear rate limiting viscosity, m the consistency parameter for the Sisko model and n the flow index, where

$$G(n, X) = \frac{\left[1 + 4 \left[\left(\frac{n+2}{n+3} \right) X + \left(\frac{2n+1}{2n+2} \right) X^2 + \left(\frac{n}{3n+1} \right) X^3 \right] \right]}{(1+X)^3} \quad (166)$$

$$X = \frac{m}{\eta_{\infty}} \gamma^{n-1} \quad (167)$$

The pressure drop for the liquid flowing alone at the same superficial velocity is:

$$-\frac{\Delta P_l}{L} = \frac{2 f_l v_{sl}^2 \rho_l}{D} \quad (168)$$

This expression for the drag ratio can be acquired:

$$\phi^2 = \frac{1}{\lambda_l} \frac{f_{tp}}{f_l} \quad (169)$$

The friction factor in the laminar flow regime can be written as

$$f = \frac{16}{Re'} \quad (170)$$

Accordingly, a general expression for the drag ratio is the following:

$$\phi^2 = \frac{1}{\lambda_l} \frac{Re'_l}{Re'_{tp}} \quad (171)$$

The drag ratio for a power-law liquid/air two-phase flow in the laminar regime is reduced to the following expression:

$$\phi^2 = \lambda_l^{1-n} \quad (172)$$

it is essential to include a coefficient C_l , related to the efficiency of the plug formation (Carleton et al., 1973), defined as the ratio between experimental and theoretical two-phase pressure drops:

$$C_l = \frac{\left(-\frac{\Delta P_{tp}}{L}\right)_{EXP}}{\left(-\frac{\Delta P_{tp}}{L}\right)_{TH}} \quad (173)$$

As a result, the general expression for the drag ratio applicable to any rheological model is the following:

$$\Phi^2 = C_l \frac{1}{\lambda_l} \frac{Re'_l}{Re'_{tp}} \quad (174)$$

Appendix B: Solid/Liquid/Gas Multiphase Flow

Solid-Liquid Flow in Pipelines

There are two separate phases in a two-phase mixture, such as liquid-solid, gas-liquid, and gas-solid, coexisting in arbitrary space. The solid phase exists as discrete particles and the fluid phase is continuously connected in most particulate two-phase flow (i.e., gas-solid and liquid-solid). The experiments with the two-phase flow are essential for practical applications (hydro-transport of particles in pipes and pneumatic transport) and understanding the natural phenomenon (biological/biomedical flow and sediment transport in water bodies). Flows with granular materials are found in the food, petrochemical, mining and chemical industry.

In the majority of industrial processes, the physics of two-phase fluids are employed as a medium of material transport. A common method used in mining, chemical, pipeline, and petroleum industries is to transport solid material in a particulate form. The general knowledge of the general principles behind the phenomena of fluid transportation is a secure and efficient system. The flow of the highly concentrated multi-sized particulate slurry is much more complicated than single phase. It is necessary to have precise information about flow regimes, pressure drop, critical velocity, hold up, etc. for designing pipelines and appropriate facilities. Nevertheless, two-phase or multiphase is common in many industries, such as the oil and gas, chemical, and petroleum industry.

In general, all single-phase liquid flows are categorized into one of two regimes – turbulent and laminar flows. The flow regime is critical for the process and design of any fluid system. The shear stress from fluid exhibited on the pipe wall requires the specific quantity of energy needed to keep the desired flow, and it is based on the flow type.

One of the main flow assurance concerns in gas-oil-sand multiphase flows through subsea tieback systems, flow-line, and the wellbore is sand particle transport. If not resolved, this can compromise the sand management (Chisholm, 1967). The type of fluid flow occurring in straight, circular pipes depends on Reynolds number, Re , or more precisely, the ratio between the inertia force and viscous force.

When the Reynolds number is smaller than 2300, laminar flow takes part. The resistance to flow does not depend on the pipe wall roughness. When Reynolds number is beyond 4000, turbulent flow takes part. Transition flow is the condition between the laminar and turbulent flow conditions, when Reynolds number is in the range from 2300 to 4000.

Laminar flow

The laminar flow condition occurs when a fluid flows through a pipe and interacts with the internal roughness of the pipe wall, which results in the local eddy currents within the fluid. It is a resistance to a flow of the fluid. The fluid that is viscous is slower and does not support eddy currents. The internal roughness of the pipe hardly impacts the frictional resistance. When the flow is laminar, fluid particles move along parallel, straight paths in layers. The magnitudes of adjacent layers differ. Laminar flow is ruled by the law connecting shear stress to the rate of angular deformation.

Turbulent flow

In turbulent flow, fluid particles move in a superficially haphazard manner in all directions. Hence, it is challenging to trace the motion of a specific fluid particle. Directions and magnitudes of shear force, pressure, and velocity fluctuate in random order.

A near-wall boundary layer is needed to describe turbulent velocity. Figure 72 below demonstrates shear stress and classic velocity near a wall. A universal velocity profile characterized by a turbulent core, a viscous sub-layer, and a buffer zone in between describes it.

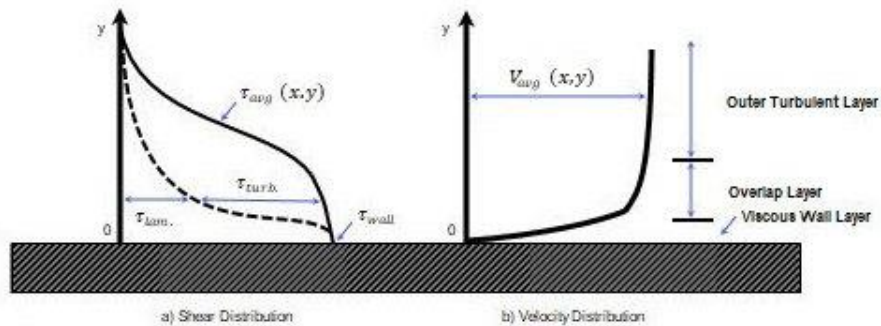


Figure 72 – Typical Velocity and Shear Stress Distributions Near a Wall in Turbulent Flow (Adapted from Kay and Nedderman, 1985 [52])

Forces from the surrounding flow act upon solid particles in the liquid flow. In particular, it depends on the force balance on the vertical axis if it will settle on the pipe bottom or not. Four common forces act on a spherical particle on a vertical axis (see Figure 73).

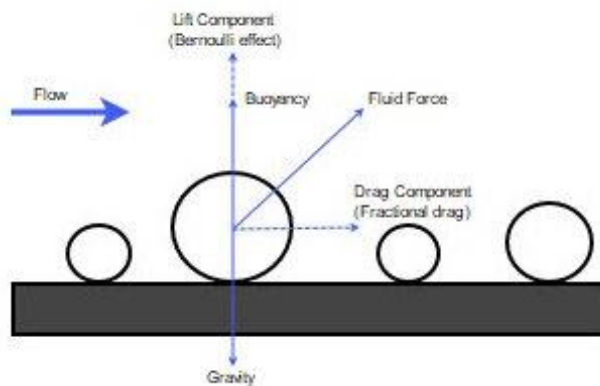


Figure 73 - Forces Acting on a Spherical Particle Within a Flow (Adapted from Green and Perry, 2007 [53])

In concentrated suspensions, the particles crash into another, and it slows down their settling. This process is known as hindered settling. The presence of the surrounding particles impacts the velocity gradients around each particle. The particles in settling displaced liquid flowing upward result in the higher particle velocity relative to the fluid in comparison to the absolute settling velocity. Viscosity and density of the fine suspension are used to determine the terminal velocity of the larger particles falling through a suspension of much finer solids.

Solid - Liquid Flow Regimes

Solid particles flowing through both single phase and multiphase pipe lines adopt several patterns or flow regimes, as illustrated by Figure 74.

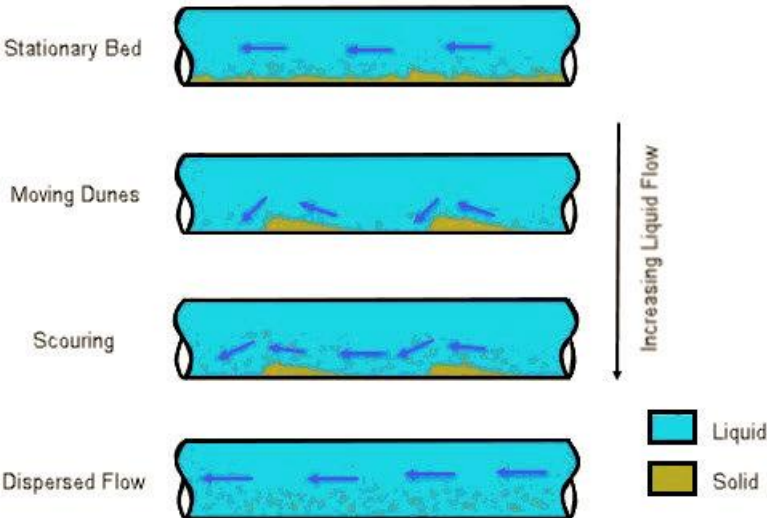


Figure 74 - Solid-Liquid flow regimes in horizontal pipelines (Adapted from Multiphase Design Handbook, 2005 [54])

Stationary Bed:

A stationary bed forms when the flowing velocity of the liquid is low with solid particles located at the bottom that do not move. When the velocity increases, a stable bed height is achieved, as the upper particles go downwards and enhance the length of the bed. When the flow rates are low, the upper surface of the bed is flat. However, with a rise in the flow rate, it becomes wavy. Moreover, with the rise in the liquid flow rate, the height of the stationary drops. To reach an equilibrium bed, solid particles should be transported downstream by the shear at the upper surface at the rate identical to the solid inflow rate.

Moving Dunes:

The bed breaks up with the further amplification of the liquid flow rate. Under this condition, the particles are rearranged into moving dunes. The grains on the dune's upper surface of the dune roll downstream, from back to front. Subsequently, the grains reach the sheltered region at the front of the dune. The dune passes particles to the top surface. The speed of smaller dunes is faster than of the big ones, and with a certain length of stationary deposit, they break into several dunes, each having a characteristic velocity and length.

Scouring:

With the further rise in the flow rate, the particles roll along the top of the dunes. At this moment, the momentum is sufficient for them to leave the sheltered downstream region. In a form of individual scouring particles, they are swept away. If the dunes are replenished by upstream particles, they can continue to exist.

Dispersed Flow:

The dunes disperse at high liquid flow-rates. At this point, the solid particles form an intermittent pattern and move into the produced fluid. Typically, it is possible to observe strong concentration gradient.

Solid – Gas - Liquid Flow Regimes

The liquid that carries the solid particles along the bottom of the pipe is lighter than the solid particles when the concentration is low. Accordingly, the flow patterns noticed in single phase solid-liquid flow are comparable to patterns observed in the stratified liquid-gas-solid flow. The reason is that the flowing velocity is constant while the liquid is located in the lower part of the pipe. Nevertheless, this does not happen when the gas-liquid flow regime is slug or plug flow due to variations in the velocities and the depth of the film. Figure 75 illustrates the flow regimes.

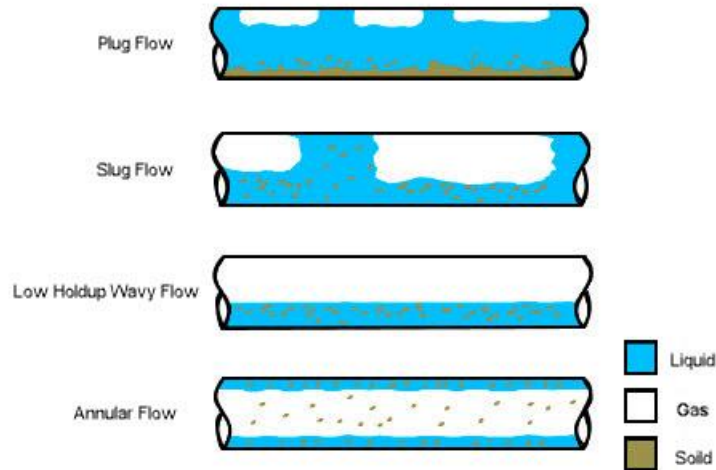


Figure 75 - Solid-Gas-Liquid flow regimes in horizontal pipelines (Adapted from Multiphase Design Handbook, 2005 [54])

Plug Flow:

In a case of the plug flow, the gas bubbles travel along the top of the pipe. Their impact on the solid phase flow is little. With a rise in the amount of gas, the bubble depth rises as well. The impact on the fluctuating velocities on the transport is comparable to the one of slug flow.

Slug Flow:

The movement of solid particles in the slug flow is complex, as they can settle while passing the film region and then transported in the slug body. It is possible to have an impact of a large diameter because of the variety of the depths of the film, as it protects the pipe's bottom from the turbulences occurring in the slug. In a case that neither the film, nor the slug transport the solid particles, a bed is formed. The motion is intermittent when only the slug transports the particles. If bed stabilization and compaction occur due to other products, there may be the frequency between slugs.

Low Holdup Wavy Flow:

When gas pipelines are wet, the liquid can move in a form of as a thin film along the bottom of the pipe. In this case, it is likely that the concentration of solid particles in the film is high. In extreme cases, it can take a form of a wet solid bed. However, there is not enough knowledge about removing the wet solid.

Annular Flow:

In this case, the solid particles may be transported in the gas core or the liquid film. In annular flow, the velocities are high. Accordingly, the greater concern is about the erosion than about the transportation of the solid particles.

Flow Loop Modifications

A technical evaluation carried out to determine if it is feasible to add solid particles to the existing system within the scope of the three-phase flow analysis in the scope of the process flow loop. Three design concepts were developed and presented.

Design 1

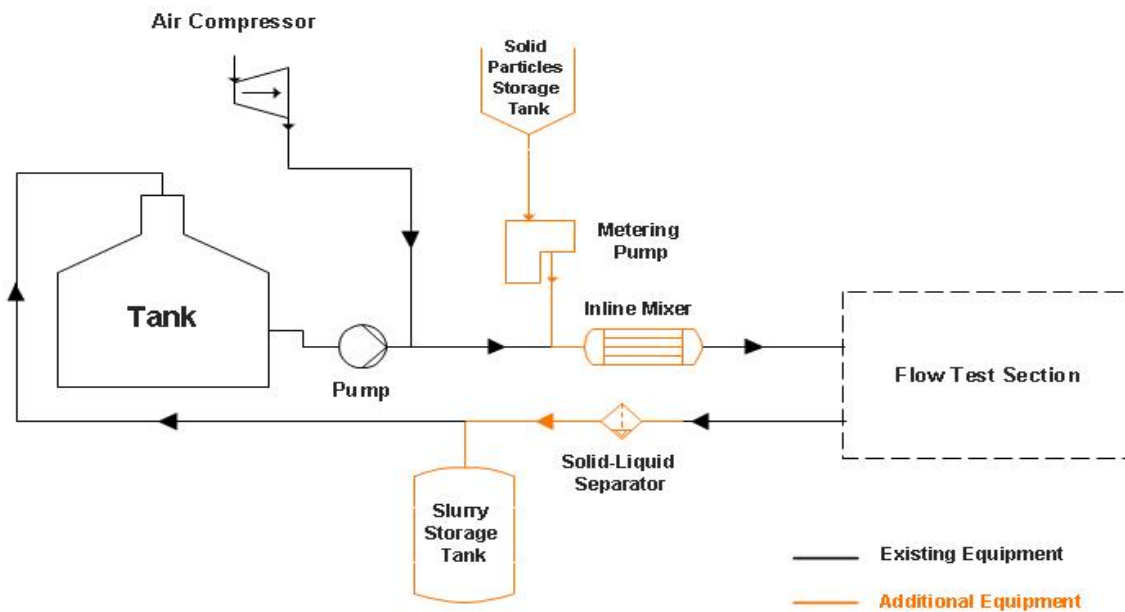


Figure 76 - Flow Loop Schematic of Design 1

Design Theory:

Introduction of solid particles into the current process flow loop following the discharges of air compressor and water pump and removal of solid particles before the inlet of the current pump.

Additional Items Required:

- Solid-liquid separator
- Inline mixer
- Rotary valve or metering pump

Advantages:

- No modification or replacement of the current pump is needed.

Disadvantages:

- A part of the solids will run through a pump continuously due to incomplete solid separation.
- Solid-Liquid separator will make the operation of the flow loop more complex.
- Liquid content of circulating Solid Particles could plug the Solid Particle Storage Tank.

Design 2

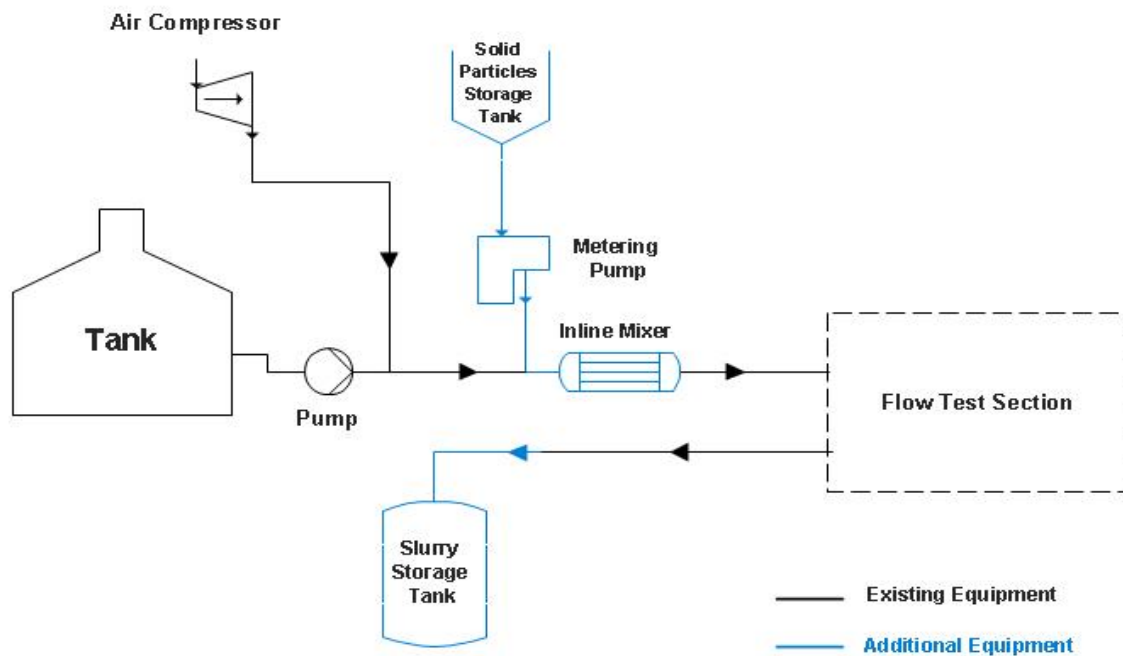


Figure 77 - Flow Loop Schematic of Design 2

Design Theory:

When a solid particle is inserted into the current system, a new slurry holding tank will gather the mixture. When the slurry tank is full, the test is over.

Additional Items Required:

- Slurry Storage Bin
- Inline mixer
- Solid Particle Storage Bin
- Rotary valve or metering pump

Advantages:

- No modification or replacement of the current pump is needed.

Disadvantages:

- High operational costs for the purchase of Solid Particles could limit the use.
- The disposal of Slurry could result in environmental complications.
- Test results may not be reliable due to transient conditions.

Design 3

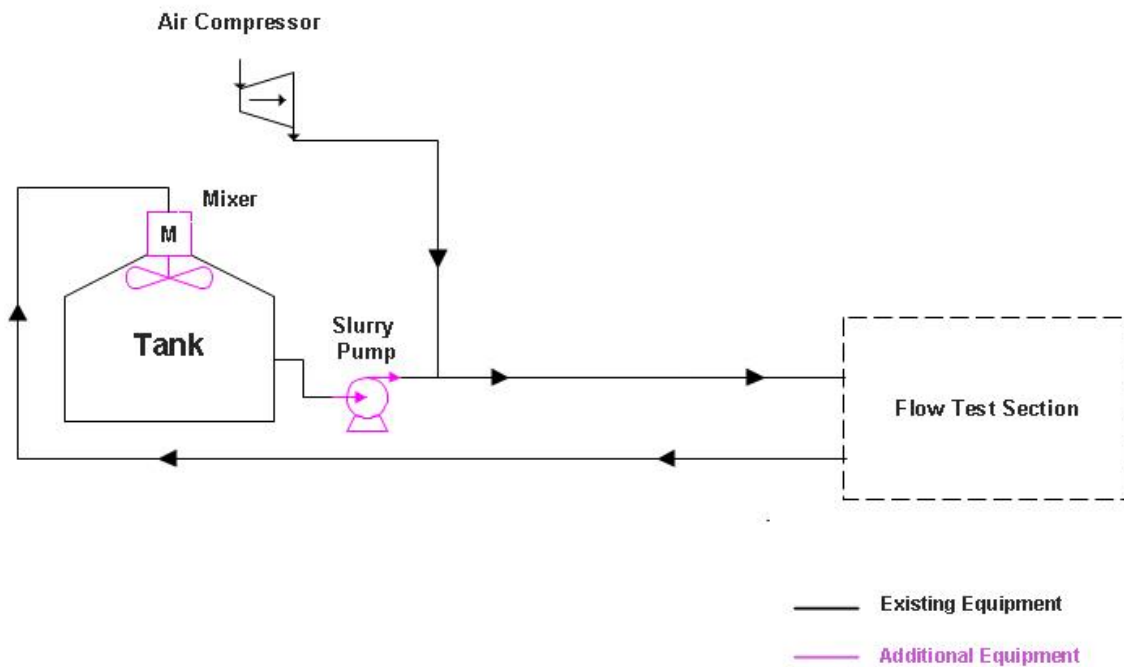


Figure 78 - Flow Loop Schematic of Design 3

Design Theory:

Solid particles are integrated into the flow loop, whereas a mixer is installed in the current storage tank to maintain a compatible pump circulates and the particles in suspension.

Additional Items Required:

- Slurry pump
- Storage Tank Agitator

Advantages:

- Some equipment replacements are needed for the introduction of solid particles smoother.

Disadvantages:

- It is possible that slurry pump is cost excessively high.

Copyright in this work rests with the author. Please ensure that any reproduction or re-use is done in accordance with the relevant national copyright legislation.